

# UC Santa Barbara

## UC Santa Barbara Electronic Theses and Dissertations

### Title

Dynamic Polyester Networks for Advanced Functional Materials

### Permalink

<https://escholarship.org/uc/item/00q12425>

### Author

Self, Jeffrey

### Publication Date

2021

Peer reviewed|Thesis/dissertation

UNIVERSITY OF CALIFORNIA SANTA BARBARA

Dynamic Polyester Networks for Advanced Functional Materials

A dissertation submitted in partial satisfaction of the  
requirements for the degree Doctor of Philosophy  
in Chemistry

by

Jeffrey Lucas Self

Committee in charge:

Professor Christopher M. Bates, Co-chair

Professor Javier G. Read de Alaniz, Co-chair

Professor Craig J. Hawker

Professor Michael L. Chabinyc

Professor R. Daniel Little

June 2021

The dissertation of Jeffrey Lucas Self is approved.

---

Christopher M. Bates, Co-chair

---

Javier G. Read de Alaniz, Co-chair

---

Craig J. Hawker

---

Michael L. Chabinyo

---

R. Daniel Little

June 2021

Dynamic Polyester Networks for Advanced Functional Materials

Copyright © 2021

by

Jeffrey Lucas Self

## ACKNOWLEDGEMENTS

First, I would like to thank my advisors, Chris Bates and Javier Read de Alaniz, for all their support and guidance over the years. I have learned so much in time at UCSB and I am incredibly appreciative of their mentorship and all the opportunities they afforded me. They encouraged me to tackle challenges that I would have thought were beyond my scope and, in doing so, fostered my development as a scientist. Beyond the countless emails, we also shared many hours engaged in thoughtful discussions on everything from career advice to lab technique to science history. They generously provided a space in which we could develop my best ideas into full-fledged projects and where we could also quietly bury my bad ideas. In short, they were great advisors.

Next, I would like to thank all my colleagues who contributed to the projects described herein. The results in Chapters I, II, and III, were collected with help from Neil Dolinski and Manuel Zayas; Caitlin Sample, Adam Levi, Cathy Li, and Renxuan Xie; Veronica Reynolds, Jacob Blankenship, Erin Mee, Renxuan Xie, and Kaitlin Albanese, respectively. I also received a great deal of help from Rachel Behrens and Hongjun Zhou, who taught me a lot about the instrumentation and experimental techniques necessary for my research. I would also like to thank all those who contributed to my time at UCSB with whom I did not have the pleasure of collaborating, including the Read de Alaniz lab, the Bates lab, the Hawker lab, and the Chabinyc lab.

Outside of lab, I had a wonderfully supportive community of friends to whom I am eternally grateful, from my early youth all the way to this past year. I do not think any list

could do justice to all the people I would like to thank in that regard, but if any of you are reading this, then please know that I appreciate you and the times we have had together.

I do want to make a special point of thanking my partner, Caitlin Sample. You have brought so much joy and adventure to my life. From our camping trips to our grocery trips, every moment with you is a gift I cherish, and I am excited about everything our future holds. Thank you for giving me the courage to prevail through the darker times of my graduate life and for reminding me to slow down and enjoy the good times. I have always admired your brilliance, your compassion, your sense of humor, and your passion, and I would not be where I am today without you. Thank you.

I also want to thank my family: my brothers, Mateo and Nico; my sister-in-law, Jessica; and my unbelievably wonderful and adorable nephews, Elliott and Anthony. I especially want to thank my parents, Mitch and Elena, who have gone such great lengths to support me. I owe them the world and, since I could never hope to pay them back, I will do my best to pay it forward. I would also like to thank my grandparents, Mary Lee and George. Thank you, Grandpa, for everything you have done for our family. And thank you so much, Grandma, for a lifetime of unconditional love; we all miss you dearly.

Finally, thank you, dear reader, for your interest in my work. Whenever and wherever you are, I hope you find something of use herein.

# Jeffrey L. Self

Department of Chemistry and Biochemistry  
University of California, Santa Barbara

(281) 841-5413  
jeffreysself@ucsb.edu

## EDUCATION

---

University of California, Santa Barbara	Aug 2016 - <i>Present</i>
Doctorate of Philosophy, Chemistry	
<i>Advisors:</i> Prof. Christopher M. Bates Prof. Javier Read de Alaniz	
The University of Texas at Austin	Aug 2011 - May 2016
Bachelor of Science with Honors, Chemistry	
Bachelor of Science with Honors, Chemical Engineering	
<i>Dual Technical Areas:</i> Materials Engineering and Energy Technology	

## RESEARCH EXPERIENCE

---

National Science Foundation Graduate Research Fellow	<i>University of California, Santa Barbara</i> Prof. Christopher M. Bates Prof. Javier Read de Alaniz	Aug. 2017 – <i>Present</i>
Graduate Research Assistant	<i>University of California, Santa Barbara</i> Prof. Christopher M. Bates Prof. Javier Read de Alaniz	Aug. 2016 – <i>Present</i>
Undergraduate Research Assistant	<i>The University of Texas at Austin</i> Prof. C. Grant Willson	May 2013 – Aug. 2016
Summer Undergraduate Research Fellow (SURF)	<i>NIST Center for Neutron Research</i> Dr. Antonio Faraone	May 2014 – Aug. 2014
Undergraduate Research Assistant	<i>The University of Texas at Austin</i> Prof. C. Buddie Mullins	Dec. 2011 – Feb. 2013

## PEER-REVIEWED PUBLICATIONS

---

- Nie, N.; Schausser, N.S.; **Self, J.L.**; Tabassum, T.; Oh, S.; Geng, Z.; Jones, S.D.; Zayas, M.S.; Reynolds, V.G.; Chabinyk, M.L.; Hawker, C.J.; Han, S.; Bates, C.M.; Segalman, R.A.; Read de Alaniz, J.G. "Light-Switchable and Self-Healable Polymer Electrolytes Based on Dynamic Diarylethene and Metal-Ion Coordination". *J. Am. Chem. Soc.* **2021**, 143 (3), 1562 – 1569.

DOI: 10.1021/jacs.0c11894

11. **Self, J.L.**; Sample, C.S.; Levi, A.E.; Li, K.; Xie, R.; Read de Alaniz, J.G.; Bates, C.M. “Dynamic Bottlebrush Polymer Networks: Self-Healing in Super-Soft Materials”. *J. Am. Chem. Soc.* **2020**, 141 (16), 7567 – 7563.  
DOI: 10.1021/jacs.0c01467
10. Nie, H.; **Self, J.L.**; Kuenstler, A.S.; Hayward, R.C.; Read de Alaniz, J.G. “Multiaddressable Photochromic Architectures: From Molecules to Materials”. *Adv. Opt. Mater.* **2019**, 1900224.  
DOI: 10.1002/adom/201900224
9. Zayas, M.S.; Dolinski, N.D.; **Self, J.L.**; Abdilla, A.; Hawker, C.J.; Bates, C.M.; Read de Alaniz, J.G. “Tuning Merocyanine Photoacid Structure to Enhance Solubility and Temporal Control: Application in Ring-Opening Polymerization”. *ChemPhotoChem.* **2019**, 3, 467–472.  
DOI: 10.1002/cptc.201800255
8. **Self, J.**; Dolinski, N.D.; Zayas, M.S.; Read de Alaniz, J.G.; Bates, C.M. “Bronsted-Acid-Catalyzed Exchange in Polyester Dynamic Covalent Networks”. *ACS Macro Lett.* **2018**, 7(7), 817-821.  
DOI: 10.1021/acsmacrolett.8b00370
7. Bertrand, C.; **Self, J.**; Copley, J.; Faraone, A. “Nanosopic Length Scale Dependence of Hydrogen Bonded Molecular Associates’ Dynamics in Methanol” *J. Chem. Phys.* **2017**, 146(5), 059901.  
DOI: 10.1063/1.4983179
6. Maher, M.; **Self, J.**; Pawel, S.; Blachut, G.; Ellison, C.; Matsen, M.; Bates, C.; Willson, C. “Structure, Stability, and Reorganization of 0.5 L<sub>0</sub> Topography in Block Copolymer Thin Films”. *ACS Nano.* **2016**, 10(11).  
DOI: 10.1021/acsnano.6b05390
5. Bertrand, C.; **Self, J.**; Copley, J.; Faraone, A. “Dynamic Signature of Molecular Association in Methanol”. *J. Chem. Phys.* **2016**, 145(1), 014502.  
DOI: 10.1063/1.4954964
4. Maher, M.; Bates, C.; Blachut, G.; Carlson, M.; **Self, J.**; Janes, D.; Durand, W.; Lane, A.; Ellison, C.; Willson, C. “Photopatternable Interfaces for Block Copolymer Lithography”. *ACS Macro Lett.* **2014**, 3(8), 824-828.  
DOI: 10.1021/mz500370r
3. Maher, M.; Bates, C.; Blachut, G.; Sirad, S.; **Self, J.**; Carlson, M.; Dean, L.; Cushen, J.; Durand, W.; Hayes, C.; Ellison, C.; Willson, C. “Interfacial Design for Block Copolymer Thin Films”. *Chem. Mater.* **2014**, 26(3), 1471-1479.  
DOI: 10.1021/cm403813q
2. Hahn, N.; **Self, J.**; Mullins, C. “BiSI Micro-Rod Thin Films: Efficient Solar Absorber Electrodes?”. *J. Phys. Chem. Lett.* **2012**, 3, 1571-1576.



DOI: 10.1021/jz300515p

1. Hahn, N.; Hoang, S.; **Self, J.**; Mullins, C. “Spray Pyrolysis Deposition and Photoelectrochemical Properties of n-type BiOI Nanoplatelet Thin Films”. *ACS Nano*. **2012**, 6, 7712-7722.

DOI: 10.1021/nn3031063

## **PATENTS AND PATENT APPLICATIONS**

---

1. Inventors: Chabinyo, M.L.; Bates, C.M.; Reynolds, V.G.; Mukherjee, S.; Xie, R.E.; Levi, A.E.; Self, J.L. Capacitive Pressure Sensor with Bottlebrush Elastomer Dielectric Layer for Low Pressure Sensing. Publication number: US2020/0362117 A1. Nov 19, 2020. Patent Pending.

## **HONORS AND AWARDS**

---

### *University of California, Santa Barbara*

2021:

-Accepted to present at the ACS POLY Excellence in Graduate Research Symposium (Spring ACS National Conference 2021) with special recognition

2020:

-2<sup>nd</sup> place in UCSB Chemical Science Student Seminar series  
-Elected as Co-President of Graduate Students for Diversity in Science

2019:

-Outstanding Service to the Department of Chemistry and Biochemistry  
-Elected as Co-President of Graduate Students for Diversity in Science

2017:

-Graduate Research Fellowship, National Science Foundation (2017-2021)  
-Phi Lambda Upsilon Award for Academic Excellence

### *University of Texas*

2016:

-Dean’s Honored Graduate  
-Undergraduate Research Fellowship  
-Departmental Honors for Undergraduate Thesis—Chemistry

2015:

-Arnold and Mabel Beckman Scholarship  
-Departmental Honors for Undergraduate Thesis—Chemical Engineering

2014:

-Howard F. Rase Scholarship in Chemical Engineering  
-Dorothy Banks Trust Charitable Scholarship

2013:

-Dwight E. Hugh Endowed Presidential Scholarship

2012:

## **MENTORING EXPERIENCE**

---

Undergraduate research assistant:		
Cathy Li	UCSB Biochemistry student	Sept. 2019 – <i>Present</i>
Cooperative International Science and Education Internship (CISEI):		
11 international summer interns		Jun. 2019 – Aug. 2019
Research Experience for Teachers (RET) assistants:		
Megan Poster	H.S. Chemistry teacher	Jun. 2019 – Aug. 2019
Paul Nolan	H.S. Physical Sciences teacher	Jun. 2018 – Aug. 2018
Kate Standerfer	H.S. Chemistry teacher	Jun. 2017 – Aug. 2017

## **STUDENT TEACHING EXPERIENCE**

---

Undergraduate Teaching Assistant (Chemistry I & II)	<i>Department of Chemistry The University of Texas at Austin</i>	Aug. 2015 – May 2016
Peer Learning Assistant (Chemistry I & II)	<i>Department of Chemistry The University of Texas at Austin</i>	Aug. 2012 – May 2015
Undergraduate Teaching Assistant (Physics Lab for Non-Majors)	<i>Department of Physics The University of Texas at Austin</i>	Jan. 2014 – May 2014
Residence Hall Study Group Tutor	<i>Student Division, CNS The University of Texas at Austin</i>	Aug. 2013 – Dec. 2013
CNS 101 Cohort Leader	<i>Student Division, CNS The University of Texas at Austin</i>	Aug. 2013 – Dec. 2013
Summer Readiness Mentor	<i>Student Division, CNS The University of Texas at Austin</i>	May 2013 – Aug. 2013

## OUTREACH EXPERIENCE

---

*Cooperative International Science and Education Internship (CISEI):* Summer internship program run through the Materials Research Laboratory wherein international students from partnering universities do an exchange program with UCSB students for 11 weeks. The students are paired with graduate mentors to participate in summer research. My role was to meet weekly with the interns to lead workshops on research methods, scientific communication, and presentation fundamentals. I also helped mediate between interns and their mentors to resolve and to coordinate the summer activities.

*Research Experience for Teachers (RET) Summer Program:* Program run through the Materials Research Laboratory for introducing local high school science teachers to university-level research. I have served as a mentor, immersing these teachers in our ongoing research projects while also educating them on the principles of investigative research, namely: safety, introductory instruction on various characterization techniques (UV-vis, NMR, etc), experiment design, and methodology. After the first summer of mentorship in a lab setting, the teachers return the following summer to work on curriculum design to bring these research concepts back to the classroom. During this second summer I assist in the development and design of chemistry experiments that are feasible yet insightful.

*UCSB Solar Car Workshop:* This program takes place every few weeks during the summers and is designed for middle to high school level students, primarily through local organizations (namely, United Way and Boys and Girls Club of Santa Barbara, and Girls Inc). The workshop involves a presentation on solar energy history and development, followed by the construction of small solar-powered cars from provided kits. I volunteered to help the students assemble their cars and race/time them before working through a handout, but my degree of involvement in the program led to a leadership role wherein I designed and delivered the presentations, as well as leading the workshops.

*It's a Materials World:* Program run through the Materials Research Laboratory wherein volunteers set up demonstrations at local elementary school Science Nights. The goal is to engage the local community and make scientific research more accessible for children, with an emphasis on lower income areas. I actively volunteered on a bimonthly basis where I would guide kids through several demonstrations dealing with science principles in a fun way; the primary demonstrations included a hydrophobicity/hydrophilicity station, a shape memory station, and a magnetic colloid station.

*Materials Outreach Teacher day:* Annual program run through the Materials Research Laboratory wherein local high school and middle school teachers spend a day on campus learning about various ongoing research and programs at UCSB. A select number of research groups can volunteer to participate. I, on behalf of the Bates group, designed/prepared hands-on demonstrations of photo-responsive gels and solutions.

# Dynamic Polyester Networks for Advanced Functional Materials

by

Jeffrey Lucas Self

## Abstract

Polyesters are of particular interest as they are well-established materials of industrial and manufacturing interest; poly(ethylene terephthalate)—the most common polyester—currently makes up nearly 20% of all plastic materials produced globally. Similarly, poly(lactic acid) is an increasingly important polymer as it can be readily sourced from natural and renewable sources (e.g., corn starch). Therefore, advances in polyester technologies, including the development of robust dynamic network systems, is of great interest to the polymer science community. To that end, we investigated 1) the effect of Brønsted acid catalyst strength on dynamic network properties in a rubbery polyester system, 2) the development of a dynamic network system using polyester bottlebrush polymers, and 3) the demonstration of a dynamic polyester bottlebrush polymer composite with CNT-filler particles to generate soft and conductive materials.

In the study of Brønsted-acid catalyzed dynamic networks, we found that with a rubbery polyester (4-methylcaprolactone) stress relaxation occurred even at mild conditions (25 to 75 °C). In comparison to the more conventional Lewis acid-catalyzed systems, Brønsted-acid-catalyzed systems have significantly lower activation energies (49 to 67 kJ mol<sup>-1</sup> as compared to 90 to 150 kJ mol<sup>-1</sup>). The rates of stress relaxation have a clear dependence on acid strength. The benefit of lower temperature compatibility was demonstrated by the reprocessing of a cylindrical sample at 85 °C over two cycles of damaging and then healing. Analysis reveals

that with increasing acid strength ( $pK_a$ ), the apparent activation energy increases and the kinetic prefactor decreases.

In the study of bottlebrush polymer dynamic networks, we found that the advantageous mechanical properties of bottlebrush polymer networks could be realized in conjunction with dynamic network properties. The samples generated showed very low moduli, from 8 to 60 kPa, significantly lower than is attainable with conventional linear networks. Furthermore, through formulation design and varying of precursor polymer molecular weight, the modulus of the final material can be targeted and predicted. In terms of their dynamic character, these networks showed activation energies in approximate agreement with reported Lewis acid activation energy systems ( $89 \text{ kJ mol}^{-1}$ ) and was invariant over the crosslinking loadings investigated. As a demonstration of the ability to self-heal, tensile samples were generated, strained to break, and re-annealed. Over two cycles of healing, the network retained >85% of its toughness.

Lastly, we report a carbon nanotube composite that uses bottlebrush polymer precursors for the matrix material. Bottlebrush polymer networks have shown promise as super-soft elastomers. While the inclusion of CNT-filler raises the modulus relative to the unfilled samples, at loadings of 0.25wt% and 0.5wt% CNT the generated composites were still characteristically soft, with modulus values of 66 kPa and 140 kPa, respectively. Despite the low loadings, the CNT-filler imbues the materials with significant conductivities. While the unfilled samples behave as insulating material, the reported composites have conductivities of  $0.006 \text{ S/m}^2$  and  $0.054 \text{ S/m}^2$ . There is ongoing work to fully understand the dynamic nature of these materials and the impact of the CNT filler particles.

## TABLE OF CONTENTS

Chapter I. Introduction to dynamic polymer networks.....	1
A brief history of crosslinked networks.....	1
Dynamic networks from dynamic bonds.....	4
Mechanisms of dynamic polymer networks.....	6
Development of dynamic bond motifs.....	10
Dynamic polymer networks for advanced applications.....	12
Thesis scope.....	15
Chapter II. Brønsted-acid-catalyzed dynamic polyester network.....	17
Abstract.....	17
Introduction.....	18
Discussion.....	21
Conclusion.....	34
Materials and Methods.....	43
Reagent and solvent information.....	43
Instrumentation.....	44
Synthesis.....	44
Chapter III. Dynamic Bottlebrush Polymer Networks: Self-Healing in Super-Soft Materials	
.....	48
Abstract.....	48
Introduction.....	49
Discussion.....	51
Conclusion.....	63

Materials and Methods .....	63
Reagents and solvent information .....	63
Instrumentation .....	64
Synthesis .....	66
Chapter IV. Carbon nanotube-containing dynamic bottlebrush polymer composites for soft electrodes .....	78
Abstract .....	78
Introduction .....	79
Results and discussion .....	80
Conclusion .....	91
Experimental methods .....	91
Reagents and solvents .....	91
Size-exclusion chromatography instrumentation .....	92
Synthetic details .....	92
Carbon nanotube dispersion .....	95
Mechanical analysis .....	96
Impedance spectroscopy .....	96
Network formation procedure .....	96
Chapter V. References .....	101

## LIST OF FIGURES

- Figure 1.** Differences in the structural connectivity of a) thermoplastics and b) thermosets result in distinct thermal properties. ....3
- Figure 2.** The different categories of dynamic bond exchange via a) a dissociative exchange reaction where the connectivity is transiently lost and b) an associative exchange reaction where the connectivity is preserved during the transformation. ....7
- Figure 3.** Angell fragility plot showing the viscosity dependence on inverse temperature of various materials. From reference <sup>11</sup>, Copyright 2016 AAAS. Reprinted with permission from AAAS. ....8
- Figure 4.** The classic suite of experiments as demonstrated by Leibler and coworker for characterizing a dynamically crosslinked network: a) confirmation of an insoluble network, b) characterization of dynamic exchange via mechanical methods (stress relaxation is shown here) and analysis of the temperature dependence of the exchange, and finally demonstrations of either the c) self-healing of the material or d) demonstration of the reprocessability. From reference 11, Copyright 2016 AAAS. Reprinted with permission from AAAS. ....9
- Figure 5.** Bronsted acids promote exchange reactions in polyesters vitrimers and offer several advantages relative to other catalysts. ....19
- Figure 6.** Flow process diagram for one-pot preparation of Brønsted-acid-catalyzed polyester vitrimers, from initial small molecule formulation to final solid network sample. ....20



**Figure 7.** (a) Schematic describing the ROP synthesis of low- $T_g$  polyester vitrimers. (b) Brønsted acid catalysts (used to promote ROP and subsequent exchange reactions via transesterification.  $pK_a$  values are referenced in H<sub>2</sub>O. ....21

**Figure 8.** Solid state <sup>13</sup>C NMR spectrum of a polyester network containing TCA catalyst. Inset: magnification of the methyl resonance. Near quantitative conversion of the monomer is evidenced by the shift to lower frequency after polymerization. ....22

**Figure 9.** The same solid state <sup>13</sup>C NMR spectrum as **Figure 4** (containing TCA catalyst) demonstrates ≈96% conversion of the cross-linker. ....23

**Figure 10.** Solid state <sup>13</sup>C NMR spectrum of a polyester network containing MSA catalyst. Inset: magnification of the methyl resonance. Near quantitative conversion of the monomer is evidenced by the shift to lower frequency after polymerization. ....24

**Figure 11.** The same solid state <sup>13</sup>C NMR spectrum as **Figure 6** (containing MSA catalyst) demonstrates quantitative conversion of the cross-linker.....25

**Figure 12.** Oscillatory rheology step-strain stress relaxation experiments on low- $T_g$  polyester vitrimer formulations containing Brønsted acid catalysts. (a) Methanesulfonic acid measured at different temperatures. (b) Various acids compared at 55 °C. Dashed lines are fits to **Equation 1**.....26

**Figure 13.** Select TCA normalized stress relaxation traces with fit model superimposed. Note the small y-axis range to better visualize the data. ....27

**Figure 14.** Select MSA normalized stress relaxation traces with fit model superimposed. Note the y-axis bounds differ from the previous figure. ....28

**Figure 15.** Select BSA normalized stress relaxation traces with fit model superimposed. Note the y-axis bounds differ from the previous figure. ....29

<b>Figure 16.</b> Select HTFSI normalized stress relaxation traces with fit model superimposed. .....	30
<b>Figure 17.</b> Select Triflic normalized stress relaxation traces with fit model superimposed.	31
<b>Figure 18.</b> Comparison of experimentally determined characteristic relaxation times to those calculated using the fit model shows good agreement. ....	32
<b>Figure 19.</b> (a) Characteristic relaxation time ( $\tau^*$ ) exhibits an Arrhenius temperature dependence for all five Brønsted acids. Solid lines are fits to <b>Equation 2</b> . Arbitrary vertical shifts $a$ were applied to improve the clarity of presentation. (b) Activation energy ( $E_a$ , filled symbols) and Arrhenius prefactor ( $\tau_0$ , open symbols) are strongly correlated with Brønsted acidity ( $pK_a$ ). Error bars are taken as the standard deviations determined from <b>Figure 23</b> . ....	34
<b>Figure 20.</b> Comparison of moduli across different samples. The relative standard deviation is 21% for storage moduli at a frequency of 1 Hz. ....	37
<b>Figure 21.</b> Effect of catalyst concentration of Arrhenius parameters for two MSA- containing samples.....	38
<b>Figure 22.</b> MSA polyester networks show excellent recyclability as expected for dynamic networks that undergo associative exchange. ....	39
<b>Figure 23.</b> Four samples of MSA demonstrate reasonable reproducibility in the temperature range studied. Activation energies agree within 4% relative standard error ( $49 \pm 2$ kJ $\text{mol}^{-1}$ ). ....	40
<b>Figure 24.</b> The temperature-dependent relaxation behavior of MSA and BSA samples exhibits a cross-over point at 52 °C (dashed line). This observation explains their	

similar characteristic relaxation time at the temperatures tested despite different Arrhenius parameters.....42

**Figure 25.** Reaction scheme for generating dynamic bottlebrush polymer networks that undergo associative bond exchange. (i) Ring-opening polymerization of 4-methylcaprolactone from a norbornene–alcohol initiator, catalyzed by Sn(Oct)<sub>2</sub> and run in the bulk at 110 °C until reaching approximately 80% conversion. (ii) Ring-opening metathesis polymerization of P4MCL macromonomer catalyzed by the Grubbs 3rd generation catalyst; 10 wt% in DCM at 25 °C for 1 h. (iii) Cross-linking bottlebrush polymers by reaction with a bis-lactone as catalyzed by Sn(Oct)<sub>2</sub> at 180 °C for 5 h. Yellow highlighting depicts the cross-linker before and after reaction.....53

**Figure 26.** (a) Normalized size-exclusion chromatography (SEC) traces (differential refractive index detection, dRI) of the macromonomers and bottlebrush polymers studied herein. (b) Summary of bottlebrush characterization data. Absolute molecular weights were determined by SEC equipped with dRI and multiangle light scattering (MALS) detectors using  $dn/dc = 0.071$  .....54

**Figure 27.** a) SEC traces (normalized differential refractive index signal) and b) characterization results from a formulation stability experiment wherein a sample was prepared ( $N_{SC} = 35$ ,  $N_{BB} = 260$ ,  $n_{cl} = 15$ , 0.2 wt% catalyst) and left at room temperature for 5 days. The before and after traces show negligible differences in their molecular weight distribution, indicating adventitious curing at room temperature is not an issue for these materials.....55

**Figure 28.** Normalized curing profiles demonstrate the cross-linking of two bottlebrush polymer 1B formulations with 15 equiv of crosslinker and different catalyst loadings. ....56

**Figure 29.** Stress-relaxation experiments with sample 1A indicate P4MCL bottlebrush networks are dynamic at elevated temperatures. Fits to a stretched exponential decay (**Equation 1**) are represented by dashed white lines.<sup>45,127,159,160</sup> (a) Inverse temperature dependence at constant cross-linker loading ( $n_{cl} = 10$ ). (b) Effect of cross-linker loading at constant temperature (160 °C). (c) Arrhenius relaxation behavior; dashed lines are fits to the Arrhenius equation (**Equation 2**). ....58

**Figure 30.** P4MCL bottlebrush polymer CANs are super-soft with a tunable storage modulus at temperatures ( $T = 25$  °C) below the onset of dynamic exchange. (a) Frequency sweeps of formulations derived from 1B, 2B, 3B, and 4B with  $n_{cl} = 25$  (filled markers: storage modulus; open symbols: loss modulus). A linear P4MCL network is included for comparison. (b) Frequency sweeps of formulations generated from bottlebrush polymer 2B ( $N_{BB} = 180$ ) with varying  $n_{cl}$ . (c) Linear scaling of the low-frequency plateau modulus ( $G_{x,bottlebrush}$ ) with  $\rho n_{cl}/M_n$ . ....60

**Figure 31.** Uniaxial tensile experiments demonstrate the self-healing and extensibility of P4MCL bottlebrush polymer CANs (sample 2B: NSC = 33,  $N_{BB} = 180$ ;  $n_{cl} = 15$ ). The toughness recovered to >85% after three cycles. ....63

**Figure 32.** Synthesis of NbOH initiator .....66

**Figure 33.** Fourier-transformed infrared (FTIR) spectrum of NbOH initiator .....67

**Figure 34.** Fourier-transformed infrared (FTIR) spectrum of 4mCL monomer .....67

**Figure 35.** Fourier-transform infrared spectrum of BD crosslinker. ....68

<b>Figure 36.</b> Synthesis of 4mCL macromonomer.....	68
<b>Figure 37.</b> Fourier-transform infrared of p4MCL macromonomer .....	69
<b>Figure 38.</b> Synthesis of 4mCL bottlebrush polymer.....	70
<b>Figure 39.</b> Fourier-transform infrared of 4mCL bottlebrush polymer.....	71
<b>Figure 40.</b> Synthesis of bottlebrush polymer network.....	72
<b>Figure 41.</b> Experimental setup for Fourier-transform infrared (FTIR) spectral analysis of P4MCL bottlebrush polymer networks. The piston was hand-tightened to form good contact, also demonstrating the compliance of dynamic bottlebrush polymer networks. ....	73
<b>Figure 42.</b> Fourier-transform infrared (FTIR) spectrum of P4MCL bottlebrush polymer networks formed from bottlebrush polymers 1B, 2B, 3B, and 4B, and cured with $n_{cl} = 25$ . ....	73
<b>Figure 43.</b> Fourier-transform infrared (FTIR) spectrum of P4MCL bottlebrush polymer networks formed from bottlebrush polymer 2B and cured with $n_{cl} = 25, 35,$ and $45$ . ....	74
<b>Figure 44.</b> Frequency sweeps of 1A-5, 1A-10, and 1A-25, demonstrating the tunability of bottlebrush polymer properties through formulation. Filled circles are storage modulus values and open circles are loss modulus values. ....	74
<b>Figure 45.</b> Raw stress-relaxation data for sample 1A-25 with superimposed fits. ....	75
<b>Figure 46.</b> Raw stress-relaxation data for sample 1A-10 with superimposed fits. ....	76
<b>Figure 47.</b> Raw stress-relaxation data for sample 1A-5 with superimposed fits. ....	77
<b>Figure 48.</b> a) Two step synthesis of a bis-lactone crosslinker with improved solubility. <i>i)</i> Cyclohexanone (2.5 eq.) was added to a solution of dithiol in dichloromethane with a catalytic amount of triethylamine (0.1 eq.) and stirred overnight at room temperature;	

ii) *meta*-Chloroperoxybenzoic acid (9 eq.) was added to a 0 °C solution of the precursor in dichloromethane and stirred overnight. b) Networks formation proceeds in a single step: iii) At room temperature, Sn(Oct)<sub>2</sub> (1.5 wt% relative to the reaction mass) was added to the reaction solution and heated to 180 °C for 20 minutes. ....81

**Figure 49.** Mechanical data showing a) the curing traces of various bottlebrush polymer resins (truncated to highlight region of interest, for full trace refer to **Figure 55**) and b) frequency-dependent modulus data capturing the room temperature rubbery plateau. 83

**Figure 50.** Frequency sweeps of the samples from **Figure 51** before curing. Samples with CNT-filler are elastic. ....85

**Figure 51.** a) Composite bottlebrush polymer samples rapidly cure at 180 °C. b) Room temperature frequency sweeps after curing show a rubbery plateau. ....86

**Figure 52.** a) Optical images of two thin films with 0.25 wt% and 0.5 wt% CNTs. b) Optical microscopy (1000× zoom) showing even CNT dispersion in the bottlebrush polymer matrix. ....87

**Figure 53.** Conductivity of the 0.25 and 0.50 wt% CNT composite samples measured in the frequency range of 0.1 Hz to 10 kHz. ....88

**Figure 54.** Bode plots of the 0.25 and 0.50 wt% CNT composite samples showing ideal resistor behavior in the range of 0.1 Hz to 10 kHz. ....89

**Figure 55.** Self-healing study of a 0.25 wt% CNT composite sample with 0.5 wt% crosslinker. a) Dynamic mechanical thermal analysis showing partial recovery of the tensile modulus (measured on cooling ramp at 5 °C/min). b) Optical microscopy of pristine and healed samples; the scale bars are 1 mm. c) Pictures taken through the healing procedure. ....90

**Figure 56.** SEC trace of macromonomer ( $M_n = 2.1$  kDa,  $M_w = 2.3$  kDa,  $\mathcal{D} = 1.1$ ) and bottlebrush polymer ( $M_n = 170$  kDa,  $M_w = 190$  kDa,  $\mathcal{D} = 1.1$ ). .....94

**Figure 57.** SEC trace of macromonomer ( $M_n = 1.7$  kDa,  $M_w = 1.9$  kDa,  $\mathcal{D} = 1.1$ ) and bottlebrush polymer ( $M_n = 150$  kDa,  $M_w = 170$  kDa,  $\mathcal{D} = 1.1$ ). .....95

**Figure 57.** Non-truncated curing traces for unfilled samples. ....97

**Figure 58.** Curing of a 0.25 wt% CNT bottlebrush polymer mixture in the absence of catalyst or crosslinker shows secondary curing events over a long time-scale. 100

## LIST OF TABLES

<b>Table 1.</b> Demonstrated exchange chemistries with corresponding chemical structures of the reaction and references to literature sources.....	10
<b>Table 2.</b> Fit parameters for stress relaxation of TCA-catalyzed sample.....	28
<b>Table 3.</b> Fit parameters for stress relaxation of MSA-catalyzed sample .....	28
<b>Table 4.</b> Fit parameters for stress relaxation of BSA-catalyzed sample.....	29
<b>Table 5.</b> Fit parameters for stress relaxation of HTFSI-catalyzed sample.....	30
<b>Table 6.</b> Fit parameters for stress relaxation of Triflic-catalyzed sample.....	31
<b>Table 7.</b> Characteristic relaxation times, both empirically determined and those calculated from the fit model, with their respective relative residual errors. ....	32
<b>Table 8.</b> Physical properties of acid catalysts included in study.....	43
<b>Table 9.</b> Measured glass transition temperatures for select polyester network samples.	44
<b>Table 10.</b> Gel-fraction and moduli of networks derived from the largest $N_{BB}$ polymer (4B) .....	59
<b>Table 11.</b> Fit parameters for 1A-25.....	75
<b>Table 12.</b> Fit parameters for 1A-10.....	76
<b>Table 13.</b> Fit parameters for 1A-10.....	77
<b>Table 14.</b> Summary of P4MCL–CNT composite properties. ....	89
<b>Table 15.</b> Formulation details of the sample with 0.5 wt% crosslinker from <b>Figure 49.</b>	98
<b>Table 16.</b> Formulation details of the sample with 1 wt% crosslinker from <b>Figure 49.</b>	98
<b>Table 17.</b> Formulation details of the sample with 2 wt% crosslinker from <b>Figure 49.</b>	98
<b>Table 18.</b> Formulation details of the sample with 3 wt% crosslinker from <b>Figure 49.</b>	99



**Table 19.** Formulation details of the 0 wt% CNT composite sample from **Figure 50.** 99

**Table 20.** Formulation details of the 0.25 wt% CNT composite sample from **Figure 50.** 99

**Table 21.** Formulation details of the 0.5 wt% CNT composite sample from **Figure 50.** 99

## **Chapter I. Introduction to dynamic polymer networks**

### **A brief history of crosslinked networks**

Materials science developments are often driven by the demands of technology and manufacturing. One insightful example of such is in the development of rubber. At the turn of the 20<sup>th</sup> century, a chemist—Charles Goodyear—discovered that natural latex from trees could transform from a sticky, viscous material to an elastic and tough solid upon heating in the presence of sulfur. Prior to his discovery, latex and rubber had experienced a tumultuous start: though initially hailed as revolutionary, these materials were found to be susceptible to cracking in the cold and melting in the heat, rendering them inadequate for many product applications. However, when subjected to Goodyear’s sulfur-based process, these products became durable over a wider range of temperatures thus triggering a boom in interest. This fortuitously coincided with the development of the automobile, where rubber played an integral role as the material foundation for tires. Goodyear named his solidification process “vulcanization”, after Vulcan—the Greek god of fire and forge. In the time since, this idea of transforming viscous polymers into solid materials has enabled a wide range of critically important technologies, touching almost all areas of the industrial sector.

To contextualize this discussion in a molecular framework, it is important to understand what is meant by “polymers.” Polymers, or macromolecules, are entities composed entirely of covalent bonds with many repeating structural units called monomers. These compounds permeate our existence in significant ways: our very DNA is a polymer composed of monomer units of nucleotides. Another important division is

the polymers found in our natural world (natural polymers) versus those made by conscious design (synthetic polymers). During the time of Goodyear's work, rubber was sourced exclusively from nature (typically rubber trees), but modern advancements have led to the majority of today's rubber being produced synthetically.

Bulk polymeric materials can be divided into one of two categories: thermoplastics and thermosets. The first is simply polymers whose intermolecular forces cause them to solidify. The defining feature of thermoplastics is that above a certain temperature, they become a viscous liquid which can then reform a solid upon cooling. The reason for this transformation is that only intermolecular forces are present to hold the polymers together such that heating provides enough energy to disassociate the polymers, as shown in **Figure 1a**. This feature has allowed for a plethora of products to be made cheaply and easily by simple heating and cooling. However, similar to the materials made before Goodyear's discovery, thermoplastics are incompatible with any application requiring elevated temperatures and typically have poor mechanical performance and chemical resistance. Conversely, thermosets are polymeric materials whose defining characteristic is that upon heating (or chemical curing) form solids which are then incapable of flowing. The reason for the irreversible change is the formation of "crosslinks" (strong covalent bonds) that transform the individual polymers into an interconnected polymer network, as shown in **Figure 1b**. These crosslinked materials typically have far superior mechanical properties and solvent resistance as well as a much wider range of compatible temperatures, making them ideal for various applications requiring more robust materials. Bakelite, a fully synthetic thermosetting material developed by Leo Baekeland in 1909, saw enormous economic success and was used in everything from toys to electrical components.<sup>1</sup> Since

then, synthetic thermosets have played an integral role in various industrial and manufacturing applications, but have one unfortunate drawback: their inability to be reprocessed.

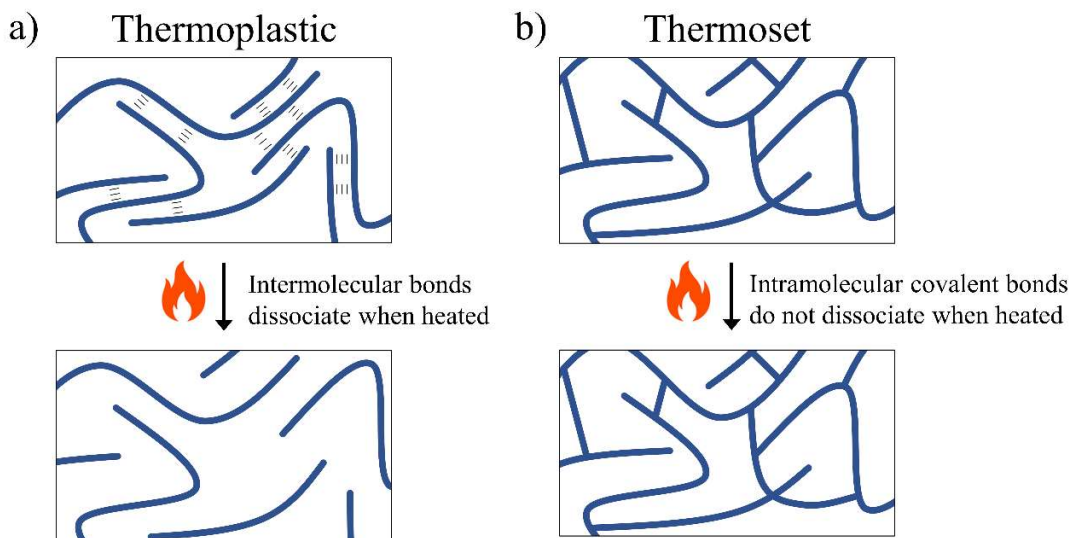


**Figure 1.** Differences in the structural connectivity of a) thermoplastics and b) thermosets result in distinct thermal properties.

Unsustainable practices in manufacturing materials that cannot be reprocessed have risen to the forefront of modern issues plaguing our world, with plastics and rubbers being major contributors. While thermoplastics can be efficiently recycled with thermal treatments, difficulties in developing an infrastructure to support a circular economy has resulted in single-use plastics often ending up in landfills or polluting our oceans. Conversely, thermosets are entirely incapable of being reprocessed due to their chemical nature as previously discussed. Instead, the usual end-of-life outcomes for these materials include being ground up as filler for composites, burned for energy, or consigned to

landfills. Just as Goodyear's development of crosslinking polymers into thermosets resulted in a substantial advancement for polymer-based technologies, the next advancement of crosslinking technologies is underway with the development of dynamically crosslinked materials.

### **Dynamic networks from dynamic bonds**

Dynamic covalent bonds are robust, covalent bonds that under certain stimuli can undergo exchange reactions resulting in a dynamic equilibrium (in which the two species are interconverting at a steady state). Strategic incorporation of these dynamic bonds into a polymer network should therefore exhibit the desirable properties of a thermoset under certain conditions, but under appropriate stimuli allow for reprocessing (similar to a thermoplastic). The realization and implementation of these ideas has developed gradually (and somewhat serendipitously) in the century following Goodyear's initial discovery.

Beginning in the late 1940s, Arthur Tobolsky and coworkers noted that at elevated temperatures, some elastomers were capable of relaxing stress *in situ*, even in the absence of catalysts or apparent reactive components.<sup>2-5</sup> In those early studies, the dynamic bonds were typically introduced incidentally to the curing chemistry (i.e., through the crosslinking agents<sup>2,3</sup> or bonds from the polymerization itself<sup>4,5</sup>), and limitations in characterization techniques available at the time made it difficult to ascertain the exact nature of the bond exchange. However, through clever experiment design and careful investigation, researchers correctly hypothesized that the dynamic nature of the networks could be attributed to the inclusion of the dynamic bonds, claiming "the stress relaxation process may consist in the breaking and reformation of these interchain bonds."<sup>2</sup>

Specifically, the bonds identified as being potentially dynamic (and later confirmed as such) were disulfides,<sup>2,3</sup> urethanes,<sup>4</sup> and siloxanes.<sup>5,6</sup> In initial investigations, this idea of stress relaxation at elevated temperatures was seen as an interesting, but ultimately detrimental, phenomenon in the elastomers studied.<sup>7</sup>

It wasn't until 1969 that James Craven at Dupont had the idea to exploit this phenomenon in thermosetting materials to generate robust and reprocessable polymer networks.<sup>8</sup> Instead of using the previously described reactions, he chose to employ Diels–Alder chemistry that had previously been shown (in 1928 by Otto Diels and Kurt Alder)<sup>9</sup> to dissociate at elevated temperatures and subsequently reform when cooled. In his original patent, Craven describes the use of these Diels–Alder crosslinks between linear polymers to allow for reprocessing via thermal treatments; in 2002 Wudl and coworker further developed this idea by generating networks where the Diels–Alder bonds were incorporated throughout the polymer network and not just at the crosslinking points.<sup>10</sup> The result of this development was a robust thermoset that upon heating to 120 °C had 30% of its mass revert to the liquid monomer precursor and then, upon cooling, reform the thermoset. By having such a dramatic change in network connectivity, this material could be readily remolded and healed, a substantially different behavior than the slowly relaxing elastomers previously described by Tobolsky. Although limited characterization was done on the material properties before and after the thermal treatment, this discovery was a notable advancement for crosslinking technologies and motivated a huge amount of research in the two decades since.

## Mechanisms of dynamic polymer networks

As the study of dynamic polymer networks has expanded, nuances have arisen in the classification and understanding of these systems. Early work from Wudl<sup>10</sup> used Diels–Alder bonds to induce dynamic bond exchange in crosslinked networks. In this case, the dynamic bond of interest could be stimulated to disassociate and—upon removal of the stimulus—would reform the original bond. This loss of connectivity results in a dramatic transformation of the material properties (namely, viscosity) as the network is transiently un-crosslinked. Systems that utilize chemistries with this mechanism are said to have a “dissociative” bond exchange, as shown in **Figure 2a**.

Leibler<sup>11</sup> and Bowman<sup>12</sup> took this concept a step further by introducing a dynamic bond that would exchange directly by reaction with other bonds without disassociation. This alternative exchange mechanism was hypothesized to improve the system design by maintaining the crosslink density throughout the transformation and became known as an “associative” bond exchange. Leibler demonstrated this associative exchange with transesterification, wherein a hydroxy group reacts with an ester to generate an unstable tetrahedral intermediate (with all the reaction components being covalently bound) which then collapses to reform an alcohol and an ester. The collapse of the intermediate either results in the reformation of the original reactive partners (no change) or swaps the two reactive groups to generate a new ester and alcohol pair (dynamic bond exchange). This process is shown in Error! Reference source not found.**b**. When the latter case occurs in a thermosetting network, the rearrangement of crosslinking points and connectivity enables the material to self-heal and be reprocessed—all while maintaining a constant crosslinking density.

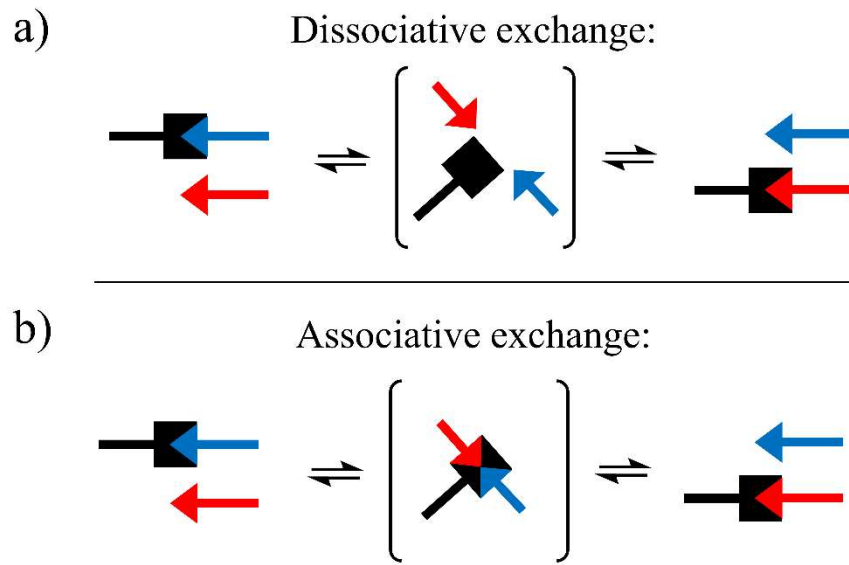


**Figure 2.** The different categories of dynamic bond exchange via a) a dissociative exchange reaction where the connectivity is transiently lost and b) an associative exchange reaction where the connectivity is preserved during the transformation.

Leibler and coworker found that these materials were able to relax stress efficiently at elevated temperatures and that the rate of relaxation increased proportionally to temperature. In measuring the zero-shear viscosity at various temperatures, they also found that the materials showed an unusual Arrhenius-like dependence on inverse temperature. Most thermoplastics experience a sharp decrease in viscosity above their glass transition temperature (as shown in Error! Reference source not found.), while thermosets show very little dependence of viscosity on temperature. In contrast, the material Leibler and coworker developed showed a very broad viscosity range that was accessible via variations in temperature. It was noted that the viscosity behavior was very similar to molten SiO<sub>2</sub> (vitreous silica) and that these materials could be considered



“strong organic glass formers,” which led them to coin the term “vitrimers” to describe these dynamic polymer networks with associatively exchanging bonds.<sup>13</sup>

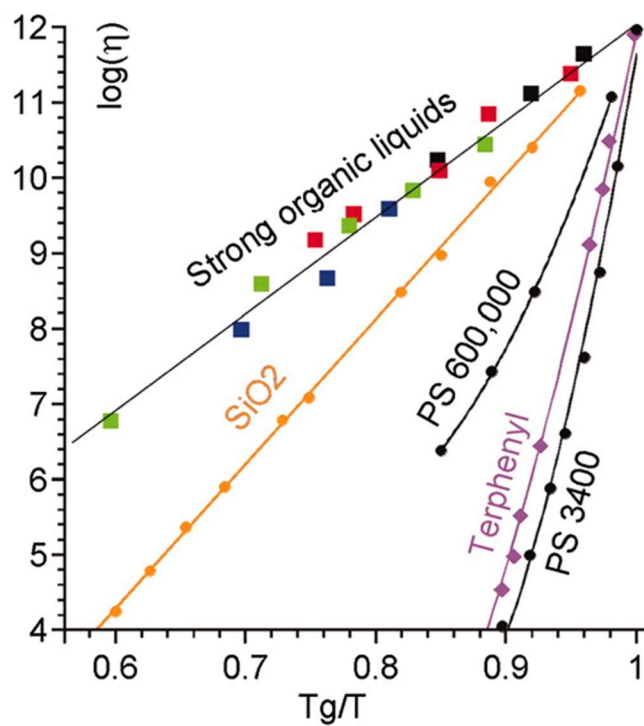


**Figure 3.** Angell fragility plot showing the viscosity dependence on inverse temperature of various materials. From reference <sup>11</sup>, Copyright 2016 AAAS. Reprinted with permission from AAAS.

In Leibler’s seminal 2011 paper, they also set the standard for characterization of these systems (**Figure 4**). Though there exists a plethora of different ways to demonstrate and highlight various aspects of a dynamic materials, a few experiments are key in establishing the nature of the network and generating the metrics necessary for comparison with other work in the literature. The first and most critical component of the investigation should be confirmation of a percolated covalent network. Insufficiently crosslinked networks can exhibit many of the same qualitative behaviors of dynamic polymer networks (such as stress relaxation and “self-healing”) which can potentially lead to improper conclusions

about the nature of the material. The confirmation of insolubility lends itself well to a sol-gel experiment wherein the gel-fraction of the network can be determined, further assessing the extent of crosslinking. Another important experiment is mechanical confirmation of the dynamic nature of the network, usually done through iterative stress relaxation at different temperatures. Evans and coworker recently published an incredibly insightful study on the various methods for quantifying temperature-dependent stress relaxation, highlighting the need for a broad temperature window and sufficiently high temperatures above the glass transition temperature to properly probe the exchange reaction and not network dynamics.<sup>14</sup> The temperature dependence of stress relaxation can then be fit to an Arrhenius function to calculate the activation energy ( $E_a$ ) associated with the relaxation process. This analysis has been particularly standardized and allows for comparison with published precedents. Lastly, a demonstration of the dynamic nature (e.g., self-healing of a damaged sample) is often useful to confirm the molecular dynamic exchange can be translated into macroscopic properties.

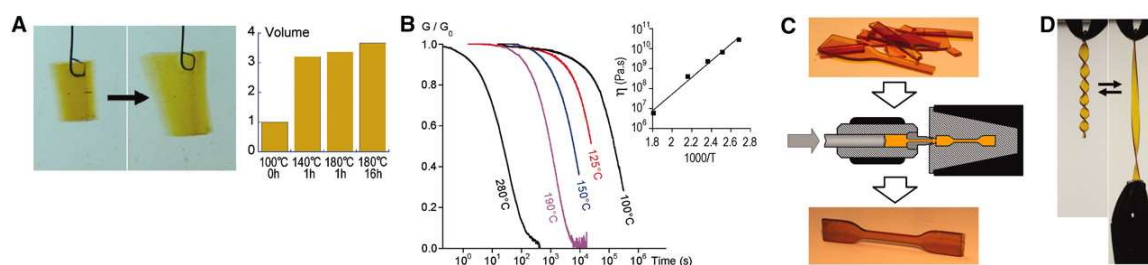


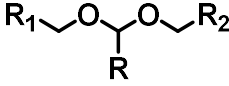
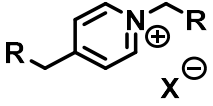
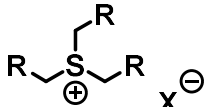
**Figure 4.** The classic suite of experiments as demonstrated by Leibler and coworker for characterizing a dynamically crosslinked network: a) confirmation of an insoluble network, b) characterization of dynamic exchange via mechanical methods (stress relaxation is shown here) and analysis of the temperature dependence of the exchange, and finally demonstrations of either

the c) self-healing of the material or d) demonstration of the reprocessability. From reference 11, Copyright 2016 AAAS. Reprinted with permission from AAAS.

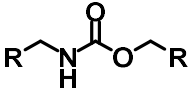
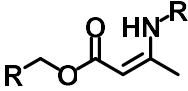
## Development of dynamic bond motifs

In the decades since dynamic polymer networks were identified as a promising new material platform, a wealth of different bond chemistries has been developed and demonstrated, with both associative and dissociative exchange mechanisms. These include acetals,<sup>15</sup> alkylated C–N species,<sup>16,17</sup> alkylated C–S species,<sup>18,19</sup> allyl sulfides,<sup>12,20,21</sup> boronic esters,<sup>22–27</sup> boroxines,<sup>14,26,28</sup> Diels–Alder adducts,<sup>8,10,29–34</sup> disulfides,<sup>3,27,35–38</sup> esters,<sup>39–45</sup> hydrazones,<sup>27,46,47</sup> imines,<sup>47–52</sup> olefins,<sup>53,54</sup> oxime-esters,<sup>55</sup> siloxanes,<sup>6,56,57</sup> silyl ethers,<sup>58–60</sup> thioester anhydrides,<sup>61–63</sup> thiourethanes,<sup>64–66</sup> urethanes,<sup>67–71</sup> and more. The structures and catalysts corresponding to these dynamic bonds are shown in **Table 1**.

**Table 1.** Demonstrated exchange chemistries with corresponding chemical structures of the reaction and references to literature sources.

Dynamic bond	Representative structure	Mechanism	Catalysts	Refs.
Acetals		Associative	-Catalyst-free	15
Alkylated C–N species		Dissociative	-Catalyst-free	16,17
Alkylated C–S species		Dissociative	-Catalyst-free	18,19

Allyl sulfides		Associative	- Radical generators	12,20,21
Boronic esters		Associative, dissociative	-Catalyst-free	22–27
Boroxines		Associative, dissociative	-Catalyst-free	14,26,28
Diels–Alder adducts		Dissociative	-Catalyst-free	8,10,29–34
Disulfides		Dissociative	-Catalyst-free	3,27,35–38
Esters		Associative	-Lewis Acids -Brønsted acids -Brønsted bases	13,40–43,45,72
Hydrazones		Associative, dissociative	-Catalyst-free -Brønsted acids	27,46,47
Imines		Associative, dissociative	-Catalyst-free	48–52
Olefins		Associative	-Grubbs catalyst	53,54
Oxime-esters		Associative	-Catalyst-free	55
Siloxanes		Associative	-Brønsted acids -Brønsted bases	6,56,57
Silyl ethers		Associative	-Catalyst-free -Lewis Acids -Brønsted acids	58–60
Thioester anhydrides		Associative, dissociative	-Brønsted bases	61–63
Thio-urethanes		Associative, dissociative	-Catalyst-free -Brønsted bases	64–66

Urethanes		Associative, dissociative	-Catalyst-free -Lewis acids -Brønsted acids -Brønsted bases	67–71
Vinylogous urethanes		Associative, dissociative	-Catalyst-free -Lewis acids -Brønsted acids	73–76

Recently, the advantage of associative over dissociative exchange has been called into question as they often show indistinguishable mechanical properties, but the importance of understanding the exchange mechanism for proper design of dynamic systems is widely acknowledged.<sup>77</sup> The emphasis in early research direction in this field was on the discovery and implementation of new dynamic chemistries so as to widen the scope of the polymer chemist’s “toolbox.” Special emphasis was placed on catalyst-free chemistries as their performance would be least affected by solvent exposure and would be least likely to leech harmful chemicals (such as the potent acids/bases commonly used to promote bond exchange). With ready access to a wealth of dynamic bond motifs, research emphasis has shifted to the application of these materials in addressing engineering problems beyond self-healing and reprocessable thermosets.

### **Dynamic polymer networks for advanced applications**

Various industrial and manufacturing processes would benefit from the incorporation of dynamic polymer network concepts. The ability to repair a thermosetting material is a clear advantage and has been well-explored, but the next phase of development seems to be at the interface of other technologies, for example composites with advanced function, additive manufacturing, and liquid crystal actuators. Although these examples represent

only a few of the technologies impacted by the incorporation of dynamic bonds, they highlight the great potential for innovation in a wide range of areas.

Composite materials are polymeric solids with heterogenous components (“filler”) dispersed throughout. Compared to the original polymer material, composites typically have far superior mechanical and thermal properties and, depending on the type of filler used, can have others like conductivity as well.<sup>78</sup> Some filler materials (like carbon fibers) give particularly impressive mechanical benefits, but are cost-prohibitive for many uses.<sup>79</sup> Currently, there are various demonstrations of the use of dynamic polymer networks being used in conjunction with these fillers to allow for complete recycling and recovery, which is expected to significantly impact their lifetime and cost.<sup>48,80-82</sup> Beyond the recovery of filler, the incorporation of dynamic bonds also allows for functionalities that conventional thermosetting composites cannot achieve, such as repairing of damage<sup>83-85</sup> and welding of multiple parts into more complex structures.<sup>86,87</sup> Some filler materials (ex. silica nanoparticles) can also be designed with specific surface functionality, enabling the direct reaction between the matrix and the filler which has been shown to improve the mechanical and dynamic properties of resulting composites.<sup>85,86,88</sup> Given the industrial interest in these materials, it is clear they will continue to be an important thrust in the investigation of dynamic polymer networks.

Additive manufacturing has traditionally been used to generate thermoplastic parts when extrusion/deposition methods are used and thermosets when light-based printing methods are used, where each has its own drawbacks intrinsic to these fundamental differences in structure.<sup>89</sup> The strategic incorporation of dynamic bonds allows for materials that exhibit the stability of thermosetting parts with the reprocessability of

thermoplastic parts.<sup>90-92</sup> This concept of printing dynamic networks has been extended to hydrogels as well,<sup>25,93,94</sup> aided by their proclivity towards shear-thinning and motivated by evidence that the biomimetic ability to relax stress makes them more viable materials for cell cultures.<sup>23,95,96</sup> Future work in this area could explore the use of multiple orthogonal dynamic bond motifs to imbue a more granular control of relaxation timescales to balance printability with functional utility of the parts. Similarly, an important future direction for this area would be the facile incorporation of dynamic moieties in commercially available printing resins to minimize re-optimization of existing systems, interface more closely with industrial needs, and take advantage of already available resources.

Another area that has benefited enormously from the introduction of dynamic bonds is liquid crystal polymer actuators.<sup>97,98</sup> Typical liquid crystal actuators work by crosslinking polymers such that liquid crystal moieties (mesogens) are embedded in the network. When these materials are heated, the mesogens undergo a phase change from an ordered to a disordered state that results in macroscopic motion.<sup>97</sup> Due to conventional crosslinking chemistry, these materials are typically “cast” in a particular configuration after which they cannot be further altered. Recent work has enabled incredible advancement of these materials by crosslinking with dynamic bonds which allows for the network to be recycled and re-cast between various configurations.<sup>29,37,56</sup> Beyond reprogramming the actuation behavior, researchers have taken advantage of the dynamic nature of these materials in other clever ways. One example of such is the “welding” of multiple actuators together to create objects with complex functions.<sup>38,42,56</sup> Furthermore, these technologies can be employed synergistically to create elegant systems such as a 3D

printable, liquid crystal actuating resin with light-responsive dynamic bonds.<sup>99</sup> This last example highlights an interesting direction in the field: developing non-thermal stimuli for dynamic bonds such that they can be employed orthogonally to thermally responsive chemistries to generate systems with a complex response.

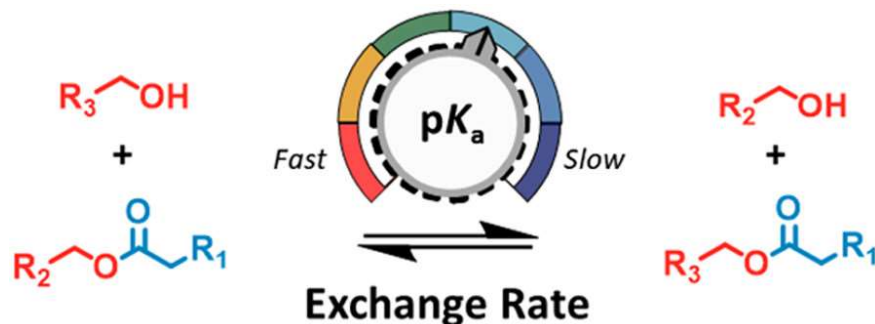
### **Thesis scope**

This thesis describes the study and development of dynamic polymer networks based on polyester transesterification as the dynamic bond motif. Chapter II details a study of the effect of Brønsted acids with varying catalytic activity (as determined from their  $pK_a$  values) on the dynamic behavior of polyester polymer networks. These networks exhibited stress relaxation even at mild temperatures (25 to 75 °C). Interestingly, stronger acid catalysts led to significantly faster stress relaxation, and further analysis revealed a clear correlation between  $pK_a$ , activation energy ( $E_a$ ), and the kinetic prefactor ( $\tau_0$ ). In Chapter III, a bottlebrush polymer architecture is combined with dynamic bond chemistry to generate networks with unique properties. Due to the bottlebrush architecture, these polymer networks exhibit moduli as low as  $\approx 10$  kPa (of order tissue and hydrogels) that can be tuned through formulation design. The tissue-like properties of this system were further demonstrated by damaging and repairing a tensile sample over two cycles, during which it recovered and retained the majority of its toughness. In Chapter IV, the bottlebrush polymer network platform is further developed to incorporate carbon nanotubes. The CNT-filler raises the modulus relative to the unfilled samples, but at loadings of 0.25wt% and 0.5wt% the generated samples were still characteristically soft,



with modulus values of 66 kPa and 140 kPa. The inclusion of the CNTs also results in a significant rise in conductivity, from a largely insulating material to composites with conductivities of  $6e-3 \text{ S/m}^2$  and  $54e-3 \text{ S/m}^2$ . Self-healing studies also indicate that the composites retain the dynamic nature of the original polyester bottlebrush polymer network. Combined, these chapters present several developments in the area of dynamic polyester network systems.

## Chapter II. Brønsted-acid-catalyzed dynamic polyester network



### Abstract

The effect of catalyst strength on polyester–alcohol dynamic covalent exchange was systematically studied using Brønsted acids and a low- $T_g$  poly(4-methylcaprolactone) vitrimer formulation. Relaxation times, activation energies, and Arrhenius prefactors are correlated with  $pK_a$ . Strong protic acids induce facile network relaxation at 25 °C on the order of  $10^4$ – $10^5$  s, significantly faster than Lewis acid alternatives that function only above 100 °C. Activation energies span 49–67 kJ/mol and increase as  $pK_a$  decreases. The opposite trend is observed with the Arrhenius prefactor. We anticipate that the quantitative understanding of Brønsted acid effects disclosed herein will be of utility in future studies that exploit acid-catalyzed dynamic covalent bond exchange.

This chapter was originally published in *ACS Macro Letters*. Reproduced with permission from *ACS Macro Lett.* **2018**, 7, 7, 389–397. Copyright 2018, American Chemical Society.

## Introduction

Dynamic covalent bonds imbue polymer networks with unique properties, for example, self-healing<sup>10</sup> and reconfigurability<sup>100</sup> in response to heat<sup>101</sup> or light.<sup>35,102</sup> The macroscopic behavior of these so-called covalent adaptable networks<sup>103</sup> (CANs) crucially depends on the mechanism of exchange between pendant reactive functional groups and crosslinks.<sup>101</sup> Both dissociative and associative are possible, but only the latter occurs without a transient change in crosslink density, producing thermoset (sometimes referred to as “vitrimers”<sup>11</sup>) that exhibit the unusual combination of solvent resistance and plasticity. Consequently, significant effort has been invested to develop different types of chemistries that undergo associative exchange, culminating in a diverse array of options including esters,<sup>11</sup> allyl sulfides<sup>12</sup>, alkenes,<sup>54</sup> carbonates,<sup>104</sup> (vinylogous<sup>73</sup>) urethanes,<sup>105</sup> boronate esters,<sup>106</sup> and Meldrum’s acid derivatives.<sup>107</sup> Many vitrimers require catalysts to stimulate bond rearrangement, for example Lewis Acids that promote transesterification,<sup>13</sup> Grubbs-type complexes for metathesis,<sup>54</sup> and photo-initiators that generate radicals.<sup>102</sup> Despite the success of these systems, a quantitative connection between catalyst strength and exchange kinetics remains poorly developed; catalyst—when necessary—are often selected merely to establish the efficacy of a new associative dynamic covalent bond. Here, we describe Brønsted acids as a new platform to systematically study the influence of catalyst strength on polyester vitrimer exchange (**Figure 5**) via correlation with the established scale that describes their activity ( $pK_a$ ). The results reveal how relaxation time, activation energies, and Arrhenius prefactors track with Brønsted acidity.

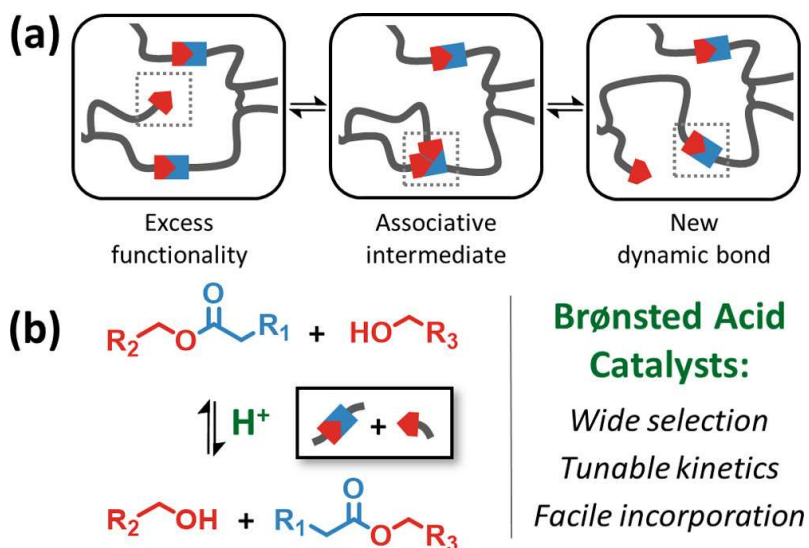


**Figure 5.** Brønsted acids promote exchange reactions in polyesters vitrimers and offer several advantages relative to other catalysts.

CANS comprising main-chain esters and pendant alcohols were selected as a model vitrimer system to study with Brønsted acid catalysts. This choice was motivated by considerations related to both the dynamic covalent bond and catalyst chemistry. Polyesters are a versatile material platform that is synthetically accessible (via condensation<sup>108</sup> or ring-opening<sup>109</sup> polymerization) with a wide range of possible mechanical properties. Leibler<sup>11</sup> and Hillmyer<sup>110</sup> have pioneered the development of polyester vitrimers using Lewis acids to promote transesterification at elevated temperatures ( $\geq 100$  °C), and we reasoned that Brønsted acids might broaden the scope of available relaxation times in addition to facilitating the quantification of catalyst strength effects. Since Brønsted acids catalyze the transesterification of small molecules<sup>111</sup> and vinylogous urethane CANS,<sup>73</sup> it seems reasonable to anticipate they should also trigger polyester vitrimer exchange.

We developed a one-pot synthesis of polyester vitrimers (**Figure 6**) using ring-opening polymerization catalyzed by a range of Brønsted acids (**Figure 7**) to cleanly form the networks of interest. This approach, inspired by recent work,<sup>110</sup> exhibits two notable differences. First, use of the bislactone crosslinker (4,4'-bioxepane-7,7'-dione<sup>112</sup>) enables in situ crosslinking instead of necessitating post-polymerization reaction with diisocyanates.<sup>110</sup> Our networks are thus exclusively composed of ester linkages, which avoids other crosslinker (e.g. urethanes) that can undergo competitive exchange reactions.<sup>105</sup> Second, the monomer 4-methylcaprolactone produces an amorphous polymer with a low glass transition temperature<sup>113</sup> ( $T_g \approx -55\text{ °C}$ ) (**Table 9**) that facilitates the analysis of vitrimer exchange at room temperature. Such rubbery mechanical properties complement the glassy and semicrystalline variants previously reported with poly(lactide)<sup>110</sup> and poly(caprolactone)<sup>114</sup> vitrimers. An additional advantage of this process is that introducing a Brønsted acid catalyst into the network during synthesis avoids any subsequent swelling/deswelling manipulations, which would complicate processing.

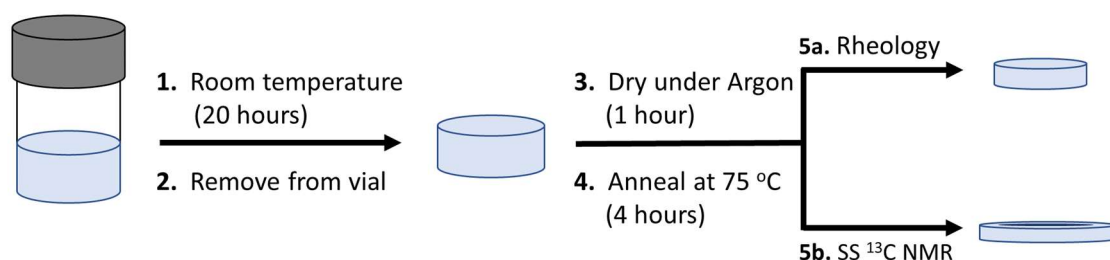


**Figure 6.** Flow process diagram for one-pot preparation of Brønsted-acid-catalyzed polyester vitrimers, from initial small molecule formulation to final solid network sample.

## Discussion

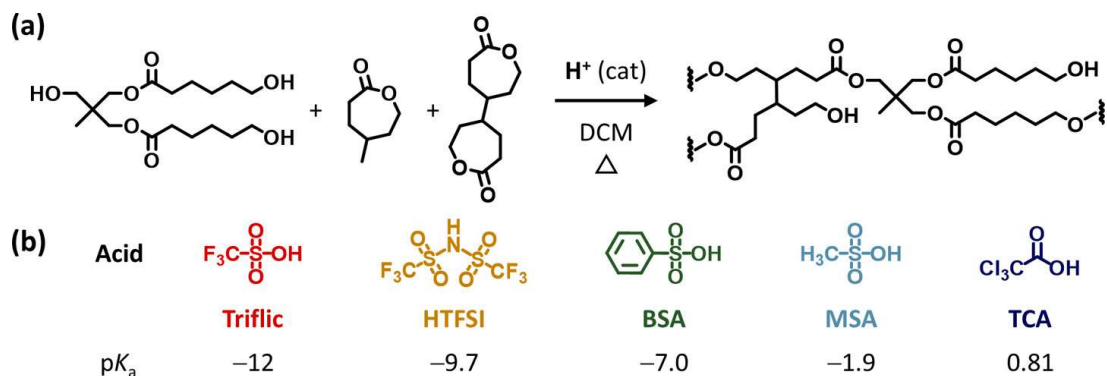


**Figure 7.** (a) Schematic describing the ROP synthesis of low- $T_g$  polyester vitrimers. (b) Brønsted acid catalysts (used to promote ROP and subsequent exchange reactions via transesterification.  $pK_a$  values are referenced in H<sub>2</sub>O.

As shown in **Figure 7b**, we used five Brønsted acid catalysts (trifluoromethanesulfonic acid, “Triflic”; bis(trifluoromethylsulfonyl)imide, “HTFSI”; benzenesulfonic acid, “BSA”; methanesulfonic acid, “MSA”; and trichloroacetic acid, “TCA”) spanning a wide range of  $pK_a$  (from -12 to 0.81) to generate the low  $T_g$  polyester vitrimers. All samples were formulated with a 1:25:3 ratio of tri-functional initiator/monomer/crosslinker to produce reasonably stiff materials (shear moduli ca. 0.5 MPa) with a sufficient density of free chain ends to facilitate the bond exchange. One molar equivalent of the given acids is added to each formulation, which catalyzes both the network formation as well as the subsequent transesterification. Qualitatively, gel time was inversely proportional to acid strength, but to verify near-complete conversion of both the monomer and crosslinker, solid-state  $^{13}\text{C}$  NMR spectra were collected for TCA and MSA—the two weakest acids tested (**Figure 8** to **Figure 11**).

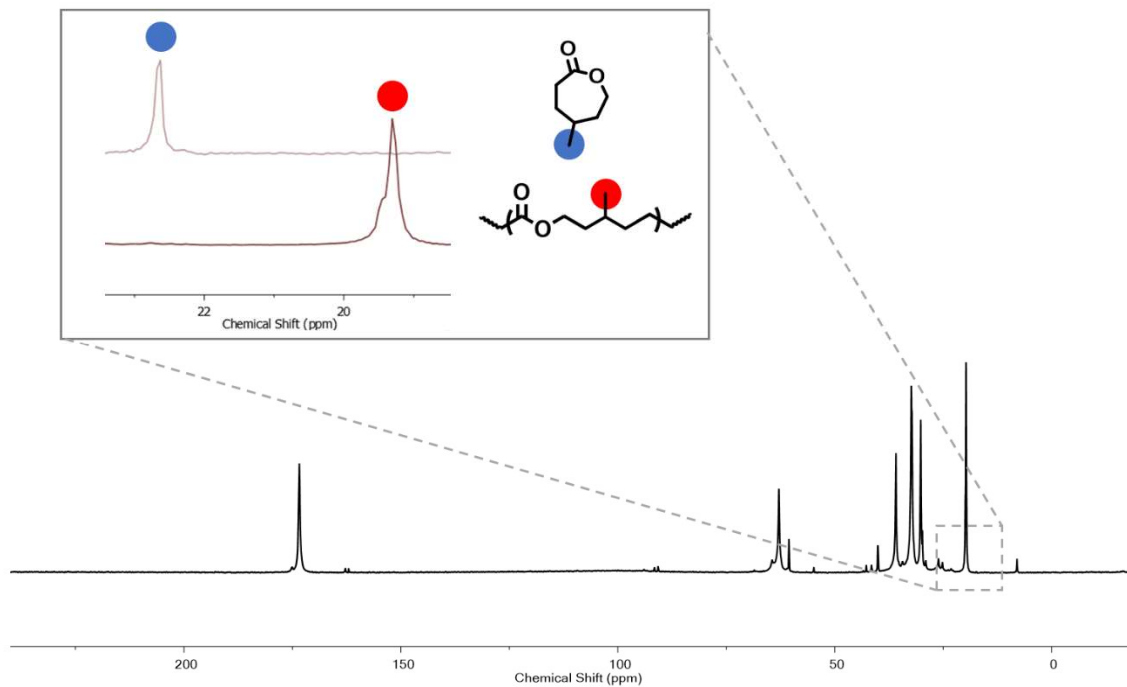


**Figure 8.** Solid state  $^{13}\text{C}$  NMR spectrum of a polyester network containing TCA catalyst. Inset: magnification of the methyl resonance. Near quantitative conversion of the monomer is evidenced by the shift to lower frequency after polymerization.

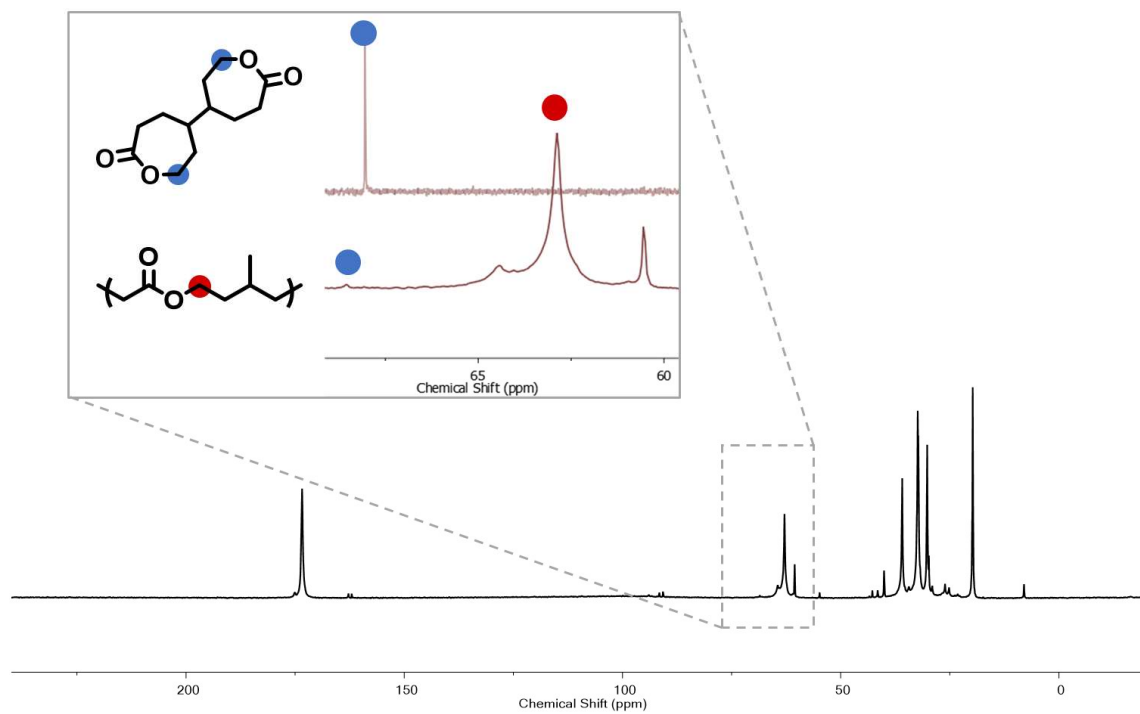


**Figure 9.** The same solid state  $^{13}\text{C}$  NMR spectrum as **Error! Reference source not found.** (containing TCA catalyst) demonstrates  $\approx 96\%$  conversion of the cross-linker.



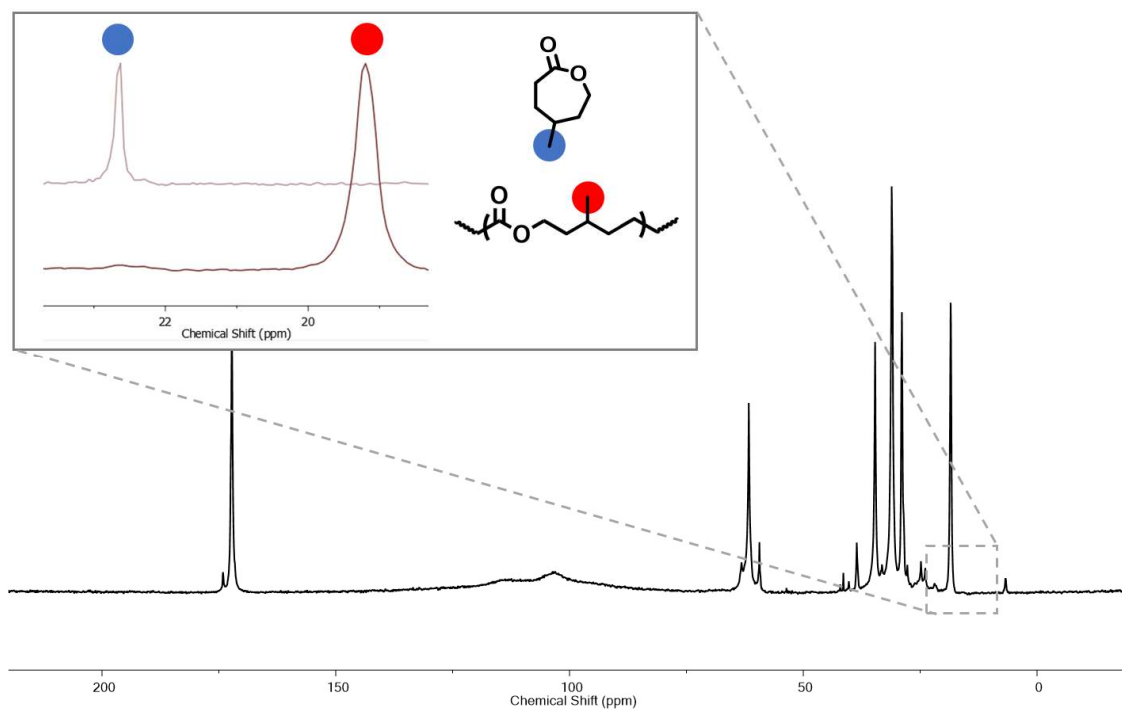


**Figure 10.** Solid state  $^{13}\text{C}$  NMR spectrum of a polyester network containing MSA catalyst. Inset: magnification of the methyl resonance. Near quantitative conversion of the monomer is evidenced by the shift to lower frequency after polymerization.

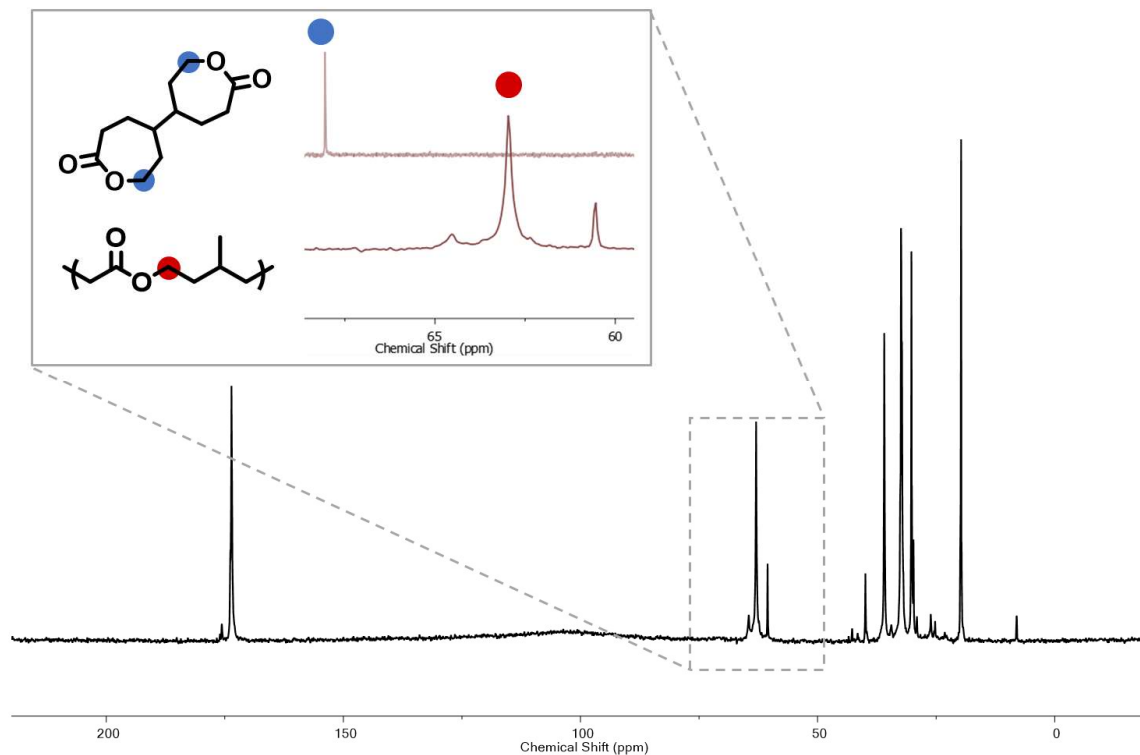


**Figure 11.** The same solid state  $^{13}\text{C}$  NMR spectrum as **Error! Reference source not found.** (containing MSA catalyst) demonstrates quantitative conversion of the cross-linker.

Solvent (dichloromethane) was removed during processing and samples were subsequently analyzed by oscillatory rheology. Step-strain stress relaxation experiments indicate these materials indeed behave as dynamic networks, with a characteristic relaxation time ( $\tau^*$ ) that depends on both temperature (**Figure 12a**) and acid chemistry (**Error! Reference source not found.Figure 12b**). Additional data for each acid sample are provided in the Materials and Methods section. Note that  $\tau^*$  is typically identified as the point in time when the normalized relaxation modulus  $G'(t)/G'(0)$  reaches a value of  $e^{-1}$  ( $\approx 0.37$ ), but these data do not perfectly adhere to a simple exponential decay. Instead, the dashed lines in **Figure 12** depict a fit to the stretched exponential (**Error! Reference source not found.**):

$$\frac{G(t)}{G(0)} = e^{-\left(\frac{t}{\tau^*}\right)^\beta}$$

**Equation 1.** Stretched exponential function used to fit stress relaxation data. Variables include plateau modulus in kPa ( $G$ ), time in seconds ( $t$ ), characteristic relaxation time in seconds ( $\tau^*$ ), and exponential stretch factor ( $\beta$ ).

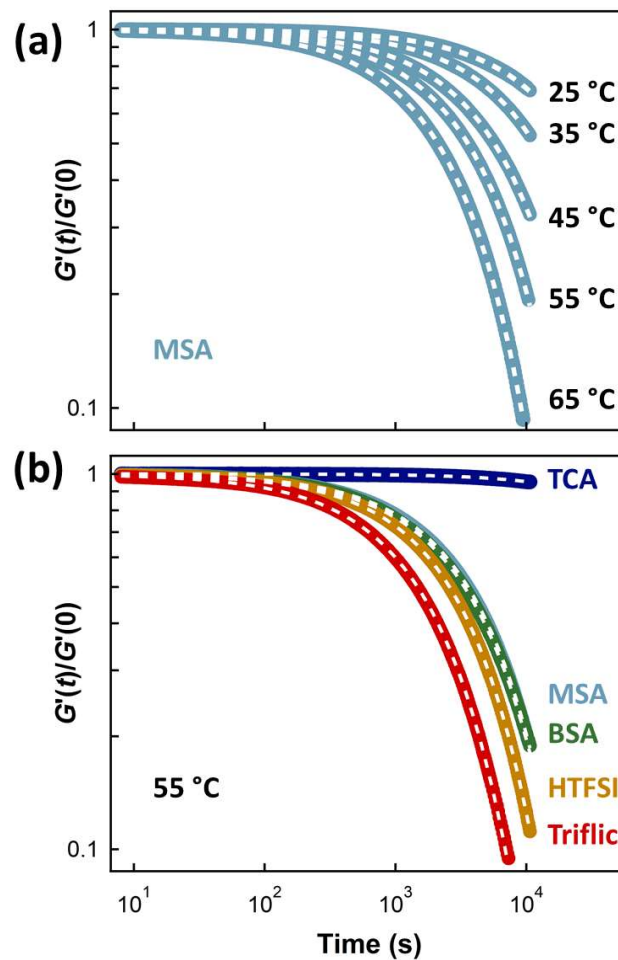


**Figure 12.** Oscillatory rheology step-strain stress relaxation experiments on low- $T_g$  polyester vitrimer formulations containing Brønsted acid catalysts. (a) Methanesulfonic acid measured at

different temperatures. (b) Various acids compared at 55 °C. Dashed lines are fits to **Error! Reference source not found.**

The stretched exponential function is commonly used to model stress–relaxation data<sup>115</sup> when there is a distribution of relaxation rates,<sup>116</sup> which seems reasonable to apply herein since primary alcohols and esters are surrounded by subtly different chemical environments depending on the exact network connectivity. Fits are in excellent agreement at all of the temperatures studied for each acid (25–75 °C, see **Figure 13** to **Figure 17**), and **Error! Reference source not found.** permits the extraction of  $\tau^*$  even for samples that do not fully relax past  $G(t)/G(0) \approx e^{-1}$  (see **Table 2** to **Table 6**). To test the veracity of the model, empirically determined relaxation times were compared with relaxation times extracted from the fits. This comparison shows good agreement between the fitted values and the empirical values, as shown in **Figure 1** and **Table 7**.

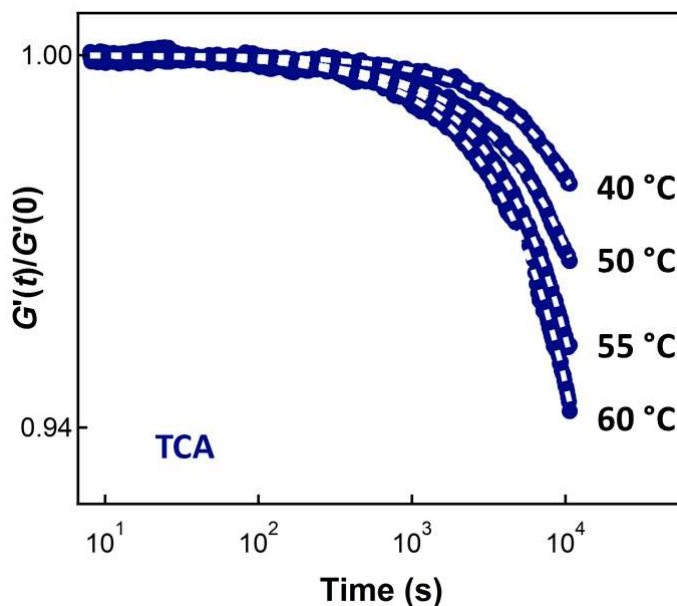


**Figure 13.** Select TCA normalized stress relaxation traces with fit model superimposed. Note the small y-axis range to better visualize the data.

**Table 2.** Fit parameters for stress relaxation of TCA-catalyzed sample.

Run #	$T$ (°C)	$(RT)^{-1}$	$\tau^* \times 10^{-5}$ (s)	$\ln \tau^*$	$\alpha$
1	45	0.378	7.71	13.6	0.79
2	55	0.367	3.00	12.6	0.90
3	60	0.361	2.71	12.5	0.88
4	50	0.372	4.31	13.0	0.91
5	40	0.384	7.09	13.5	0.92

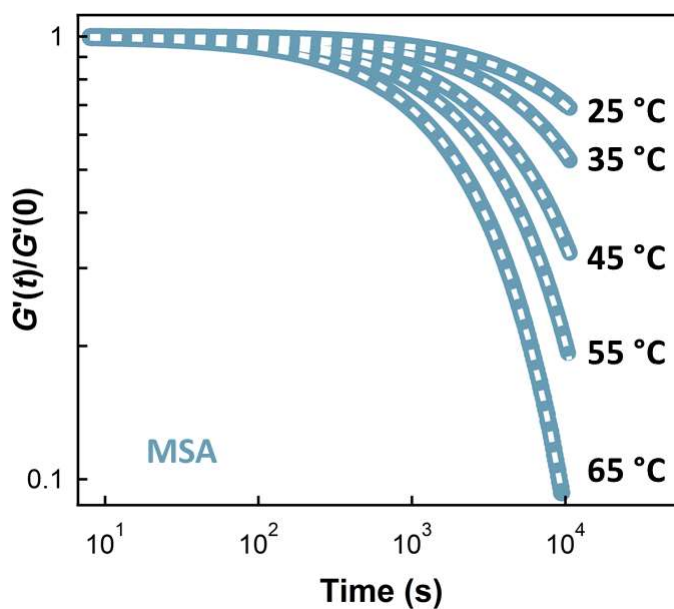


**Figure 14.** Select MSA normalized stress relaxation traces with fit model superimposed. Note the y-axis bounds differ from the previous figure.

**Table 3.** Fit parameters for stress relaxation of MSA-catalyzed sample

Run #	$T$ (°C)	$(RT)^{-1}$	$\tau^* \times 10^{-3}$ (s)	$\ln \tau^*$	$\alpha$
1	45	0.378	9.04	9.11	0.80
2	35	0.391	18.0	9.80	0.82
3	55	0.367	5.62	8.63	0.81

4	25	0.404	34.9	10.5	0.83
5	65	0.356	3.30	8.10	0.82

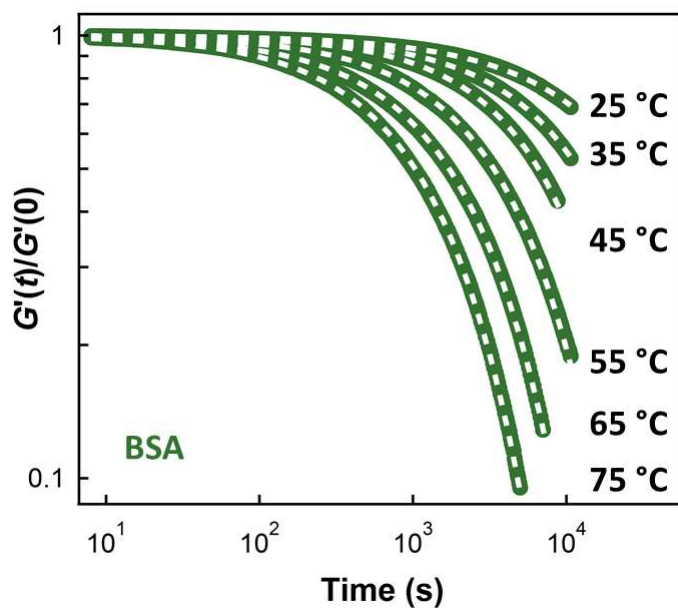


**Figure 15.** Select BSA normalized stress relaxation traces with fit model superimposed. Note the y-axis bounds differ from the previous figure.

**Table 4.** Fit parameters for stress relaxation of BSA-catalyzed sample.

Run #	$T$ (°C)	$(RT)^{-1}$	$\tau^* \times 10^{-3}$ (s)	$\ln \tau^*$	$\alpha$
1	35	0.391	19.3	9.87	0.77
2	55	0.367	5.36	8.59	0.78
3	75	0.346	1.65	7.41	0.78
4	65	0.356	2.77	7.93	0.77
5	25	0.404	43.9	10.7	0.72
6	45	0.378	10.3	9.23	0.83

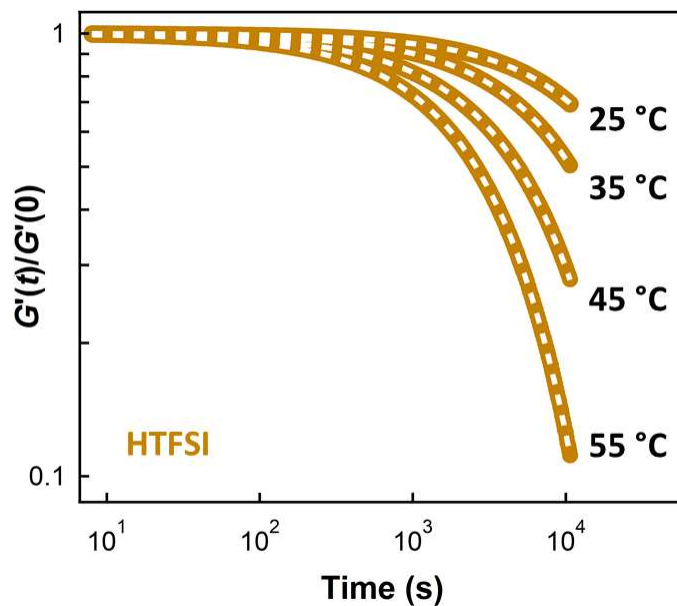


**Figure 16.** Select HTFSI normalized stress relaxation traces with fit model superimposed.

**Table 5.** Fit parameters for stress relaxation of HTFSI-catalyzed sample.

Run #	$T$ (°C)	$(RT)^{-1}$	$\tau^* \times 10^{-3}$ (s)	$\ln \tau^*$	$\alpha$
1	55	0.367	4.07	8.31	0.81
2	45	0.378	7.77	8.96	0.78
3	35	0.391	17.1	9.74	0.80
4	25	0.404	36.7	10.52	0.82

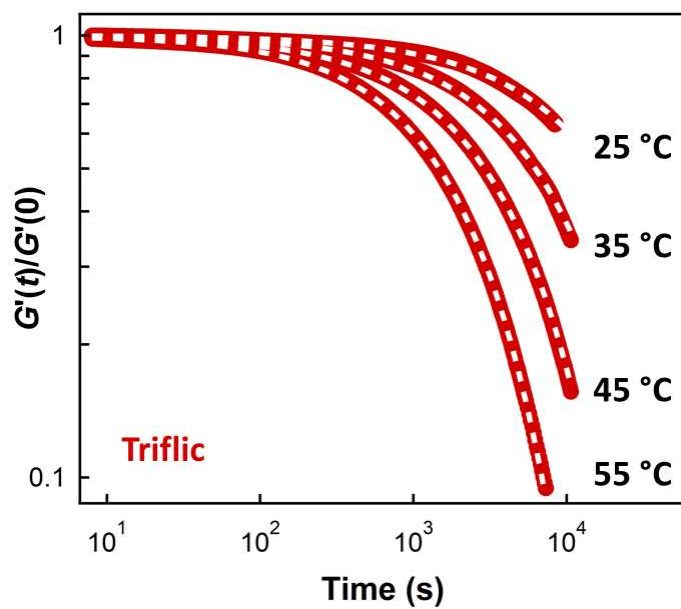


**Figure 17.** Select Triflic normalized stress relaxation traces with fit model superimposed.

**Table 6.** Fit parameters for stress relaxation of Triflic-catalyzed sample.

Run #	$T$ (°C)	$(RT)^{-1}$	$\tau^* \times 10^{-3}$ (s)	$\ln \tau^*$	$\alpha$
1	55	0.367	2.36	7.77	0.78
2	45	0.378	4.77	8.47	0.75
3	35	0.391	10.3	9.24	0.74
4	25	0.404	26.9	10.2	0.72



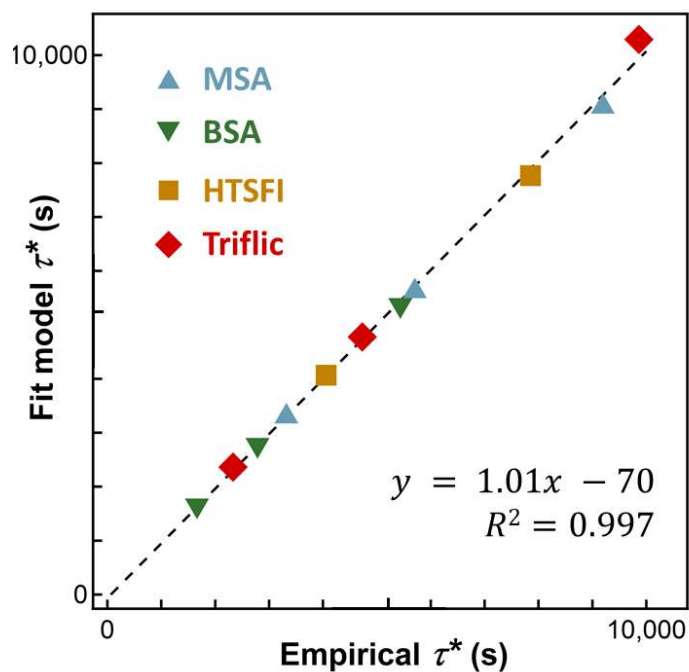


**Figure 18.** Comparison of experimentally determined characteristic relaxation times to those calculated using the fit model shows good agreement.

**Table 7.** Characteristic relaxation times, both empirically determined and those calculated from the fit model, with their respective relative residual errors.

Acid	$T$ (°C)	$\tau^*$		% error
		Experimental (s)	Fit model (s)	
Triflic	35	9,865	10,291	-4.3
	45	4,731	4,774	-0.9
	55	2,332	2,363	-1.3
HTFSI	45	7,852	7,767	1.1
	55	4,060	4,065	-0.1
BSA	55	5,436	5,367	1.3
	65	2,785	2,773	0.4
	75	1,661	1,652	0.5
MSA	45	9,194	9,040	1.7
	55	5,704	5,623	1.4

As shown in **Figure 19a**, the temperature-dependent relaxation time,  $\tau^*(T)$ , determined using **Error! Reference source not found**. shows a strongly linear Arrhenius dependence for all acids tested. In this case, to characterize the activation energy of the relaxation process, an “inverse” Arrhenius equation is used. While typical Arrhenius analysis is done using reaction rates ( $s^{-1}$ ), this analysis instead uses relaxation time (s), hence the “inverse” qualifier. Solid lines are fits to the following equation:

$$\tau^* = \tau_0 e^{\left(\frac{E_a}{RT}\right)}$$

**Equation 2.** Inverse Arrhenius equation. Variables include characteristic relaxation time in seconds ( $\tau^*$ ), kinetic prefactor in seconds ( $\tau_0$ ), activation energy in  $\text{kJ mol}^{-1}$  ( $E_a$ ), universal gas constant in  $\text{kJ K}^{-1} \text{mol}^{-1}$  ( $R$ ), and absolute temperature ( $K$ ).

The linear trend observed for each acid (on a semi-log scale) is a hallmark of associative network rearrangement, one distinctive trait of all vitrimeric materials.<sup>101</sup> Both  $E_a$  and  $\tau_0$  are monotonic functions of Brønsted acid  $\text{p}K_a$  (**Figure 19b**). Stronger acids have higher activation energies, implying the characteristic relaxation time will depend more strongly on temperature than that of weaker analogues.  $\tau_0$  can be interpreted as the characteristic relaxation time at infinite temperature when the exponential asymptotes to 1. We find this trend to be inversely related to that of the activation energy, with weaker acids exhibiting larger  $\tau_0$  values.

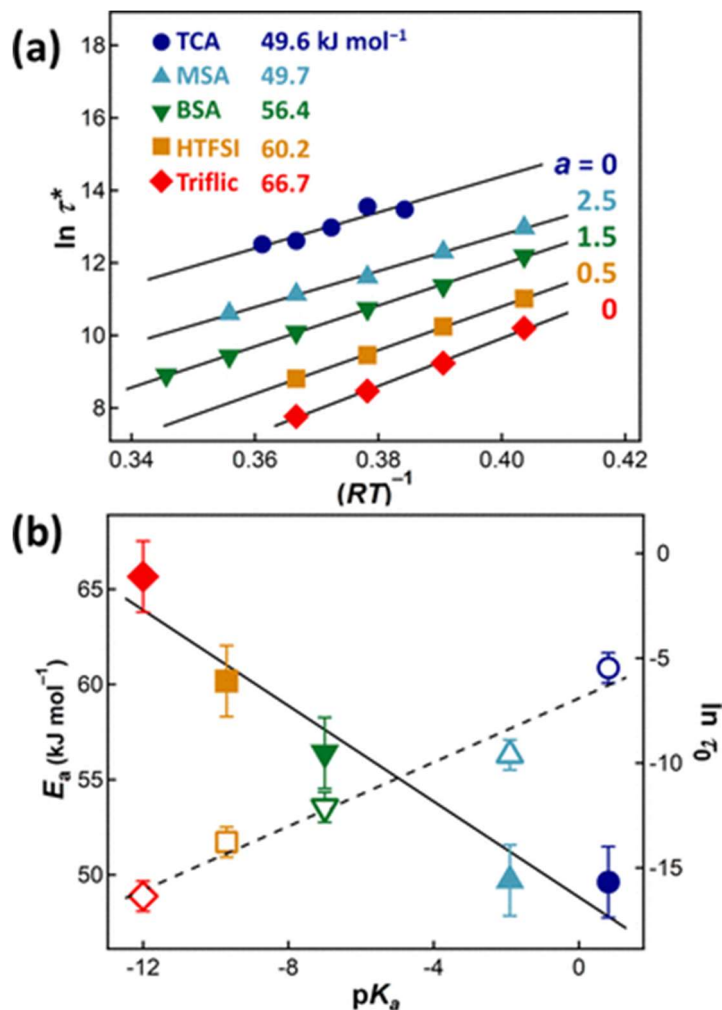


**Figure 19.** (a) Characteristic relaxation time ( $\tau^*$ ) exhibits an Arrhenius temperature dependence for all five Brønsted acids. Solid lines are fits to **Error! Reference source not found.** Arbitrary vertical shifts  $a$  were applied to improve the clarity of presentation. (b) Activation energy ( $E_a$ , filled symbols) and Arrhenius prefactor ( $\tau_0$ , open symbols) are strongly correlated with Brønsted acidity ( $pK_a$ ). Error bars are taken as the standard deviations determined from **Figure 23**.

## Conclusion

Brønsted acid strength is clearly correlated with vitrimer exchange kinetics and thermodynamics as evidenced by **Figure 12** and **Figure 19**. Consequently, relaxation

times and their temperature dependence are tunable over a relatively broad range by the choice of Brønsted acid. While we have selected 5 catalysts that span a fairly disparate  $pK_a$  range, many other options are commercially available and presumably follow similar trends. In contrast, no studies to date have established firm quantitative relationships using more conventional Lewis acid catalysts. Such a correlation is in principle possible, for example using Gutmann-Beckett acceptor numbers that assess Lewis acid strength via reference chemical shifts in nuclear magnetic resonance spectra.<sup>117</sup> Nevertheless, Lewis acid catalysts exhibit important qualitative and quantitative differences with the Brønsted acids described herein. Liu et al. reported a systematic study of different tin-based catalysts and found that activation energy and characteristic relaxation time increase concurrently.<sup>43</sup> Brønsted acids seemingly exhibit the opposite trend; stronger acids relax faster (having a smaller  $\tau^*$  at a given temperature, as seen in **Figure 12**) while having higher activation energies (**Figure 19**) than their weaker analogues. The underlying cause for this behavior is not yet fully understood, but has been recently reported in a similar system; thiol-acrylate derived vitrimers with transesterification as the dynamic motif were catalyzed by Brønsted acids and the trend presented here between  $pK_a$  and  $E_a$  was also observed, further supporting our findings.<sup>41</sup> Moreover, typical Lewis acids tend to activate significant transesterification rates only at elevated temperatures ( $\geq 100$  °C) with essentially no exchange observed at room temperature. Brønsted acids clearly promote transesterification at much lower temperatures (**Figure 12**). Even though the activation energies we measure for Brønsted-acid-catalyzed transesterification (circa  $55 \text{ kJ mol}^{-1}$ ) are roughly half that of Lewis acids ( $100 - 150 \text{ kJ mol}^{-1}$ ),<sup>11,43,110</sup> extrapolation of the Arrhenius fits from **Figure 19a** indicate that select Brønsted-acid-catalyzed systems

would still relax stress at comparable rates to some Lewis acids at elevated temperatures. For example, a triflic acid-containing networks at 140 °C is predicted to have  $\tau^* = 16$  s, in contrast to systems catalyzed by either  $\text{Zn}(\text{acetate})_2$  (which was measured to have  $\tau^* \approx 10^4$  s) or  $\text{Sn}(\text{2-ethylhexanoate})_2$  (measured to have  $\tau^* \approx 10^1$  s). Parallels with Grubbs-catalyzed olefin metathesis vitrimers that exchange at room temperature are also interesting.<sup>54</sup> The activation energy reported herein are again two times smaller, yet the Brønsted acid  $\tau^*$  values are around ten times larger at 25 °C. These comparisons require acknowledgement that the backbone chemistry, catalyst loading, and crosslinking density vary across these literature reports, but in an approximate sense, order-of-magnitude differences or similarities in kinetics and thermodynamics likely reflect at least in part the effect(s) of catalyst choice.

Factors other than  $\text{p}K_a$  could theoretically account for the trends in relaxation behavior (**Figure 12**) and Arrhenius parameters (**Figure 19**) calculated for the various Brønsted acids. For example, both crosslink density<sup>118</sup> and catalyst loading<sup>43,110</sup> have been demonstrated to influence relaxation times and Arrhenius parameters. To circumvent these complicating factors, all samples were prepared with identical constituent molar ratios in an attempt to constrain materials to a single crosslink density and catalyst loading. However, as noted above, weaker acids exhibited a slower transesterification rate and therefore required longer reaction times to form a gel. To probe if this potentially resulted in a higher sol fraction and incomplete network formation (which would result in a lower effective crosslink density), solid-state  $^{13}\text{C}$  NMR experiments were conducted. These results indicate that even the weakest acids reach >95% conversion of both monomer and crosslinker after processing (**Figure 8** to **Figure 11**). Moreover, the modest variability

observed in the initial storage modulus across samples (**Figure 20**) likely cannot account for the orders-of-magnitude changes in stress relaxation behavior as a function of acid chemistry. All processing conditions and rheology analysis were performed at temperatures of 25 to 75 °C, well below the boiling point of each catalyst, to minimize evaporative changes in acid concentration (as that can also affect calculated Arrhenius parameters, as seen in **Figure 21**).

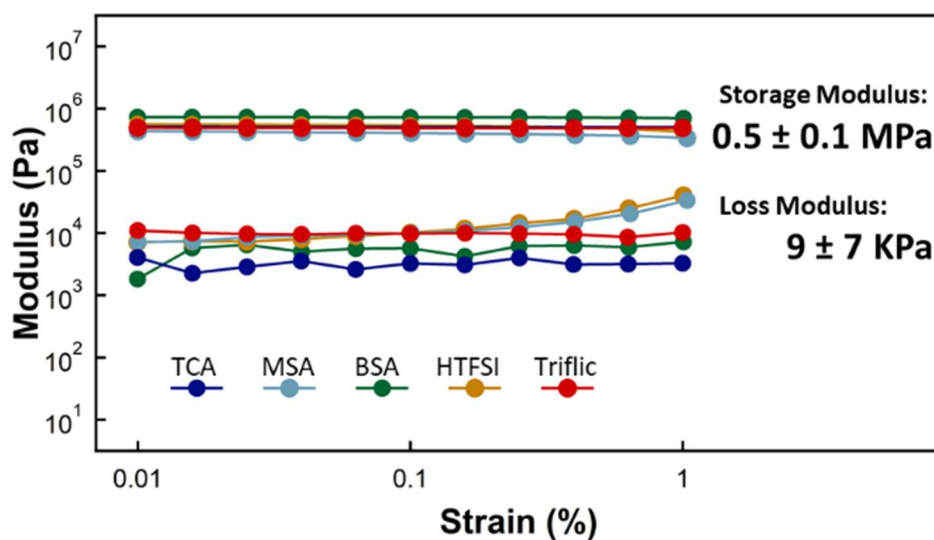


**Figure 20.** Comparison of moduli across different samples. The relative standard deviation is 21% for storage moduli at a frequency of 1 Hz.

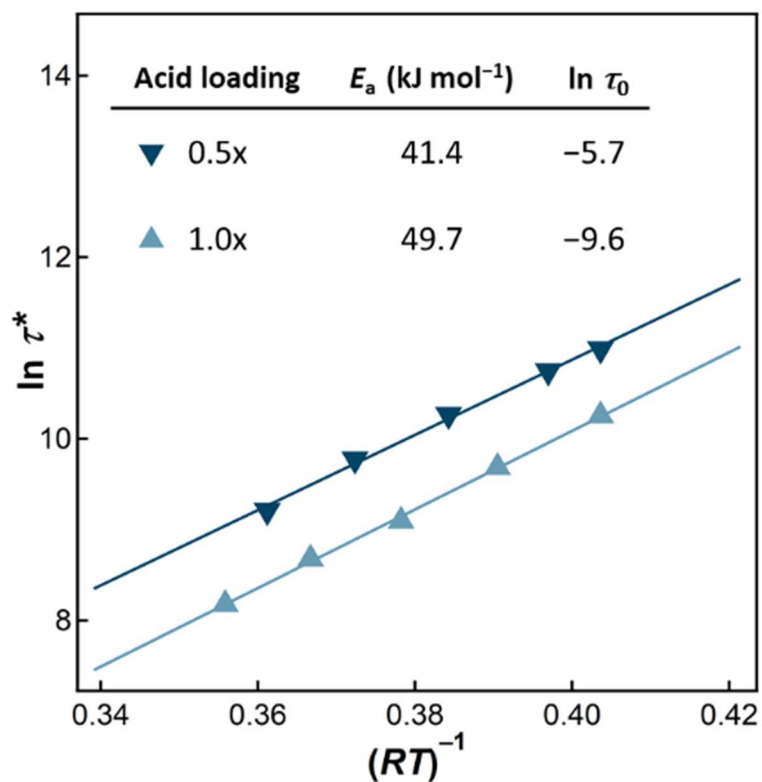


**Figure 21.** Effect of catalyst concentration of Arrhenius parameters for two MSA-containing samples.

Note also that there is no correlation between acid strength and boiling with the acids used herein, which might otherwise explain the monotonic dependence of activation energy ( $E_a$ ), kinetic prefactor ( $\tau_0$ ) and characteristic relaxation times ( $\tau^*$ ) on  $pK_a$ . There is some sensitivity of the Arrhenius parameter to recycling, but an MSA sample that experienced two additional iterations of grinding/remolding can still undergo stress relaxation at room temperature at similar rates (**Figure 22**). Finally, replicate samples of MSA demonstrate reasonable reproducibility and activation energies in agreement within 4% relative standard error (**Figure 23**).

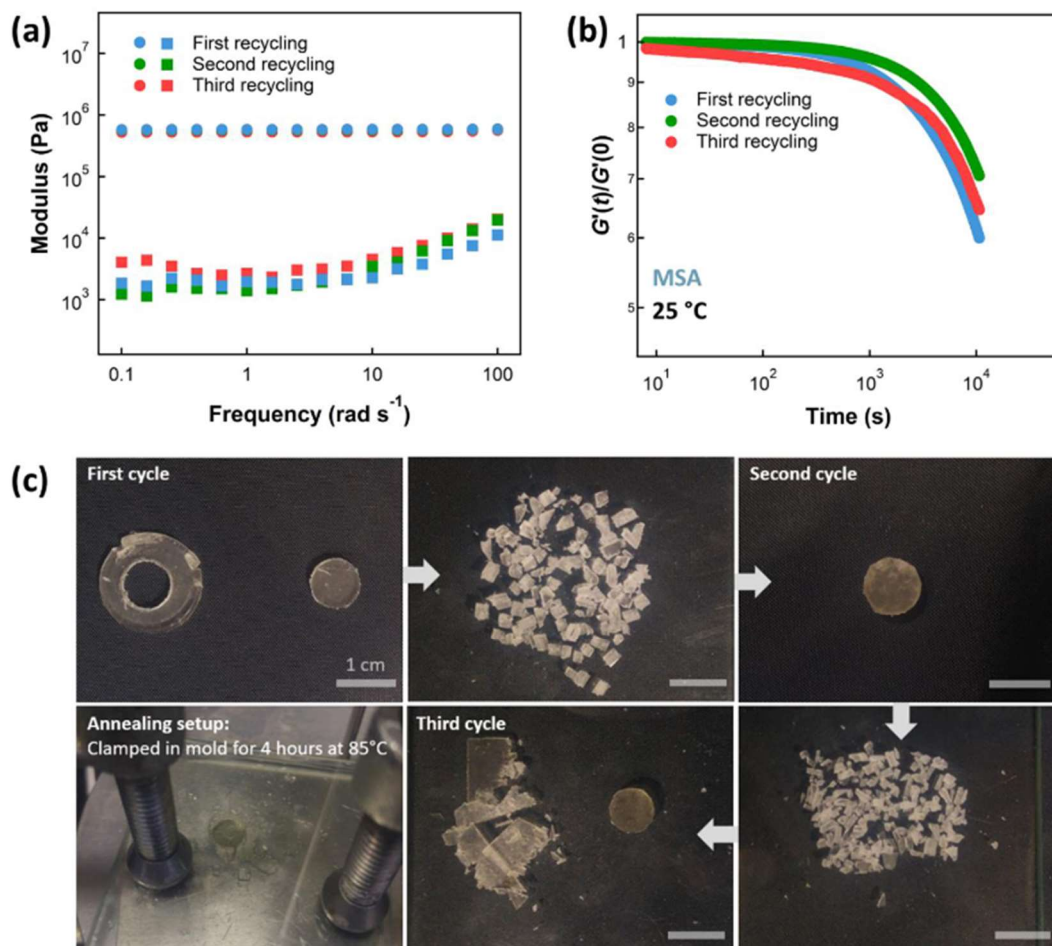


**Figure 22.** MSA polyester networks show excellent recyclability as expected for dynamic networks that undergo associative exchange.



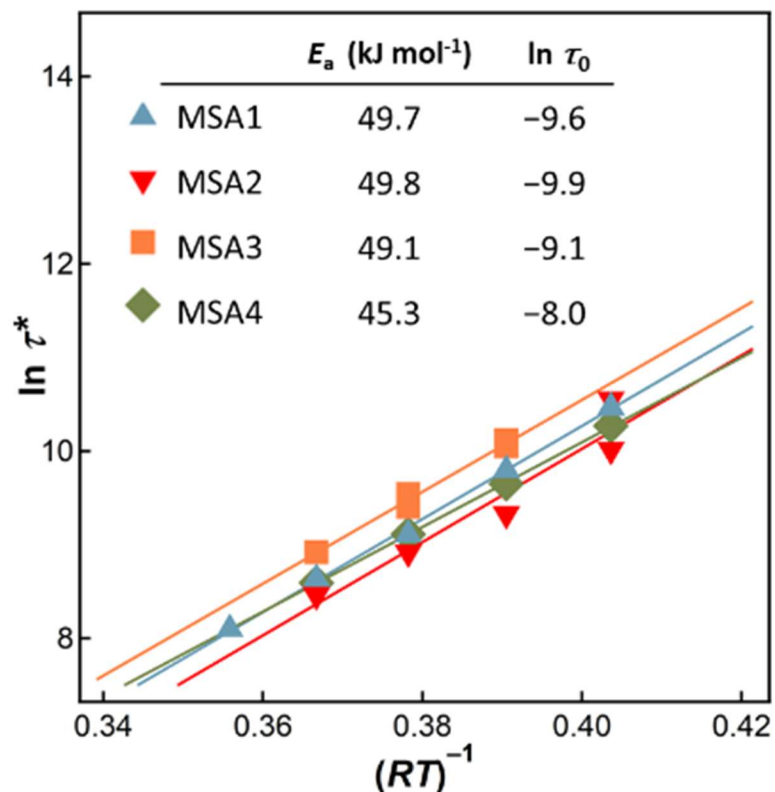


**Figure 23.** Four samples of MSA demonstrate reasonable reproducibility in the temperature range studied. Activation energies agree within 4% relative standard error ( $49 \pm 2$  kJ mol<sup>-1</sup>).

The logarithmic acid dissociation constant ( $pK_a$ ) reflects the thermodynamic equilibrium between a given Brønsted acid and its conjugate base plus a proton. However, disassociated protons in general interact with solvent molecules and their effective concentration thus depends on the medium in which they are embedded.<sup>119</sup> The  $pK_a$  values of the five acids referenced in **Figure 7b** are taken from literature reports in water: triflic acid (-12),<sup>120</sup> bis(trifluoromethane)sulfonimide (-9.7),<sup>121</sup> benzenesulfonic acid (-7.0),<sup>122</sup> methanesulfonic acid (-1.9),<sup>123</sup> and trichloroacetic acid (0.81).<sup>124</sup> While these absolute

values probably change when the acids are incorporated into poly(4-methylcaprolactone) networks, the relative trend between values should still hold. The measurement of  $pK_a$  within our materials is difficult, but two factors are of anticipated importance to understand any differences. Pendant network alcohol functionality is slightly less basic than water (as measured in an aqueous environment)<sup>125</sup> which would decrease the donating power of the surroundings and also the apparent Brønsted acidity of the a catalyst.<sup>119</sup> This effect is amplified by a significant reduction in dielectric constant (as a reference, water  $\approx 80$  and isopropanol  $\approx 18$ ) that would destabilize ionic species, thereby pushing the equilibrium back towards the conjugate acid. Thus, we propose that the monotonic trend plotted in **Figure 19** would still persist if the matrix-induced difference in  $pK_a$  for every acid is similar, simply with a corresponding shift along the x-axis.

One of the most striking features of **Figure 12** is that MSA and BSA exhibit nearly indistinguishable stress relaxation traces at 55 °C, yet evidently different Arrhenius parameters (**Figure 19**). In **Figure 24** both data sets are plotted together as  $\ln(\tau^*)$  vs  $(RT)^{-1}$ . A crossover point exists near room temperature, which explains this apparent incongruity. We have opted to report the behavior of both acids for this reason.

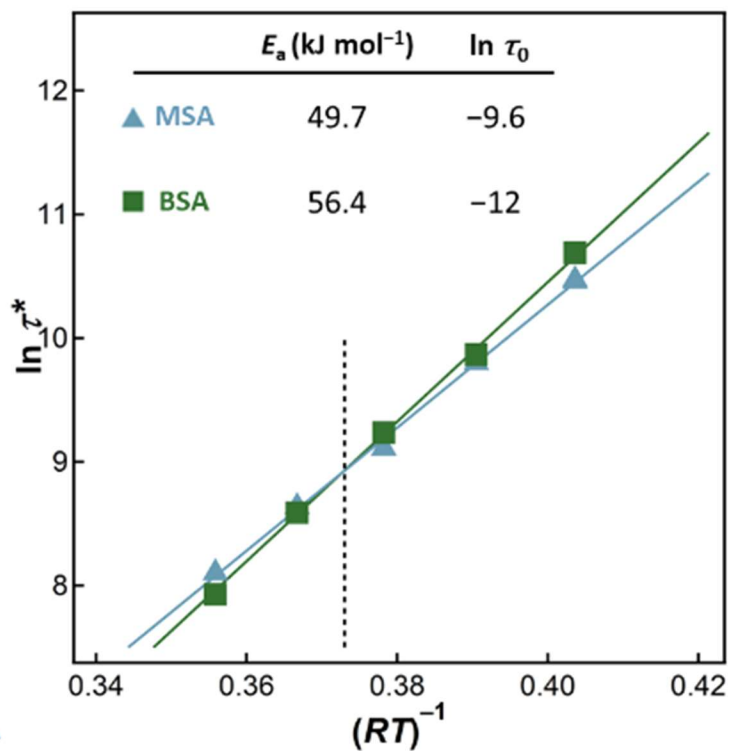


**Figure 24.** The temperature-dependent relaxation behavior of MSA and BSA samples exhibits a cross-over point at 52 °C (dashed line). This observation explains their similar characteristic relaxation time at the temperatures tested despite different Arrhenius parameters.

Brønsted acids catalyze polyester-alcohol dynamic covalent bond exchange. Reaction kinetics are significantly accelerated at lower temperatures compared to Lewis acid analogues, and exchange at 25 °C is facile in materials with sufficiently low  $T_g$ . Relaxation times, activation energies, and Arrhenius prefactors are all correlated with Brønsted acid  $pK_a$ . Stronger acids tend to relax stress faster, exhibit higher activation energies, and asymptote to shorter relaxation times as  $T$  approaches infinity. Expanding the scope of catalysts used to induce vitrimer plasticity, in conjunction with a quantitative

understanding of the associated kinetics and thermodynamics, should prove useful in the future design of materials with tailored properties, for example, shape memory polymers,<sup>39,114</sup> particles with controlled topology,<sup>72</sup> and high performance composites.<sup>48,86</sup>

## Materials and Methods

### *Reagent and solvent information*

Reagents and solvents were used as received except where otherwise stated. Triflic acid (98%), benzenesulfonic acid (98%), methanesulfonic acid (HPLC grade,  $\geq 95\%$ ), trichloroacetic acid ( $\geq 99\%$ ), and 4-methylcyclohexanone ( $\geq 99\%$ ) were purchased from Sigma-Aldrich. Tone 3031 (triol initiator) and 4,4'-bicyclohexanone ( $>98\%$ ) were purchased from TCI America. Bistriflimide ( $\geq 99\%$ ) and 3-chloroperoxybenzoic acid (70–75%) were purchased from Acros Organics. Dichloromethane (ACS grade,  $\geq 99.5\%$ ) was purchased from Fisher Chemicals and passed through activated alumina before use. The summary of catalyst properties and glass transition temperature for resultant polyester networks are given below in **Table 8** and **Table 9**.

**Table 8.** Physical properties of acid catalysts included in study.

Acid	Molar Mass (g/mol)	$pK_a$	Melting point <sup>126</sup> (°C)	Boiling point <sup>126</sup> (°C)	$\rho^{126}$ (g/cm <sup>3</sup> )
TCA	163.4	0.81 <sup>124</sup>	57–58	196	1.63
MSA	96.10	–1.9 <sup>123</sup>	20.	167	1.48
BSA	158.2	–7.0 <sup>122</sup>	51	190.	1.32
HTFSI	281.2	–9.7 <sup>121</sup>	46–57	91.0	1.36
Triflic	150.1	–12 <sup>120</sup>	–40.	162	1.70

**Table 9.** Measured glass transition temperatures for select polyester network samples.

Acid	$T_g$ (°C)
TCA	-55
MSA	-52
BSA	-56

### *Instrumentation*

Proton nuclear magnetic resonance ( $^1\text{H}$  NMR) spectra were collected using a 600 MHz Varian spectrometer. All chemical shifts ( $\delta$  ppm) are reported relative to residual protic- $\text{CHCl}_3$  (7.26 ppm) in deuterated  $\text{CDCl}_3$ . The  $^{13}\text{C}$  solid-state MAS NMR measurements were performed on a Bruker AVANCE III 500 MHz (11.7 T) wide bore spectrometer, operating at 500.24 MHz and 125.79 MHz for  $^1\text{H}$  and  $^{13}\text{C}$ , respectively, with a 4 mm zirconia rotor system at a spinning frequency of 10 kHz. The  $^{13}\text{C}$  MAS experiments were performed with a 30-degree  $^{13}\text{C}$  excitation pulse of 1.33  $\mu\text{s}$ , a 3 s relaxation delay, a 80.9 ms acquisition time, and an accumulation of about 20,000 scans. 60 kHz proton decoupling was applied during  $^{13}\text{C}$  data acquisition. The chemical shifts were referenced to a TMS standard. Parallel plate oscillatory rheology experiments were conducted on a TA Instruments AR-G2 magnetic bearing rheometer with a Peltier heating stage.

### *Synthesis*

**4-methylcaprolactone (4mCL):** The following procedure was adapted from Hillmyer et al.<sup>113</sup> In a typical reaction, a 500 mL round bottom flask was charged with a stir bar and 3-chloroperoxybenzoic acid (72 g, 321 mmol, 1.2 eq). To this vessel was added

dichloromethane (300 mL) while stirring. Due to impurities in the 3-chloroperoxybenzoic acid, an aqueous layer formed on top after complete dissolution, which was promptly removed. The reaction vessel was then degassed with a purge of Ar gas for 10 minutes while stirring and cooled to 0 °C. 4-Methylcyclohexanone (30 g, 267 mmol, 1.0 eq) was added dropwise to the solution, which was left stirring for 16 hours. Afterwards a large quantity of precipitated 3-chlorobenzoic acid was observed, to which 100 mL of dichloromethane was added, followed by aqueous washes: 400 mL of 10% sodium bisulfite (twice), 400 mL of saturated sodium bicarbonate (twice), and 400 mL of saturated brine (once). The organic layer was dried over magnesium sulfate and the solvent removed *in vacuo* to yield a colorless liquid. This crude product was distilled from calcium hydride to give 4-methylcaprolactone in >95% purity and 66% isolated yield (23 g, 203 mmol). <sup>1</sup>H NMR (600 MHz, Chloroform-d) δ 4.22 (ddd, J= 12.9, 5.8, 1.9 Hz, 1H), 4.14 (dd, J= 12.9, 10.4 Hz, 1H), 2.60(m, 2H), 1.89(dt, J = 15.3, 4.0Hz, 1H), 1.83 (m, 1H), 1.73 (m, 1H), 1.45 (dtd, J= 15.3, 10.8, 1.9 Hz, 1H), 1.28 (dtd, J= 14.0, 11.3, 2.6 Hz, 1H), 0.95 (d, J= 6.6 Hz, 3H).

**4,4'-bioxepane-7,7'-dione (BOD):** The following procedure was adapted from Wiltshire et al.<sup>112</sup> In a typical reaction, a 250 mL round bottom flask was charged with a stir bar and 3-chloroperoxybenzoic acid (11g, 46 mmol, 3eq.). To this vessel was added dichloromethane (150mL) while stirring. Due to impurities in 3-chloroperoxybenzoic acid, an aqueous layer formed on top after complete dissolution which was promptly removed. The reaction vessel was then degassed with a purge of Ar gas for 10 minutes while stirring and subsequently cooled to 0°C. 4,4'-Bicyclohexanone (3.0 g, 15 mmol, 1 eq) was dissolved in a minimal amount of dichloromethane, added dropwise to the

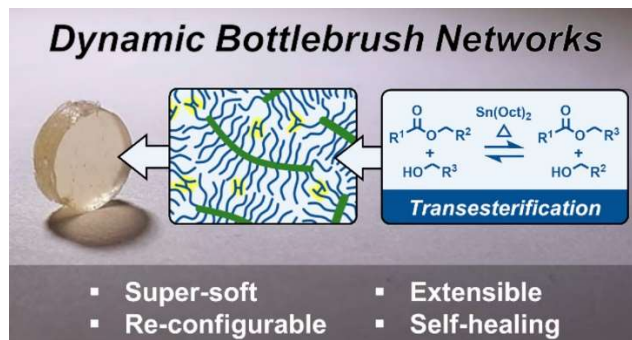
solution, and the resulting solution was left stirring for 16 hours. Thereafter, 200 mL of dichloromethane was added to the solution, followed by four aqueous washes: 400 mL of 10% sodium bisulfite (twice), 400 mL of saturated sodium bicarbonate (four times), and saturated brine (once). The organic layer was dried over magnesium sulfate and the solvent removed *in vacuo* to give 2.6 g of a white solid (26 g, 203 mmol) in 74% isolated yield with 97% purity. <sup>1</sup>H NMR (600 MHz, Chloroform-d) δ 4.33 (dd, J = 5.1, 7.2 Hz, 2H), 4.15 (dd, J= 13.1, 9.2 Hz, 2H), 2.72 (ddd, J= 14.2, 7.4, 1.6 Hz, 2H), 2.59 (ddt, J= 14.5, 12.5, 2.3 Hz, 2H), 1.89 (m, 2H), 1.84 (m, 2H), 1.4(m, 4H), 1.48 (q, J= 12.1 Hz, 2H).

**Network formation:** A dram vial was with the initiator Tone 3031 (0.035 g, 0.1 mmol, 1.0 eq). 4mCL monomer (0.320 g, 2.5 mmol, 25 eq), BOD crosslinker (0.068 g, 0.3 mmol, 3.0 eq), and dichloromethane (0.2 mL) were sequentially added and the vial was sonicated until all reagents were completely dissolved. Finally, 1 stoichiometric equivalent of acid catalyst was added. For liquid catalysts, the acid was measured by micro-syringe and injected directly into the reaction vial. Conversely, for solid catalysts, the acid was first dissolved in 0.1 mL of dichloromethane and then added to the reaction vial. In both cases, the vial was rapidly shaken to ensure homogeneity and then left quiescent at room temperature for 20 hours to gel. Thereafter, the dram vials were broken, and the polyester gel was gently removed. The gel was then subjected to a flow of argon for 1 hour to promote evaporation of residual dichloromethane and then annealed on a hot block at 75 °C. To ensure the correct geometry for characterization experiments, a rheology punch was used to isolate the center of the samples (where they tended to be most uniform). The sample was left annealing at 75 °C for 4 hours before being removed and immediately loaded on the rheometer for testing. For samples containing TCA and

MSA, excess material was removed by hand and submitted for solid state  $^{13}\text{C}$ NMR analysis to quantify conversion.



## Chapter III. Dynamic Bottlebrush Polymer Networks: Self-Healing in Super-Soft Materials



### Abstract

We introduce a design strategy to expand the range of accessible mechanical properties in covalent adaptable networks (CANs) using bottlebrush polymer building blocks. Well-defined bottlebrush polymers with rubbery poly(4-methylcaprolactone) side chains were cross-linked in formulations that include a bis-lactone and strong Lewis acid (tin ethyl hexanoate). The resulting materials exhibit tunable stress-relaxation rates at elevated temperatures (160–180°C) due to dynamic ester cross-links that undergo transesterification with residual hydroxy groups. Varying the cross-linker loading or bottlebrush backbone degree of polymerization yields predictable low-frequency shear moduli ca. 10–100 kPa, well below values typical of linear polymer CANs (1MPa). These extensible networks can be stretched to strains as large as 350% before failure and undergo efficient self-healing to recover >85% of their original toughness upon repeated fracture and melt processing. In summary, molecular

architecture creates new opportunities to tailor the mechanical properties of CANs in ways that are otherwise difficult to achieve.

This chapter was originally published in the *Journal of the American Chemical Society*.

Reproduced with permission from *J. Amer. Chem. Soc.* **2020**, 142, 16, 7567–5737.

Copyright 2020, American Chemical Society.

## Introduction

Dynamic covalent bonds provide a unique opportunity to tailor the viscoelasticity of crosslinked polymers (i.e., covalent adaptable networks, CANs) for a variety of applications including self-healing rubbers<sup>22,24,58</sup> and plastics,<sup>11,49,106</sup> three-dimensional cell culture,<sup>25,95,96</sup> and recyclable thermosets.<sup>52,127,128</sup> While significant efforts have been directed toward developing new types of dynamic bond chemistries<sup>18,24,51,54,58,107</sup> and catalysts<sup>44,45,73,105,129</sup> to promote exchange reactions in CANs under various stimuli (e.g., temperature,<sup>45,104</sup> light,<sup>12,23</sup> and carbon dioxide<sup>130</sup>), far fewer studies have addressed other design principles that are known to influence the properties of conventional polymeric materials. For example, only recently have block sequence<sup>131,132</sup> and crystallinity<sup>35,114</sup> been exploited to tailor the macroscopic creep resistance and shape-memory behavior of CANs despite decades of prevalence in traditional thermoplastics and thermosets.<sup>133</sup> Sparser yet are reports discussing the impact of architecture on CAN performance—the most common network topology involves linear chains connected on both ends to a network junction.

Of the various polymer architectures that can be constructed with controlled polymerization techniques (e.g., stars,<sup>134–136</sup> combs,<sup>137</sup> cycles,<sup>138</sup> ...), bottlebrush polymers are a particularly attractive target for CANs since they should broaden the spectrum of available physical properties to include “super-soft” elastomers (herein defined as networks with a high gel fraction and an equilibrium shear modulus  $G_x < 100$  kPa for consistency with previous reports<sup>139,140</sup>). Individual bottlebrush molecules are highly branched, containing a polymeric side chain protruding from each backbone repeat unit.<sup>141–143</sup> When crosslinked via chemical<sup>36,144–146</sup> or physical<sup>147,148</sup> bonds to form rubbery, non-dynamic networks, past work has established that the resulting bottlebrush polymer elastomers are unusually soft due to the suppression of entanglements and a high density of network defects (non-crosslinked, dangling side chains).<sup>139,149</sup> The shear modulus ( $G$ ) of these materials can approach 1–100 kPa, even in the absence of solvent, which is significantly smaller than the plateau modulus of a typical entangled rubber without plasticizer ( $\sim 1$  MPa).<sup>143,150,151</sup> Such softness is advantageous in a number of emerging applications ranging from high-sensitivity capacitive pressure sensors<sup>152</sup> to efficient dielectric actuators<sup>153</sup> and biomimetic materials<sup>145,154</sup> (the low values of  $G$  approximate various types of living tissue<sup>155</sup>). However, because bottlebrush polymers are usually crosslinked with static covalent bonds, these traditional approaches do not enable self-repair, which is critical to mitigate device damage or emulate biological healing processes. To the best of our knowledge, there are only two literature examples that have started to explore dynamically cross-linked bottlebrush polymers, both of which rely on the use of dissociative bonds (disulfides<sup>36</sup> or Diels–Alder adducts<sup>156</sup>). Like all dissociative CANs, decomposition of the polymer crosslinks occurs before bond exchange, yielding a

temporary decrease in mechanical integrity. In contrast, CANs with dynamic bonds that rearrange via an associative mechanism, also known as “vitrimers”,<sup>11,101,127</sup> maintain a constant crosslink density and therefore desirable mechanical properties throughout the exchange process. Broadening the scope of reconfigurable bottlebrush polymer elastomers to include associative dynamic pathways such as transesterification<sup>11,45</sup> would therefore create opportunities to tailor properties in new ways.

Here, we introduce a robust synthetic platform that combines the benefits of molecular architecture and CANs to access dynamically crosslinked bottlebrush polymer elastomers with super-soft and reconfigurable properties via associative bond exchange. Our approach involves the stepwise isolation of well-defined bottlebrush polymer precursors and subsequent thermal crosslinking to generate networks with fast curing kinetics, tunable stress-relaxation rates, and predictable shear moduli that are 10–100× lower than traditional CANs. As evidenced by tensile experiments, these dynamic bottlebrush polymer elastomers exhibit >300% strain-at-break and retain >85% toughness after repeated cycles of fracture and annealing. The design concept outlined herein—rooted in molecular architecture—represents a new strategy to tune the performance of CAN-based materials beyond the conventional constraints imposed by linear dynamic networks.

## **Discussion**

We opted to design bottlebrush polymer CANs with polyester side chains as a model system that undergoes associative dynamic covalent bond exchange via transesterification.<sup>11,45,110,128,157</sup> Poly(4-methylcaprolactone) (P4MCL) was specifically

selected as the side-chain chemistry due to its low glass transition temperature ( $T_g \approx -60$  °C), lack of crystallinity, and synthetic accessibility.<sup>45,113,135</sup> As depicted in **Figure 25**, macromonomers of P4MCL were generated from norbornene–alcohol initiators using ring-opening polymerization<sup>135</sup> and characterized by size-exclusion chromatography with multiangle light scattering detection to determine absolute side-chain degrees of polymerization ( $N_{SC}$ ). Two different macromonomers were synthesized, denoted A ( $N_{SC} = 47$ ) and B ( $N_{SC} = 33$ ). The macromonomers were then further polymerized into bottlebrush polymers via ring-opening metathesis polymerization (ROMP). From a single batch of macromonomer, multiple distinct bottlebrush polymers are easily synthesized on multigram scales with different backbone degrees of polymerization ( $N_{BB}$ ) by varying the equivalents of Grubbs catalyst. For example, with macromonomer B, four bottlebrush polymers were synthesized spanning  $N_{BB} = 53$ –380 while maintaining a constant average side-chain length ( $N_{SC} = 33$ ) and low molar-mass dispersity ( $D = 1.1$ –1.3). An advantage of this approach to forming networks is the ability to fully characterize each well-defined bottlebrush polymer precursor before cross-linking, as summarized in **Figure 26**.

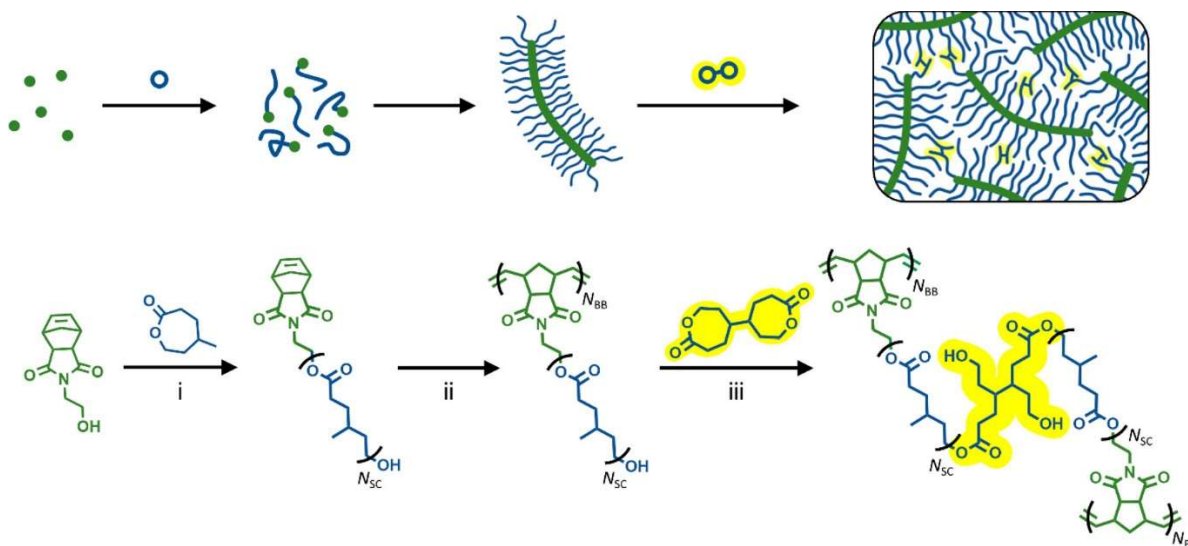


**Figure 25.** Reaction scheme for generating dynamic bottlebrush polymer networks that undergo associative bond exchange. (i) Ring-opening polymerization of 4-methylcaprolactone from a norbornene–alcohol initiator, catalyzed by  $\text{Sn}(\text{Oct})_2$  and run in the bulk at 110 °C until reaching approximately 80% conversion. (ii) Ring-opening metathesis polymerization of P4MCL macromonomer catalyzed by the Grubbs 3rd generation catalyst; 10 wt% in DCM at 25 °C for 1 h. (iii) Cross-linking bottlebrush polymers by reaction with a bis-lactone as catalyzed by  $\text{Sn}(\text{Oct})_2$  at 180 °C for 5 h. Yellow highlighting depicts the cross-linker before and after reaction.

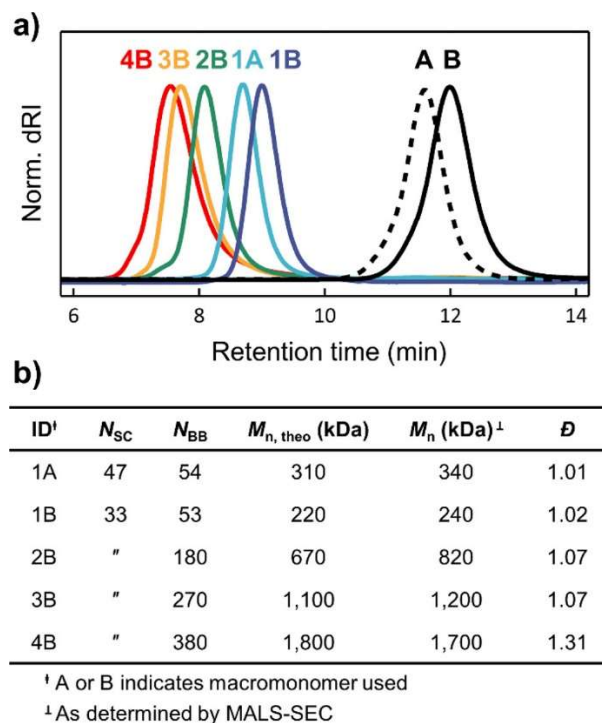


**Figure 26.** (a) Normalized size-exclusion chromatography (SEC) traces (differential refractive index detection, dRI) of the macromonomers and bottlebrush polymers studied herein. (b) Summary of bottlebrush characterization data. Absolute molecular weights were determined by SEC equipped with dRI and multiangle light scattering (MALS) detectors using  $dn/dc = 0.071$

Bottlebrush precursors were then cross-linked by reacting hydroxy groups at the termini of P4MCL side chains with 4,4'-bioxepane-7,7'-dione and a Lewis acid catalyst. Note that the catalyst used in this step will remain in the material after cross-linking and promote dynamic bond exchange via transesterification. Although both Brønsted<sup>45</sup> and Lewis acids<sup>44,110,128,157</sup> are viable choices, we opted for the latter because they require elevated temperatures to promote exchange in polyester networks,<sup>101</sup> which facilitates the characterization of nondynamic mechanical properties near room temperature. During formulation, bottlebrush, cross-linker, and tin(II) 2-ethylhexanoate ( $\text{Sn}(\text{Oct})_2$ ) were homogenized with a minimal amount of dichloromethane (DCM); these mixtures are

bench stable for at least 5 days without premature crosslinking as evidenced by SEC analysis, given below in **Figure 27**. To ensure full removal of the solvent prior to crosslinking and testing, samples were dried under vacuum for 48 h.

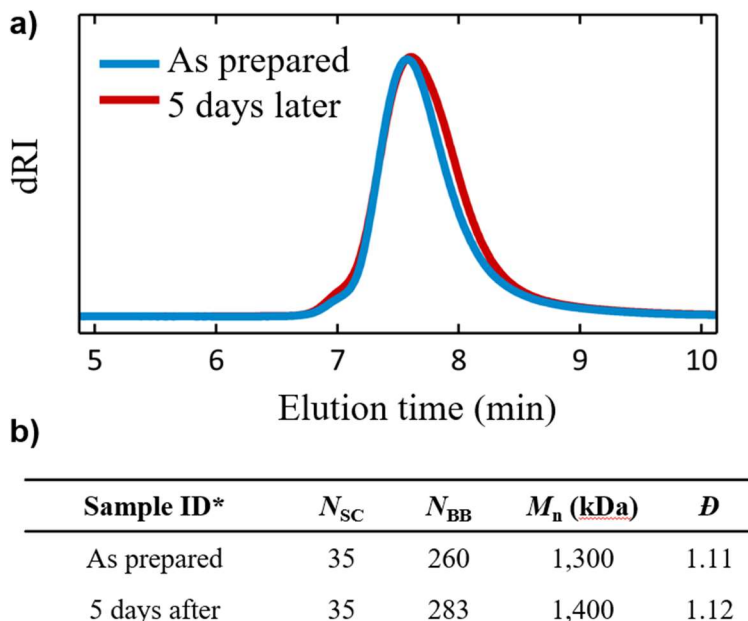


**Figure 27.** a) SEC traces (normalized differential refractive index signal) and b) characterization results from a formulation stability experiment wherein a sample was prepared ( $N_{SC}=35$ ,  $N_{BB}=260$ ,  $n_{cl}=15$ , 0.2 wt% catalyst) and left at room temperature for 5 days. The before and after traces show negligible differences in their molecular weight distribution, indicating adventitious curing at room temperature is not an issue for these materials.

Two representative formulations of bottlebrush 1B ( $N_{BB}=53$ ,  $N_{SC}=33$ ) were cured at 180 °C *in situ* in an oscillatory rheometer to continuously monitor the curing process (**Figure 28**). In both samples, the stoichiometric ratio of crosslinker to bottlebrush molecules ( $n_{cl}$ ) was held at 15 equiv. Note that this definition of  $n_{cl}$  implies bottlebrush polymer precursors with larger  $N_{BB}$  and  $N_{SC}$  will have a lower crosslink density at identical



crosslinker loading. The modulus of both samples plateaued to a constant value but with different time scales needed to reach 95% completion (83 vs 200 min) depending on catalyst loading. The higher catalyst loading (1.7 wt%) was used for all subsequent formulations with a curing time of 5 hours (approximately three times longer than 95% conversion) to ensure complete cross-linking.

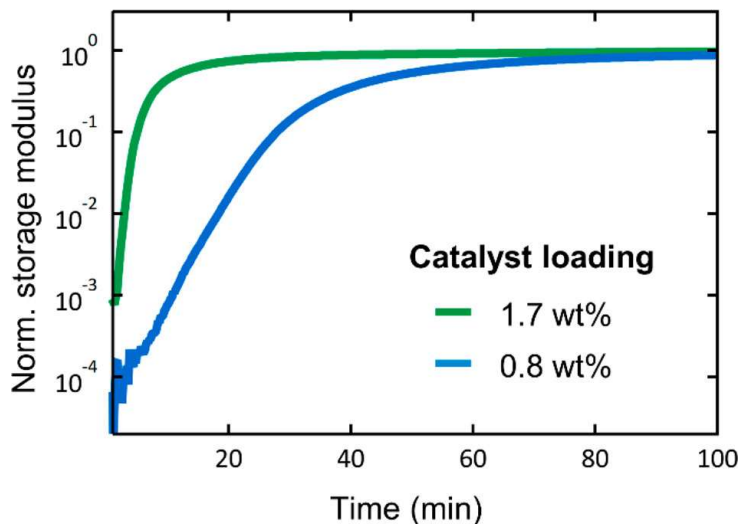


**Figure 28.** Normalized curing profiles demonstrate the cross-linking of two bottlebrush polymer 1B formulations with 15 equiv of crosslinker and different catalyst loadings.

We initially established the dynamic properties of P4MCL bottlebrush networks with various formulations of 1A ( $N_{SC} = 47$ ,  $N_{BB} = 54$ ). Three samples were cured with 5, 10, or 25 equiv of the bis-lactone crosslinker ( $n_{cl}$ ) while maintaining a constant catalyst loading (15 equiv, 1.7 wt %) (frequency sweeps are given in **Figure 44**). Selected compressive stress-relaxation experiments at elevated temperatures (160–180 °C) are shown in **Figure 29**. All three samples exhibit significant stress relaxation. The rate increases monotonically with increasing temperature (**Figure 29a**) and decreases with larger  $n_{cl}$  (**Figure 29b**). The characteristic relaxation time ( $\tau^*$ ) in each case was extracted

by fitting to a stretched exponential decay (non-normalized traces are given in **Figure 45** to **Figure 47**. Raw stress-relaxation data for sample 1A-5 with superimposed fits, and the fitting parameters are given in **Table 11** to **Table 13**). Values of  $\tau^*$  range from 18 m ( $T = 180\text{ }^\circ\text{C}$ ,  $n_{cl} = 5$ ) to 86 m ( $T = 160\text{ }^\circ\text{C}$ ,  $n_{cl} = 25$ ). While this is a longer time scale than some dynamic chemistries,<sup>22,24,45</sup> it is fairly comparable to other Lewis-acid-catalyzed dynamic polyester networks.<sup>11</sup> Further analysis revealed a linear Arrhenius dependence of  $\ln \tau^*$  with  $T^{-1}$  as shown in **Figure 29c**, which is common for dynamic networks that undergo associative bond exchange.<sup>11,127,158</sup> In all cases, similar activation energies were observed ( $89 \pm 2\text{ kJ mol}^{-1}$ ) that are roughly consistent with several other studies involving Lewis acids within a polyester matrix.<sup>11,44,157</sup>

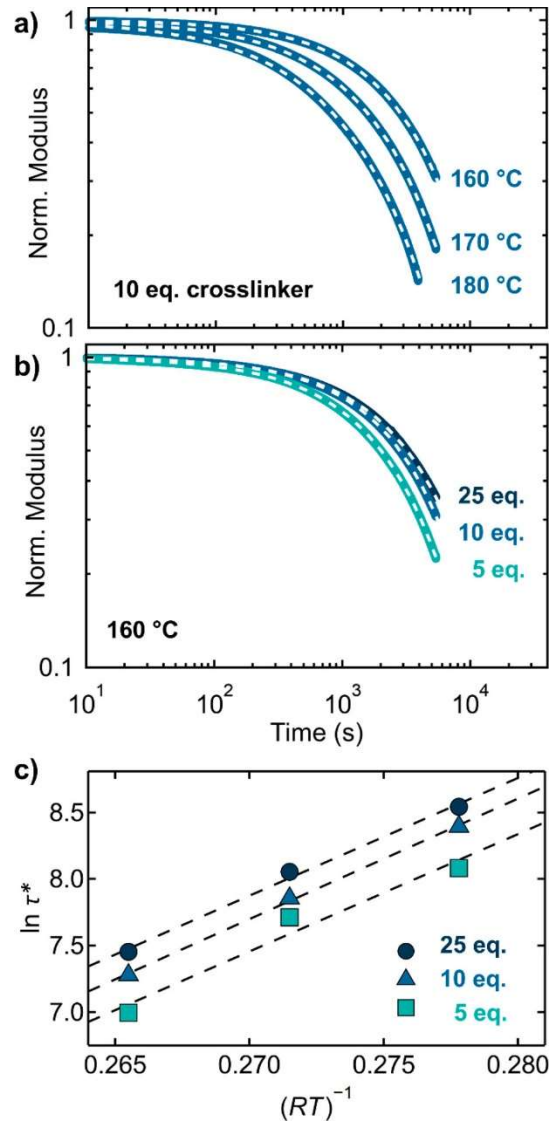


**Figure 29.** Stress-relaxation experiments with sample 1A indicate P4MCL bottlebrush networks are dynamic at elevated temperatures. Fits to a stretched exponential decay (**Equation 1**) are represented by dashed white lines.<sup>45,127,159,160</sup> (a) Inverse temperature dependence at constant crosslinker loading ( $n_{cl} = 10$ ). (b) Effect of cross-linker loading at constant temperature (160 °C). (c) Arrhenius relaxation behavior; dashed lines are fits to the Arrhenius equation (**Equation 2**).

To showcase the tunable mechanical properties of P4MCL bottlebrush CANs, four samples derived from macromonomer B (constant  $N_{SC} = 33$ ) with  $N_{BB} = 53$  (denoted 1B),

180 (2B), 270 (3B), and 380 (4B) at  $n_{cl} = 25$  were cured in molds, loaded on the rheometer, and analyzed by oscillatory experiments (**Figure 30a**). The measured value of  $G'$  at low frequencies, which we define as the plateau modulus  $G_{x,bottlebrush}$ , varies in the range 10–100 kPa depending on  $N_{BB}$ . As  $N_{BB}$  increases at constant  $n_{cl}$ ,  $G_{x,bottlebrush}$  decreases due to a reduction in cross-link density. Consequently, a long bottlebrush precursor ( $N_{BB} = 380$ ) produces materials as soft as 15 kPa at 25 °C, even with a fairly high  $n_{cl} = 25$ . The loading of cross-linker also determines  $G_{x,bottlebrush}$ . By changing  $n_{cl}$  from 5 to 45 with bottlebrush 2B ( $N_{BB} = 180$ ),  $G_{x,bottlebrush}$  varies between 8 and 62 kPa (**Figure 30b**). Collectively, these moduli are far smaller than CANs derived from linear network building blocks (most reported materials have  $G_x > 1 \text{ MPa}^{58,129,160}$ ) and are more typical of highly solvated hydro- or organogels.<sup>139,161</sup> Gel fraction experiments indicate this is not the result of a large sol fraction, in contrast to commercially available soft (nondynamic) elastomers like EcoFlex. For example, the gel fraction of our softest material (4B,  $N_{BB} = 380$ ) averages >90% across three different cross-linker loadings,  $n_{cl} = 15, 25,$  and 35. These results are given below in **Table 10**. Moreover, all formulations reported in **Figure 30** show good network integrity as evidenced by the prominent plateau in  $G'$  at low frequencies and a 1–2 order-of-magnitude separation between  $G'$  and  $G''$ .<sup>162</sup>

**Table 10.** Gel-fraction and moduli of networks derived from the largest  $N_{BB}$  polymer (4B)

Sample name	$M_n$ (kDa)	$n_{cl}$	Modulus (kPa)	Gel-fraction (%)
4B-15	1,680	15	11.3	91
4B-25	1,680	25	15	92
4B-35	1,680	35	22.6	89

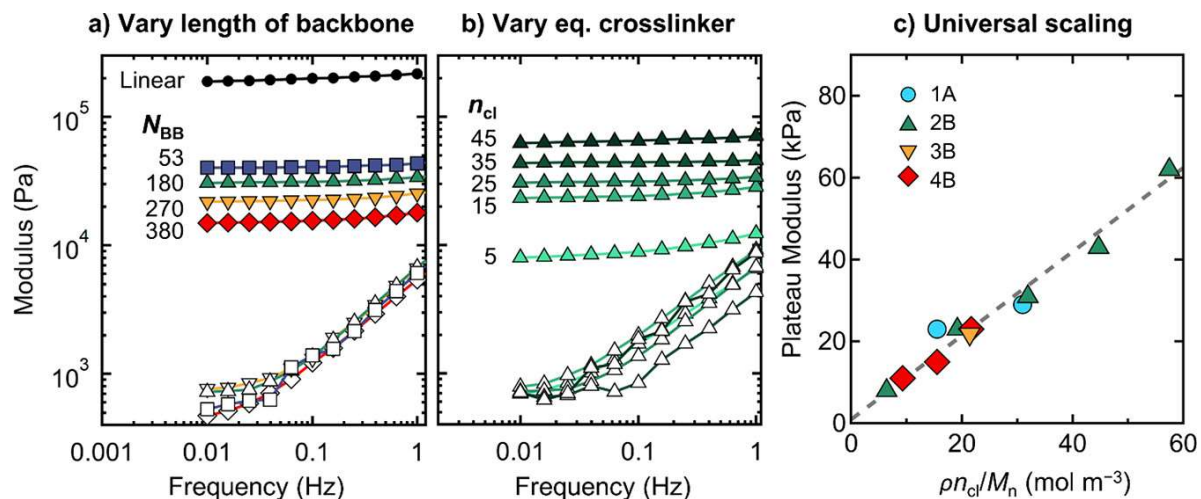


**Figure 30.** P4MCL bottlebrush polymer CANs are super-soft with a tunable storage modulus at temperatures ( $T = 25\text{ }^{\circ}\text{C}$ ) below the onset of dynamic exchange. (a) Frequency sweeps of formulations derived from 1B, 2B, 3B, and 4B with  $n_{cl} = 25$  (filled markers: storage modulus; open symbols: loss modulus). A linear P4MCL network is included for comparison. (b) Frequency sweeps of formulations generated from bottlebrush polymer 2B ( $N_{BB} = 180$ ) with varying  $n_{cl}$ . (c) Linear scaling of the low-frequency plateau modulus ( $G_{x,bottlebrush}$ ) with  $\rho n_{cl}/M_n$ .

For comparison, **Figure 30a** also includes a linear P4MCL network with a low frequency plateau modulus  $G_{x,linear} \approx 200\text{ kPa} \gg G_{x,bottlebrush}$  that is significantly larger than all of the bottlebrush polymer CANs (**Figure 30a**). This sample was designed with a target molecular weight between cross-links ( $M_{x,theo} = 9.6\text{ kDa}$ ) slightly larger than the entanglement molecular weight ( $M_e = 2.9\text{ kDa}^{113}$ ) in an attempt to maximize softness by striking a balance between trapped entanglements ( $M_{x,theo} \approx 3M_e$ ) and crosslink density, both of which contribute to  $G_{x,linear}$  at low frequencies.<sup>162</sup>  $G_{x,linear}$  in this case is dominated by the crosslink density since its value is roughly consistent with rubber elasticity theory based on  $M_{x,theo}$  ( $G_{x,linear} \approx \rho RT/M_{x,theo} = 266\text{ kPa}$  calculated using  $\rho_{P4MCL} = 1.04\text{ g/cm}^3$ ,  $T = 295\text{ K}$ , the gas constant  $R$ , and  $M_{x,theo} = 9.6\text{ kDa}$ ). While decreasing  $G_{x,linear}$  somewhat

further may be possible through careful formulation optimization, it is unlikely to ever approach  $G_{x,\text{bottlebrush}}$ ; in the limit of vanishing crosslinker loading, a strongly entangled P4MCL melt is even stiffer:  $G_e = \rho RT/M_e = 880 \text{ kPa}$ .<sup>113</sup> In contrast, bottlebrush polymer networks generate far softer materials while retaining excellent network integrity, highlighting a unique advantage imparted by molecular architecture.

A quantitative understanding of the structure–property relationships in dynamic bottlebrush polymer networks would allow for targeting specific moduli without tedious, Edisonian optimization, for example to mimic different types of biological tissue. Similar to nondynamic bottlebrush polymer networks,<sup>144</sup> there exists a linear correlation between  $G_{x,\text{bottlebrush}}$  and  $\rho n_{cl}/M_n$ , where  $\rho$  is the mass density ( $\rho_{\text{P4MCL}} = 1.04 \text{ g/cm}^3$ ) and  $M_n$  is the number-average molar mass of a bottlebrush polymer precursor molecule as shown in **Figure 30c**. Physically,  $\rho n_{cl}/M_n$  is the number density (mol/volume) of cross-linker in a bottlebrush polymer network. The relationship in **Figure 30c** remains true for four different combinations of  $N_{\text{BB}}$  and  $N_{\text{SC}}$  (samples 1A, 2B–4B) below a threshold value of  $\rho n_{cl}/M_n$  (about  $60 \text{ mol/m}^3$ ), above which the crosslinker is not fully soluble in a given bottlebrush polymer. (At higher cross-linker loadings, some persistent cloudiness or, in extreme cases, small white crystals remain visible by eye.) Overall, **Figure 30** provides quantitative insight into the connection between molecular design, formulation, and mechanical performance of bottlebrush polymer CANs.

Finally, the extensibility and recyclability of P4MCL bottlebrush polymer CANs were investigated (**Figure 31**) with a network of intermediate backbone length (2B,  $N_{\text{BB}} = 180$ ) and cross-linker loading ( $n_{cl} = 15$ ). Three uniaxial tensile experiments were performed on the following: (1) a pristine dogbone that was formulated and hot-pressed at  $180 \text{ }^\circ\text{C}$  for 5

h, (2) the broken specimen from (1) that was re-hot-pressed under the same conditions, and (3) the sample resulting from (2) that was reprocessed a third time. In all cases, similar values of the strain-at-break (325–350%) and toughness (>85% recovery) were measured. The good recovery of mechanical properties upon repeated reprocessing is likely tied to dynamic bond formation/exchange rather than other mechanisms, e.g., reptation across fresh interfaces, since the bottlebrush polymer architecture suppresses backbone entanglements and the P4MCL side chains are relatively short (of order  $M_e$ ). Moreover, any entanglements that happen to form would not support a significant amount of stress since P4MCL is rubbery at room temperature. We suspect the stress–strain behavior in **Figure 31** can be further tailored by the values of  $N_{BB}$  and  $N_{SC}$  which are synthetically encoded into the well-defined bottlebrush polymer precursors before cross-linking. These studies highlight the self-healing and recyclability of CANs derived from bottlebrush polymer elastomers.

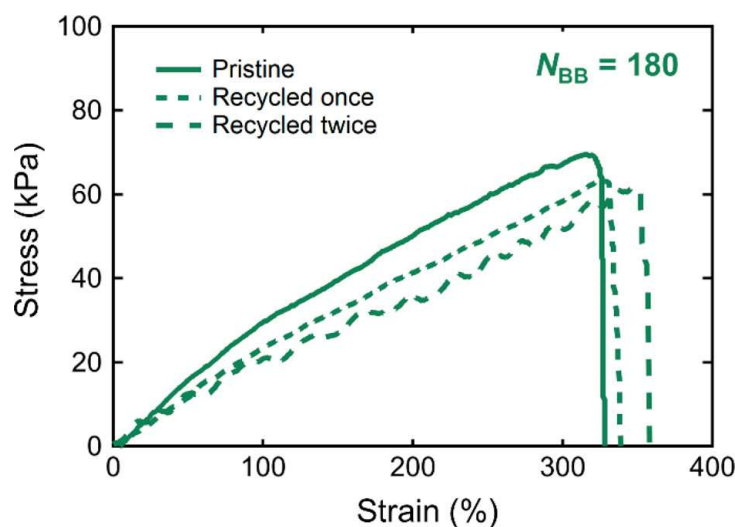


**Figure 31.** Uniaxial tensile experiments demonstrate the self-healing and extensibility of P4MCL bottlebrush polymer CANs (sample 2B: NSC = 33,  $N_{\text{BB}} = 180$ ;  $n_{\text{cl}} = 15$ ). The toughness recovered to >85% after three cycles.

## Conclusion

In conclusion, we have introduced a new type of covalent adaptable network (CAN) comprising bottlebrush polymer building blocks that undergoes dynamic bond exchange via an associative mechanism. The use of rubbery poly(4-methylcaprolactone) side chains produces materials with tunable exchange dynamics that are exceptionally soft (shear moduli 10–100 kPa), extensible, and tough. We anticipate this class of dynamic networks will find use in applications that would benefit from the combination of super-soft and self-healing properties, for example, next-generation sensors, actuators, and tissue-mimetic biomaterials. Expanding the scope of covalent adaptable networks to include nonlinear molecular architectures creates new opportunities at the intersection of chemistry, materials science, and engineering.

## Materials and Methods

### *Reagents and solvent information*

Reagents and solvents were used as received except where otherwise noted. 4,4'-bicyclohexa-none ( $\geq 98\%$ ) was purchased from TCI America. Methylene chloride ("DCM", ACS grade,  $\geq 99.5\%$ ), methanol ("MeOH", 99%), and ethyl vinyl ether ("EVE", 99%) were purchased from Fischer Scientific and used as received. Tin(II) ethyl hexanoate ( $\text{Sn}(\text{Oct})_2$ , Aldrich, 92.5–100%) was purified by fractional distillation ( $3\times$ ) under reduced pressure (0.05 Torr, 150 °C) and kept in a nitrogen-filled glovebox. 4-



Methylcaprolactone (“4MCL”) was prepared according to previously reported methods<sup>113</sup> and further purified by three consecutive fractional distillations over calcium hydride (CaH<sub>2</sub>, Fisher Scientific, 93%). Crosslinker (4,4'-bioxepane-7,7'-dione, “BD”) was prepared according to previously reported methods<sup>45</sup> and further purified by recrystallization from ethyl acetate. Macromonomer initiator (N-(hydroxyethyl)-cis-5-norbornene-exo-2,3-dicarboximide, “NbOH”) was also prepared according to previously reported methods<sup>36</sup> and further purified by recrystallization from chloroform. Grubbs second-generation metathesis catalyst [(H<sub>2</sub>IMes)(PCy<sub>3</sub>)<sub>2</sub>(Cl)<sub>2</sub>Ru=CHPh, “G2”) was generously provided by Materia. G2 was converted to Grubbs third-generation metathesis catalyst [(H<sub>2</sub>IMes)(Pyr)<sub>2</sub>(Cl)<sub>2</sub>Ru=CHPh, “G3”) following a previously reported method.<sup>163</sup>

### *Instrumentation*

<sup>1</sup>H NMR spectra were collected on a Varian Unity Inova AS600 600MHz using the residual un-deuterated solvent peak as an internal reference (CHCl<sub>3</sub> at 7.26 ppm). The following abbreviations (or combinations thereof) were used to explain the multiplicities: s = singlet, d = doublet, t = triplet, q = quartet, m = multiplet, br = broad. FTIR spectra were collected on a Thermo Nicolet iS10 FTIR Spectrometer equipped with a Smart Diamond attenuated total reflectance (ATR) accessory. Size-exclusion chromatography with multi-angle light scattering detection (SEC-MALS) was performed using two Agilent columns (PLgel, 5µm Mini MIX-D, 250×4.6 mm) connected to a Waters Alliance HPLC System, 2690 separation module pump, Wyatt 18-angle DAWN HELEOS-II light scattering detector, and Wyatt REX differential refractive index detector using THF as the

mobile phase. The absolute molar mass was determined by light scattering using online determination of  $dn/dc$  by assuming 100% mass elution under the peak of interest. Mass spectrometry data were collected on a Waters GCT Premier high-resolution time-of-flight mass spectrometer in the electron ionization mode. This instrument has a working mass range up to 800 m/z.

Frequency and strain sweeps were run on a TA Instruments AR-G2 with an 8 mm parallel-plate geometry. After running strain sweeps from 0.1% to 100%, frequency sweeps were collected at a sufficiently low strain to ensure they were within the linear viscoelastic regime (with a typical value being 1% strain). The plateau modulus was taken to be the modulus at the lowest measured frequency (0.01 Hz). In situ curing experiments were run on a TA Instruments ARES-G2 equipped with a nitrogen-purged forced convection oven. The advanced sensitivity of the instrument allowed for high-resolution characterization of the uncured polymer melt while also enabling in situ monitoring of the entire curing process. A room-temperature frequency sweep was collected on both the cured and uncured material from 0.01 Hz to 10 Hz and a strain of 1%. Curing was monitored during a rapid temperature ramp from 25 to 180 °C (<3 minutes) followed by holding at 180 °C until completion. Stress-relaxation experiments were conducted on a TA Instruments DMA 850 in compression mode with a sample diameter of 8 mm to allow for the same specimens to be used from the rheology experiments. For the stress-relaxation experiments, samples were first brought to thermal equilibrium for 20 minutes at the desired testing temperature, after which a preload force of 0.2 N was first applied and the sample was subjected to a 1% strain.

## Synthesis

***N*-(hydroxyethyl)-*cis*-5-norbornene-*exo*-2,3-dicarboximide, “NbOH initiator”**: In a 500 mL round-bottom flask charged with a stir bar, 20 g of *cis*-5-norbornene-*exo*-2,3-dicarboxylic anhydride (121.8 mmol, 1.0 eq) was combined with 7.8 g (7.8 mL, 127.9 mmol, 1.05 eq) of ethanol amine and 240 mL of toluene. A Dean–Stark trap equipped with a condenser was placed on top of the round-bottom flask, and the reaction was refluxed at 120 °C overnight until all the *cis*-5-norbornene-*exo*-2,3-dicarboxylic anhydride was consumed, as determined by NMR. The reaction was then cooled, and the solvent was removed in vacuo. The contents were dissolved in 500 mL of DCM, washed three times with 100 mL of 0.1 M HCl, and once with 100 mL of brine before drying over MgSO<sub>4</sub>. Solvent was removed in vacuo and compound was recrystallized from chloroform. <sup>1</sup>H NMR (500 MHz, Chloroform-*d*) δ = 6.29 (s, 2H), 3.78 (t, J= 5.8, 4.4 Hz, 2H), 3.71 (t, J= 5.8, 4.4 Hz, 2H), 3.29 (s, 2H), 2.72 (s, 2H), 1.52 (d, J= 10.0, 1.7 Hz, 1H), 1.35 (d, 1H). <sup>13</sup>C NMR (125MHz, CDCl<sub>3</sub>) δ = 178.8, 137.9, 60.6, 47.9, 45.3, 42.8, 41.4. MS for C<sub>11</sub>H<sub>13</sub>NO<sub>3</sub>Na [M+Na]<sup>+</sup>, calculated: 230.0793, and found: 230.0783.

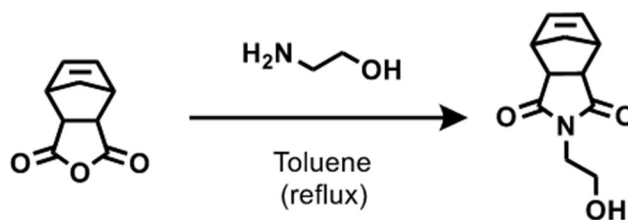


**Figure 32.** Synthesis of NbOH initiator

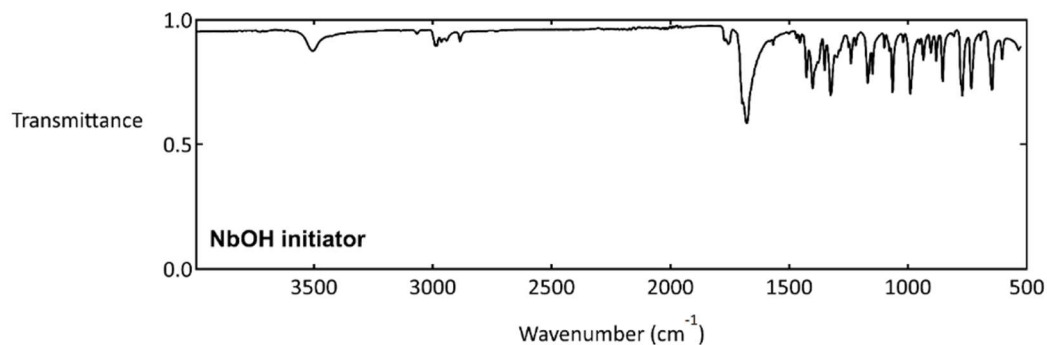


**Figure 33.** Fourier-transformed infrared (FTIR) spectrum of NbOH initiator

**4-methylcaprolactone, “4MCL monomer”:** Synthesized according in the same method as described in the synthesis section of Chapter 2.

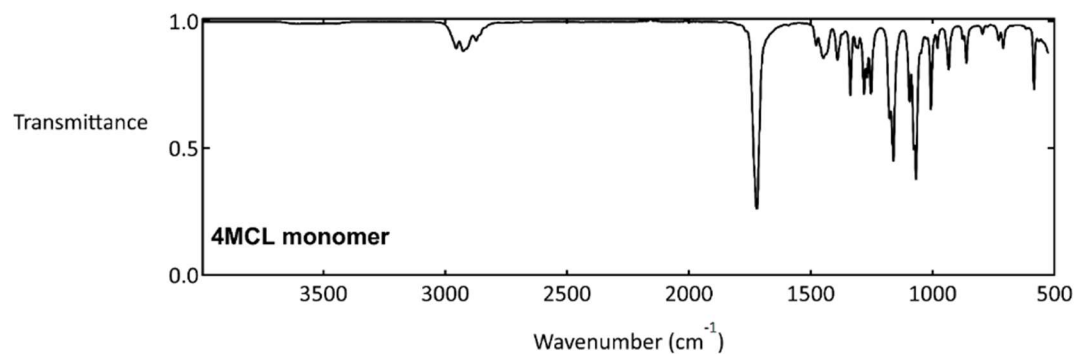


**Figure 34.** Fourier-transformed infrared (FTIR) spectrum of 4mCL monomer

**4,4'-bioxepane-7,7'-dione, “BD crosslinker”:** Synthesized according in the same method as described in the synthesis section of Chapter II.

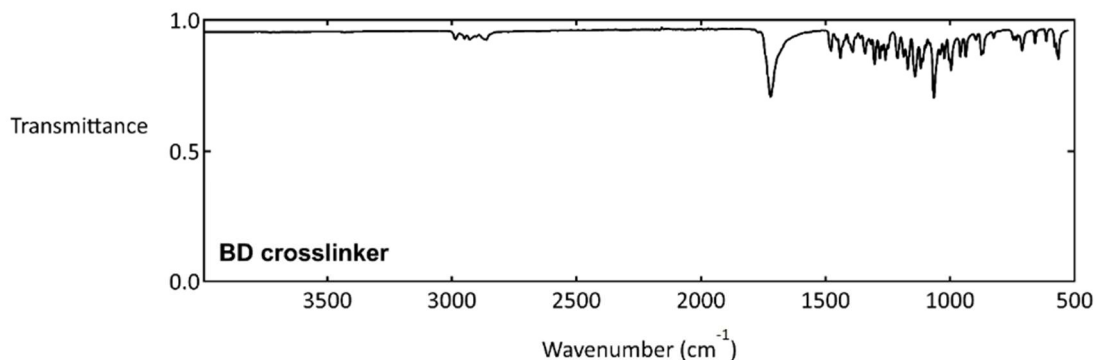


**Figure 35.** Fourier-transform infrared spectrum of BD crosslinker

**4mCL macromonomer by ring-opening polymerization (ROP):** The following procedure was used to prepare both macromonomer batches (A and B); the representative spectroscopic characterization reported is for macromonomer B.

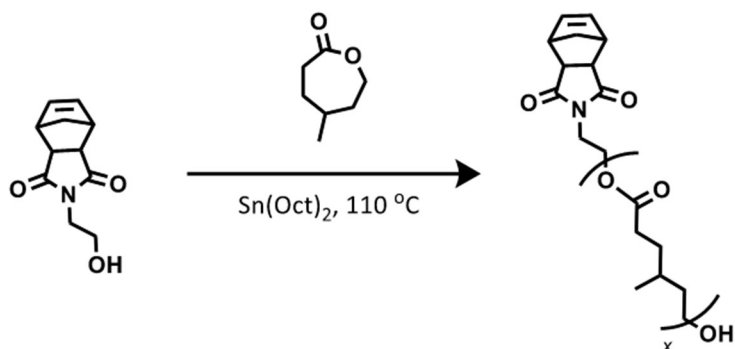


**Figure 36.** Synthesis of 4mCL macromonomer.

In a nitrogen-filled glovebox, 50 g of 4mCL monomer (390 mmol, 40 eq.) were added to an oven-dried round-bottom flask equipped with a stir bar. To this reaction vessel, initiator NbOH (9.76 mmol, 1 eq.) and catalyst Sn(Oct)<sub>2</sub> (0.97 mmol, 0.1 eq.) were also added before sealing the reaction vessel. This mixture was then removed from the glovebox and stirred in a pre-heated oil bath at 110 °C, during which the initiator rapidly

dissolved to form a homogeneous reaction solution. An aliquot was periodically extracted to determine the conversion of monomer by  $^1\text{H}$  NMR. Once the desired conversion was achieved, the vessel was immediately removed and quenched to  $0\text{ }^\circ\text{C}$  in an ice bath. DCM was added to dilute the polymerization after which it was precipitated into cold MeOH ( $-78\text{ }^\circ\text{C}$ ). The cold methanol was then decanted off to yield a concentrated and viscous polymer. This dissolution/precipitation process was repeated twice more to thoroughly remove unreacted monomer and catalyst. The final p4mCL was then rigorously dried under high vacuum (10 mTorr) for 24 hours to ensure adequate removal of residual DCM and MeOH. The product was isolated as 46.2 g of a clear oil (92% yield).  $^1\text{H}$  NMR (600 MHz, Chloroform-d)  $\delta$  = 6.26 (s, 2H), 4.27–4.12 (m, 4H), 4.11–4.03 (m, 56H), 3.73–3.70 (m, 2H), 3.25 (p,  $J$ = 1.7 Hz, 2H), 2.67 (d,  $J$ = 1.4 Hz, 2H), 2.66–2.55 (m, 2H), 2.34–2.21 (m, 58H), 1.70–1.60 (m, 60H), 1.58–1.50 (m, 31H), 1.49–1.39 (m, 59H), 1.32–1.25 (m, 2H), 0.89 (d,  $J$ = 6.6 Hz, 88H).  $^{13}\text{C}$  NMR (126 MHz,  $\text{CDCl}_3$ )  $\delta$  = 177.8, 174.0, 173.7, 173.7, 173.2, 137.8, 68.0, 62.6, 62.5, 60.6, 47.8, 45.2, 42.6, 39.4, 37.6, 37.2, 35.2, 33.2, 31.9, 31.7, 31.5, 31.4, 30.8, 29.5, 29.4, 29.1, 22.1, 19.3, 19.0.  $M_n(1\text{H NMR}) = 4.0\text{ kg mol}^{-1}$ . MALS SEC ( $dn/dc = 0.071$ ):  $M_n = 4.5\text{ kg mol}^{-1}$ ,  $D = 1.06$ .

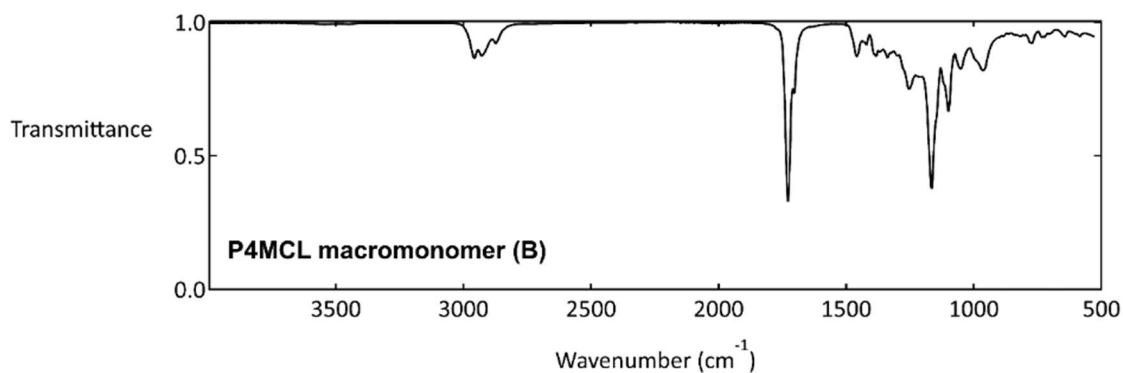


**Figure 37.** Fourier-transform infrared of p4MCL macromonomer

**Bottlebrush polymer by ring-opening metathesis polymerization (ROMP):** The following procedure was used to prepare all bottlebrush polymers (1A, 1B, 2B, 3B, and 4B); the representative spectroscopic characterization reported is for bottlebrush polymer 1B.

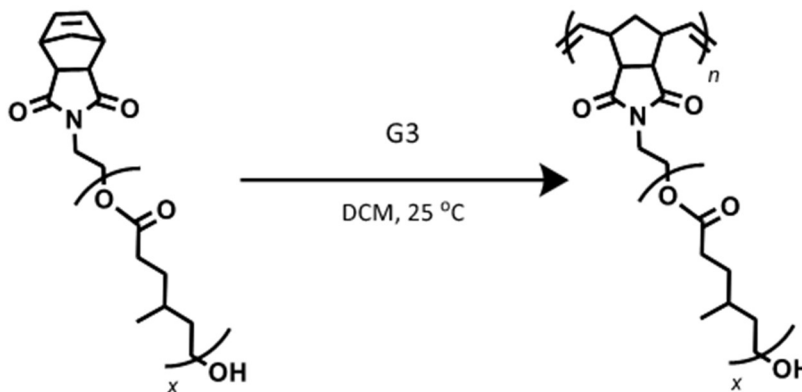


**Figure 38.** Synthesis of 4mCL bottlebrush polymer.

In a nitrogen-filled glovebox, 20 g of P4MCL macromonomer (50 eq., 4.4 mmol) were added to an oven-dried round-bottom flask equipped with a stir bar. DCM was added until a concentration of 20wt% macromonomer was reached. Separately, 65 mg of G3 (1 eq., 0.1 mmol) was added to a scintillation vial and dissolved in a minimal amount of solvent (typically, <0.5 mL DCM). The solution with macromonomer was stirred vigorously to ensure full dissolution and to promote rapid mixing upon the addition of catalyst. To the stirring solution, G3 was quickly added. As the reaction progressed, the color of the solution changed from its initial green to a dull brown. After an hour of stirring, a large excess of EVE (approximately 1 mL, 120 eq.) was added to quench the G3. The reaction was then stirred an additional two hours to ensure sufficient quenching and precipitated

into cold methanol three times, with the precipitate being centrifuged, filtered, and re-dissolved between each precipitation. To ensure complete removal of solvent, the bottlebrush polymer was dried in a vacuum oven for 24 hours at room temperature. The final material was isolated as 16.6 g of a clear, slightly yellow oil (83% yield).  $^1\text{H}$  NMR (500 MHz, Chloroform-d)  $\delta$  = 5.74 (br, s, 2H), 4.08 (br, tt,  $J$ = 11.0, 5.5 Hz, 154H), 3.98 – 3.88 (br, m, 1H), 3.76 – 3.58 (br, m, 7H), 2.52–2.02 (br, m, 163H), 1.67 (br, ddt,  $J$ = 20.6, 14.4, 6.4 Hz, 168H), 1.60 – 1.50 (br, m, 89H), 1.52 – 1.34 (br, m, 162H), 1.27 – 1.06 (br, m, 5H), 0.91 (br, d,  $J$ = 6.5 Hz, 242H).  $^{13}\text{C}$  NMR (125MHz,  $\text{CDCl}_3$ )  $\delta$  173.8, 62.6, 60.8, 50.8, 39.5, 35.2, 31.9, 31.8, 29.6, 29.1, 19.0.

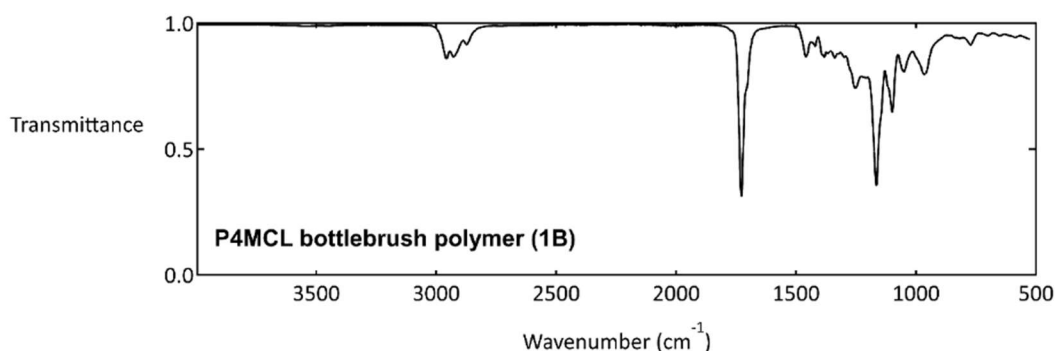


**Figure 39.** Fourier-transform infrared of 4mCL bottlebrush polymer.

**Network curing:** The procedure for network generation was the same across all sample sets used, but the values in the following representative procedure were calculated based on the molecular weight for bottlebrush polymer 1B. First, 300 mg of bottlebrush polymer (1 eq., 1.3  $\mu\text{mol}$ ) were weighed out in a dram vial. Next, a stock solution of 20  $\text{mg mL}^{-1}$  was made for both the crosslinker and catalyst. From the crosslinker stock solution, 215  $\mu\text{L}$  (4.3 mg, 15 eq., 19  $\mu\text{mol}$ ) of solution were added to the bottlebrush. Next,



from the catalyst stock solution, 256  $\mu\text{L}$  (5.1 mg, 10 eq., 12.7  $\mu\text{mol}$ ) of solution were added to the bottlebrush. Another approximate 0.5 mL of DCM was then added to ensure good mixing. After mixing to homogeneity, the solution was then dried under vacuum (approximately 25 mTorr) for 48 hours. The resulting homogeneous paste was loaded into a mold and heated at 180  $^{\circ}\text{C}$  for five hours to yield a cured network.

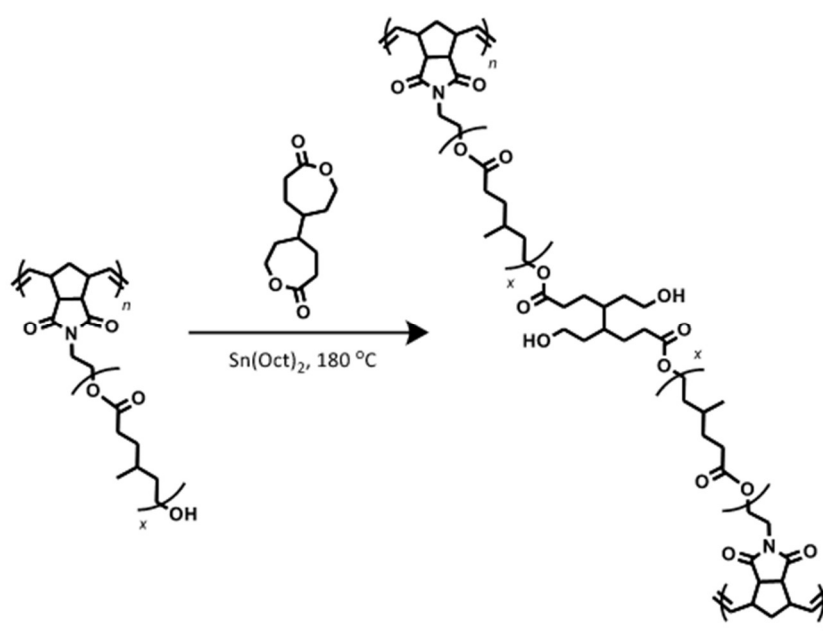


**Figure 40.** Synthesis of bottlebrush polymer network

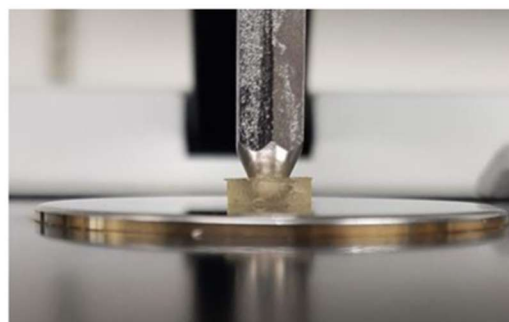
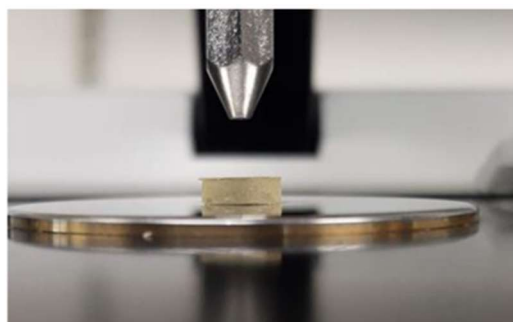


**Figure 41.** Experimental setup for Fourier-transform infrared (FTIR) spectral analysis of P4MCL bottlebrush polymer networks. The piston was hand-tightened to form good contact, also demonstrating the compliance of dynamic bottlebrush polymer networks.

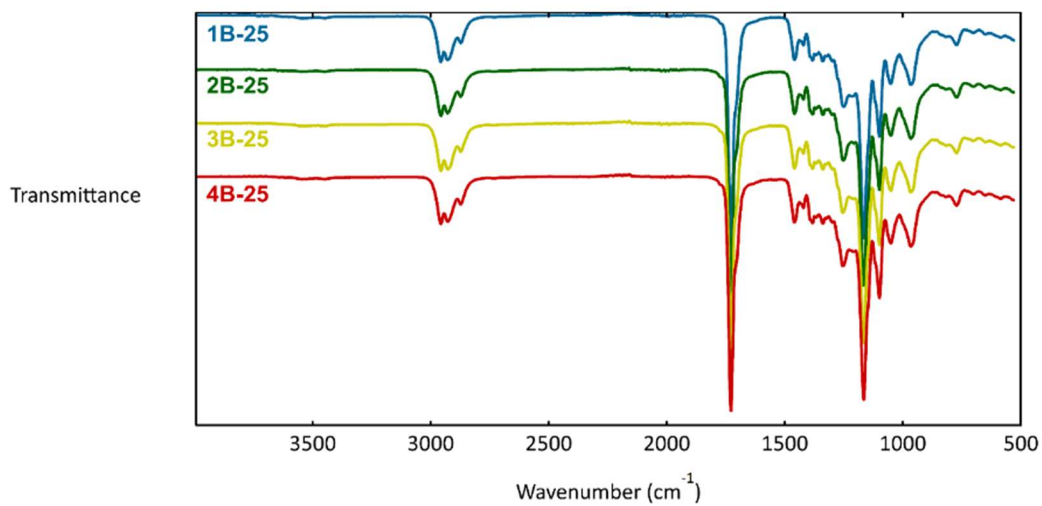


**Figure 42.** Fourier-transform infrared (FTIR) spectrum of P4MCL bottlebrush polymer networks formed from bottlebrush polymers 1B, 2B, 3B, and 4B, and cured with  $n_{cl} = 25$ .

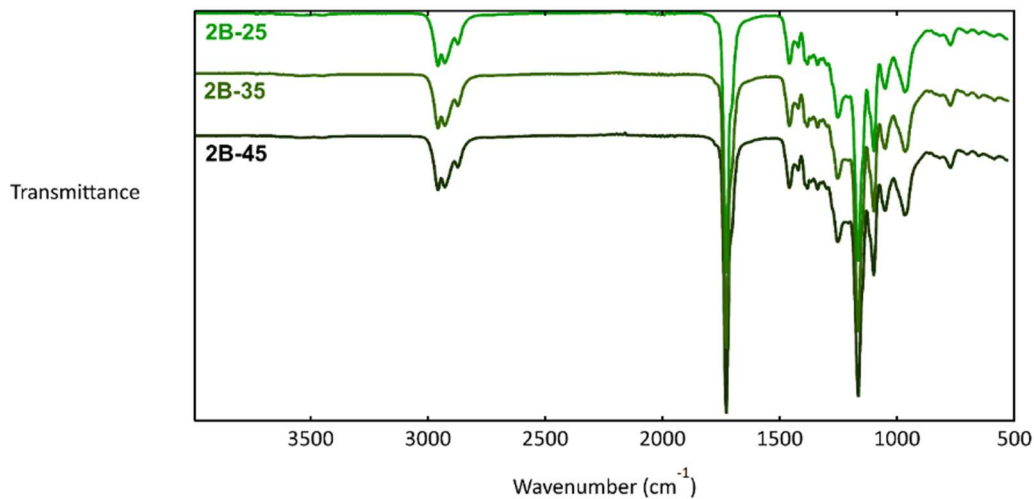


**Figure 43.** Fourier-transform infrared (FTIR) spectrum of P4MCL bottlebrush polymer networks formed from bottlebrush polymer 2B and cured with  $n_{cl} = 25, 35,$  and  $45$ .

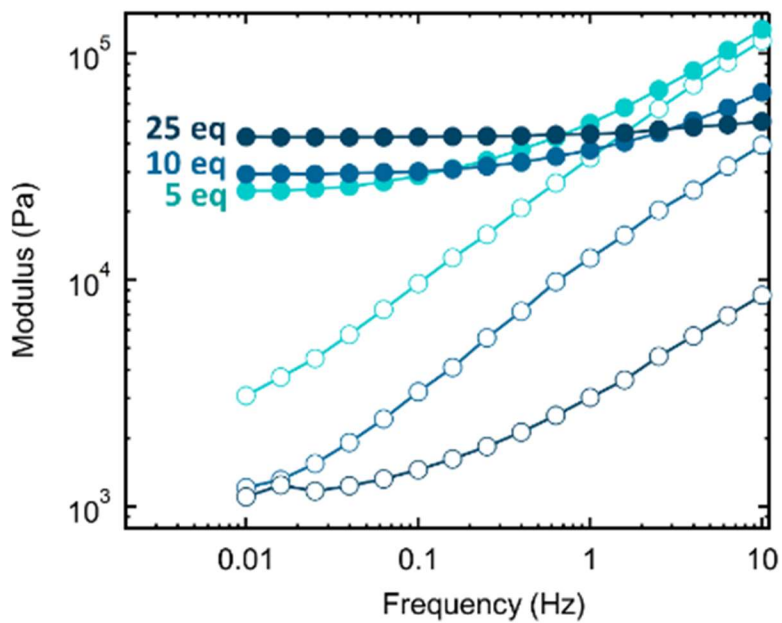


**Figure 44.** Frequency sweeps of 1A-5, 1A-10, and 1A-25, demonstrating the tunability of bottlebrush polymer properties through formulation. Filled circles are storage modulus values and open circles are loss modulus values.

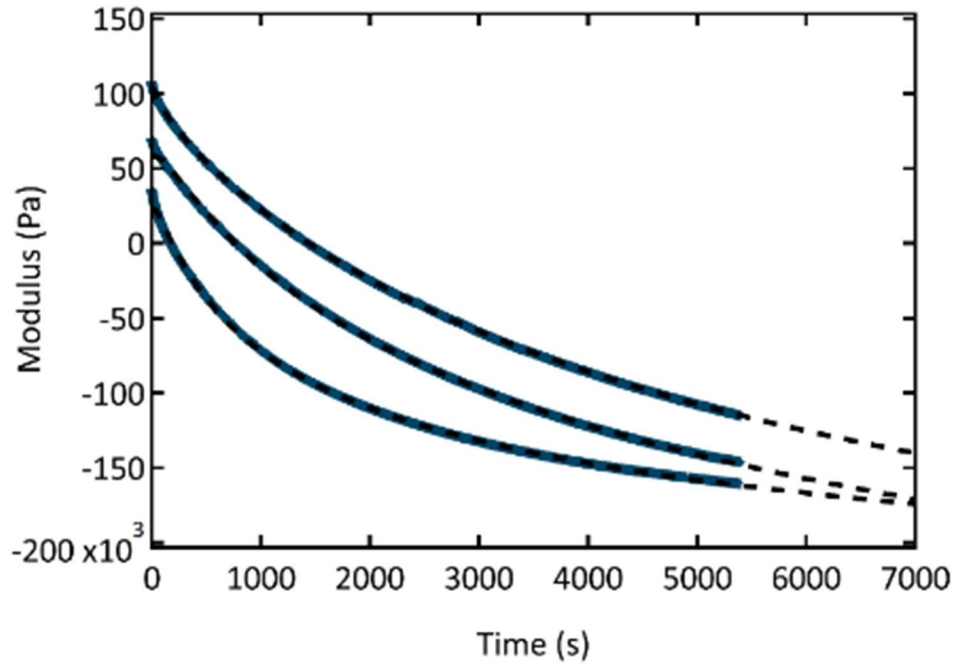


**Figure 45.** Raw stress-relaxation data for sample 1A-25 with superimposed fits.

**Table 11.** Fit parameters for 1A-25

$T$ ( $^{\circ}\text{C}$ )	$A$ (kPa)	$\tau^*$ (sec)	$\beta$	$b$ (kPa)	$(RT)^{-1}$	$\ln(\tau^*)$
180	221	1,700	0.71	-183	0.266	7.45
170	270	3,200	0.87	-201	0.272	8.05
160	341	5,100	0.78	-236	0.278	8.54

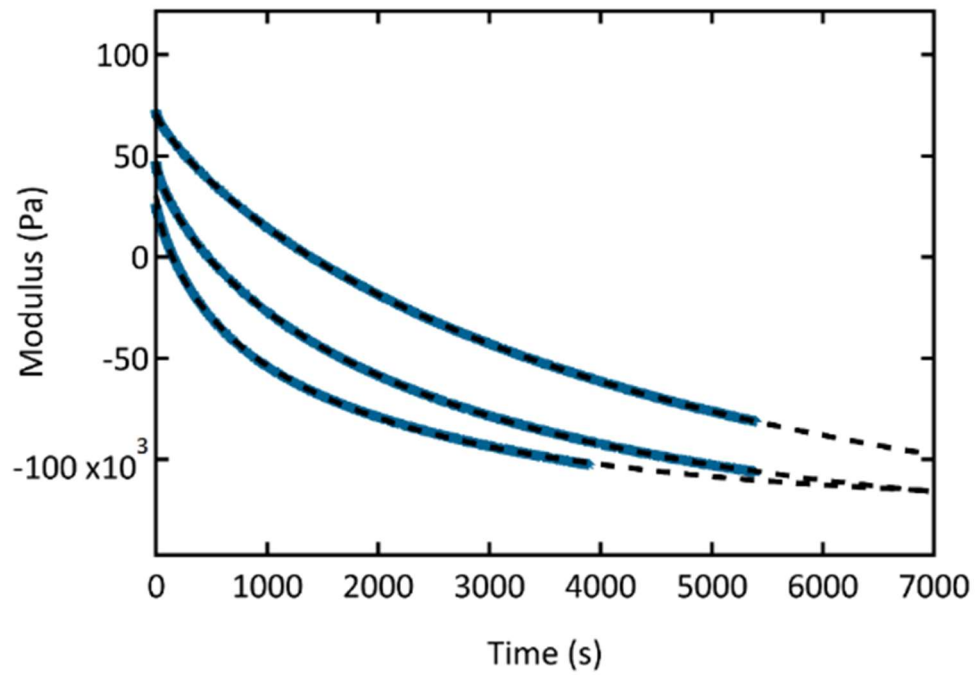


**Figure 46.** Raw stress-relaxation data for sample 1A-10 with superimposed fits.

**Table 12.** Fit parameters for 1A-10

$T$ ( $^{\circ}\text{C}$ )	$A$ (kPa)	$\tau^*$ (sec)	$\theta$	$b$ (kPa)	$(RT)^{-1}$	$\ln(\tau^*)$
180	157	1,500	0.65	-125	0.266	7.28
170	188	2,600	0.72	-140	0.272	7.86
160	220	4,400	0.82	-149	0.278	8.39

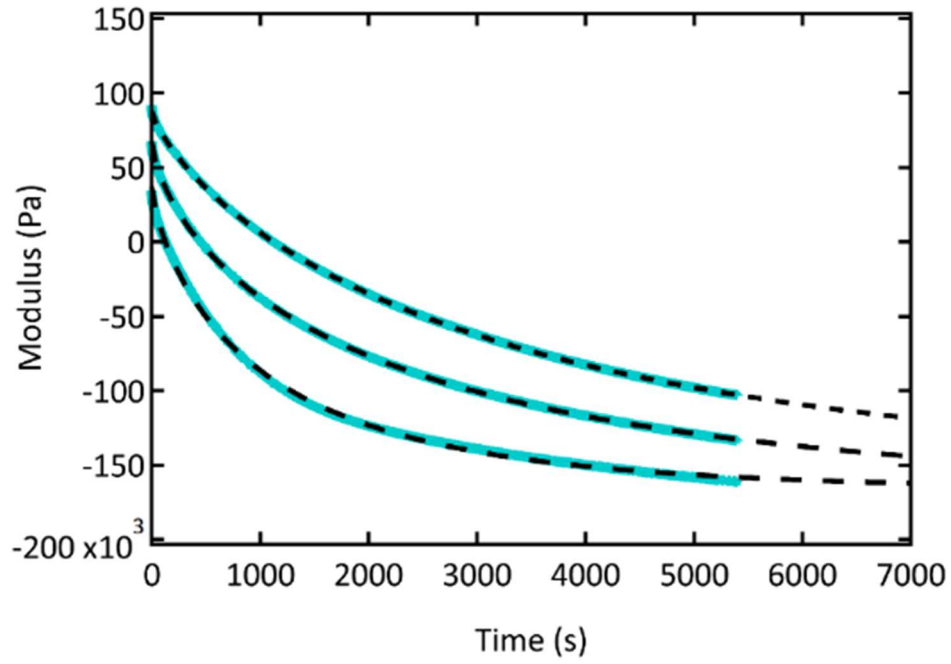


**Figure 47.** Raw stress-relaxation data for sample 1A-5 with superimposed fits.

**Table 13.** Fit parameters for 1A-10

$T$ ( $^{\circ}\text{C}$ )	$A$ (kPa)	$\tau^*$ (sec)	$B$	$b$ (kPa)	$(RT)^{-1}$	$\ln(\tau^*)$
180	205	1,100	0.73	-167	0.266	7.00
170	240	2,200	0.68	-172	0.272	7.71
160	247	3,200	0.77	-159	0.278	8.08

## **Chapter IV. Carbon nanotube-containing dynamic bottlebrush polymer composites for soft electrodes**

### **Abstract**

The advancement of wearable electronics and biointerfacing technologies requires materials that are simultaneously compliant and conductive. Conventional rubbery materials are already at the limit of stiffness compatible with biotissue ( $\geq 0.1$  MPa) and the addition of filler particles generally leads to a substantial increase in modulus, so a strategy to generate soft composites is highly desirable. Herein, we report carbon nanotube (CNT) composites containing super-soft bottlebrush polymers as the matrix to generate soft and conductive materials. At loadings of 0.25 wt% and 0.5 wt% CNT the generated composites had modulus values of 66 kPa and 140 kPa, respectively. These materials are several orders of magnitude softer than comparable composites in the literature. Despite the low loadings, the CNT-filler imbues the materials with significant conductivities. While unfilled samples are insulating, the reported composites have conductivities of  $0.006 \text{ S/m}^2$  and  $0.054 \text{ S/m}^2$ . Preliminary self-healing studies indicate these composites also retain some of the dynamic nature of the original polyester bottlebrush polymer network. We anticipate this new strategy of designing soft composites by using tailored bottlebrush polymer architecture will be of great interest to the community.

## Introduction

Electronic devices made with soft and elastic components offer unique functionality compared to conventional, rigid silicon-based technology.<sup>164</sup> Flexible and stretchable electronics have been developed for applications such as biomonitoring of physiological signals (e.g., electrocardiography, electroencephalography),<sup>165</sup> electronic skin for prosthetics and soft robotics,<sup>166,167</sup> and body motion tracking for injury rehabilitation monitoring and the assessment of motor control disorders.<sup>168</sup> Biointerfacing or biomimicking devices require elastomers with electrical and mechanical properties not typical of conventional rubbery networks. The electrical properties of elastomers can be modified through the addition of a second material, including blends (e.g., adding semiconducting polymers to create an elastic semiconductor) and composites (e.g., adding a conductive particle to create an elastic conductor).<sup>169–174</sup> Carbon nanotubes (CNTs) are ideal fillers due to their flexibility and high aspect ratio, which enables percolation at lower loadings than spherical particles.<sup>175</sup> Inclusion of these particle fillers in polymer systems presents as intrinsic challenge—the percolated particle network that imparts conductivity also increases stiffness.<sup>176</sup>

Bottlebrush polymer networks have been demonstrated to have comparable bulk mechanical properties to hydrogels without the use of solvent or plasticizer.<sup>40,139,142</sup> The development of bottlebrush polymer networks has impacted many technologies, from elastomers with unusually low moduli<sup>139</sup> to capacitive pressure sensors with enhanced sensitivity<sup>152</sup> and dielectric actuators with increased actuation.<sup>153,156</sup> The underlying principle behind these advancements is the suppression of physical entanglements due to the highly branched polymer architecture, resulting in a final polymer network with a significantly lower modulus than linear polymer analogues.<sup>139</sup> We reasoned that this same advantage could



be realized in CNT-containing composites to generate bulk materials with high conductivity and compliance which could further improve the performance of flexible electronics.

Previously, the incorporation of CNTs into dynamic networks was shown to create stiff, conductive, and self-healing materials.<sup>177–179</sup> Here, the choice of a polyester bottlebrush polymer generates low modulus materials despite the inclusion of filler materials. We present a series of dynamically crosslinked CNT-filled bottlebrush elastomers which are soft (shear modulus 66–140 kPa) and conductive (0.006–0.054 S/m). These findings broaden the utility of bottlebrush polymers to improve the properties of advanced composites.

## Results and discussion

### *Molecular design and synthesis*

P4MCL side chains were used as the bottlebrush matrix chemistry due to its low  $T_g$  and lack of crystallinity, which are crucial properties for soft elastomers.<sup>40,45</sup> Similarly, tin ethylhexanoate ( $\text{SnOct}_2$ ) was used as the transesterification catalyst as it has been well-established to promote exchange at elevated temperatures while being largely dormant under ambient conditions.<sup>40,110,178</sup> The previously used bis-lactone crosslinker had limited solubility in 4MCL monomer so a newly reported bis-lactone with a PEG-based linker was synthesized to have improved solubility.<sup>45,112</sup> The network curing chemistry is given below in **Figure 48**.

Bottlebrush polymer network design principles suggest that longer backbones (i.e., higher degree of polymerization of the backbone,  $N_{BB}$ ) are preferable for soft networks as they allow access to lower crosslinking densities, but the viscosity of bottlebrush polymers also scales with  $N_{BB}$  (assuming the sidechain  $M_n$  is held constant). Thus, high  $N_{BB}$  ( $\approx 400$ ) samples were too viscous to be incompatible with our CNT dispersion process (as detailed

in the experimental methods). More moderate  $N_{BB}$  polymers ( $\approx 100$ ) better balanced the trade-off of pre-cured viscosity and post-cured softness. To further facilitate mixing, the bottlebrush polymer was plasticized 4MCL monomer. Due to the living nature of the ring-opening polymerization, this plasticizer is incorporated directly into the network—by propagating from the ends of side chains or alcohols generated from crosslinking—during the annealing process as shown in **Figure 48**. Full synthetic methods and characterization of the materials used in this study are described in the experimental methods section.

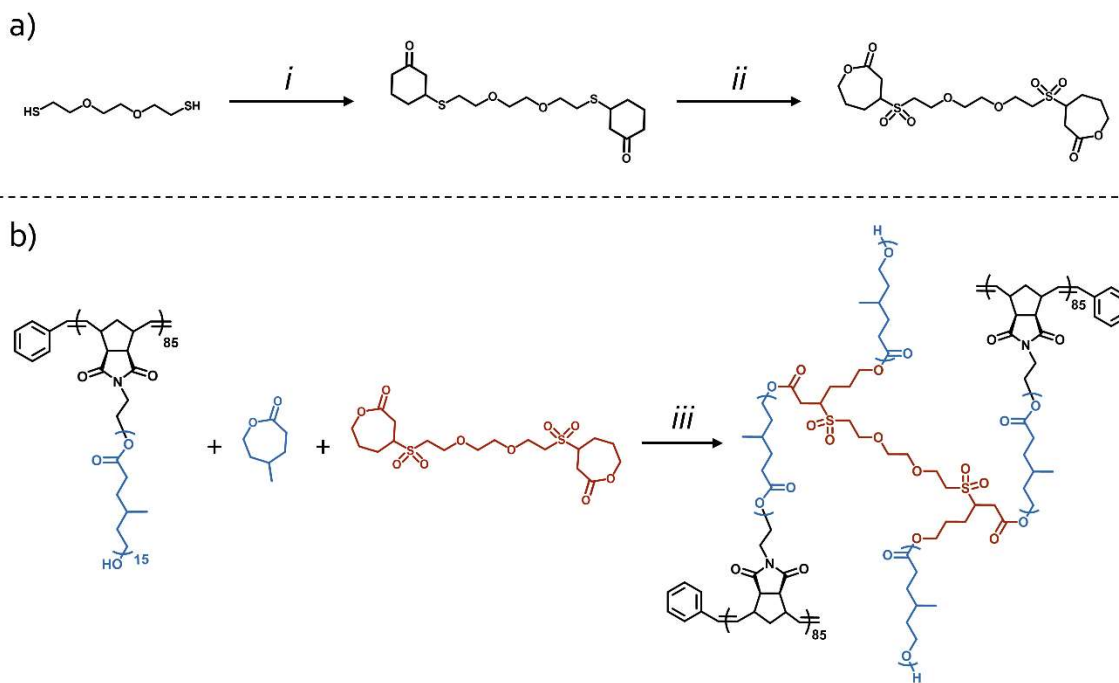


**Figure 48.** a) Two step synthesis of a bis-lactone crosslinker with improved solubility. *i*) Cyclohexanone (2.2 eq.) was added to a solution of dithiol in dichloromethane with a catalytic amount of triethylamine (0.1 eq.) and stirred overnight at room temperature; *ii*) *meta*-Chloroperoxybenzoic acid (9 eq.) was added to a 0 °C solution of the precursor in dichloromethane and stirred overnight. b) Networks formation proceeds in a single step: *iii*) At room temperature,  $\text{Sn}(\text{Oct})_2$  (1.5 wt% relative to the reaction mass) was added to the reaction solution and heated to 180 °C for 20 minutes.

### *Mechanical characterization of polymer and composite networks*

A series of samples was prepared from a 170 kDa bottlebrush polymer ( $N_{\text{BB}} = 85$ ,  $N_{\text{SC}} = 15$ ) with varying amounts of crosslinker (from 0.5 wt% to 3 wt%) to assess the efficiency of the new crosslinker. The catalyst and crosslinker loadings were kept constant at 1.5 wt% and 20 wt%, respectively (complete formulations with calculated equivalents are provided in **Table 15****Table 16****Table 17****Table 18**). Network formation proceeds rapidly at 180 °C, nearing complete conversion within 20 minutes (**Figure 49a**). After curing, the samples were cooled immediately to 25 °C and frequency sweeps were used to measure the rubbery plateau modulus (**Figure 49b**). The final material showed low plateau moduli from 18 kPa to 160 kPa (values well within range of various biological tissues)<sup>155</sup> that were easily tuned through formulation. For composite samples, the lowest crosslinker loading was used to determine if the bulk polymer softness could be retained despite the inclusion of CNT-filler particles.

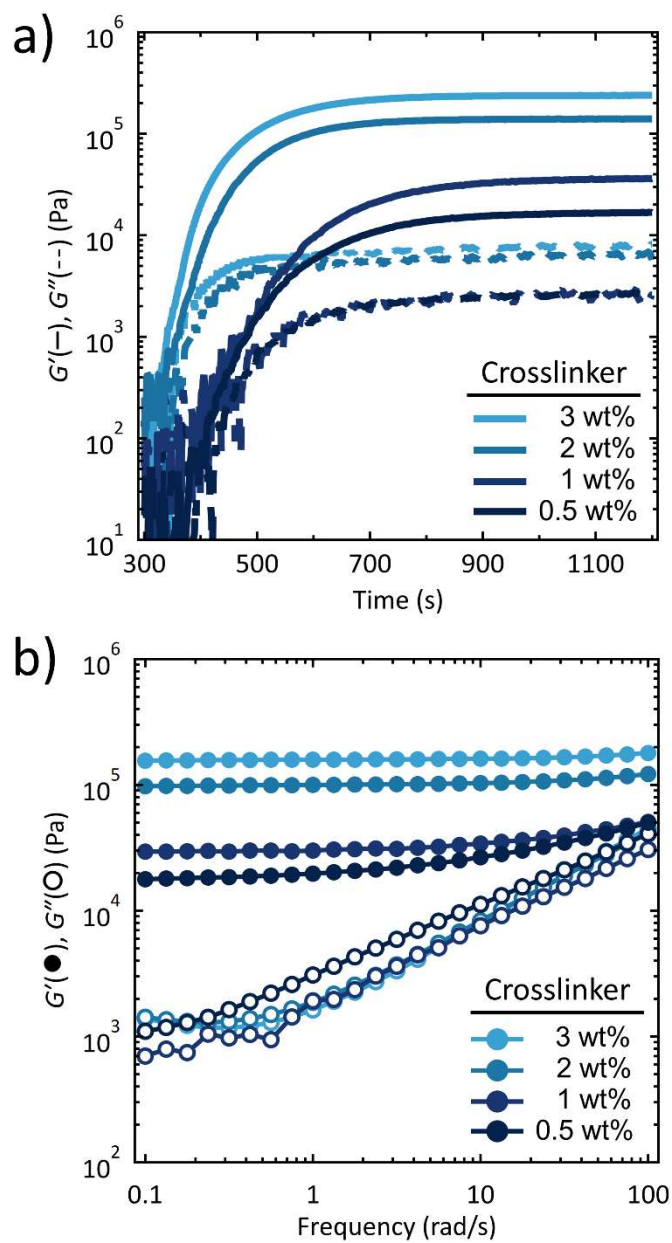


**Figure 49.** Mechanical data showing a) the curing traces of various bottlebrush polymer resins (truncated to highlight region of interest, for full trace refer to **Figure 58**) and b) frequency-dependent modulus data capturing the room temperature rubbery plateau.

The dispersion of carbon nanotubes was achieved by mechanically mixing CNT bundles into a bottlebrush polymer precursor ( $M_n = 150$  kDa,  $N_{BB} = 88$ ,  $N_{SC} = 12$ ) plasticized by 14

wt% 4MCL monomer. For the composite materials, guided by previous formulation results, a crosslinker loading of 0.5 wt% was targeted to minimize the resulting sample stiffness. The final formulation of these samples was analogous to those shown in **Figure 49**, but with the inclusion of CNT-filler: 0, 0.25, and 0.5% by weight (full formulations given in **Table 19**,

**Table 20**, and **Table 21**). As evidenced by optical microscopy (**Figure 52**), the simple mixing process works well on a gram scale to generate homogeneously dispersed CNT-doped bottlebrush polymer resins. Because high quality dispersion is critical to achieve optimal composite properties, various strategies for improving dispersion have been developed. These include, increasing the chemical compatibility of the CNTs and polymer matrix (e.g., CNT surface functionalization or addition of surfactant/dispersant molecules) and employing aggressive mixing techniques (e.g., ultrasonication or bead milling). To our delight, we found that a simple, solvent-free mixing process resulted in composites with good electrical and mechanical properties. Our process involved centrifugal mixing with ceramic cylinders added to promote shear forces to break up the CNT agglomerates. Although batch sizes in our studies rarely exceeded one gram, this mixing process can be readily scaled up.

The curing traces in **Figure 51a** show that the inclusion of CNT-filler obfuscates the development of a plateau, so the composite samples were annealed under the same conditions as the unfilled samples. Analysis of the curing traces is complicated by the fact that these materials behave elastically even prior to crosslinking as a result of their percolated filler content. This is readily observed in the pre-curing frequency sweeps, which show a rubbery plateau at low frequencies (**Figure 50**).

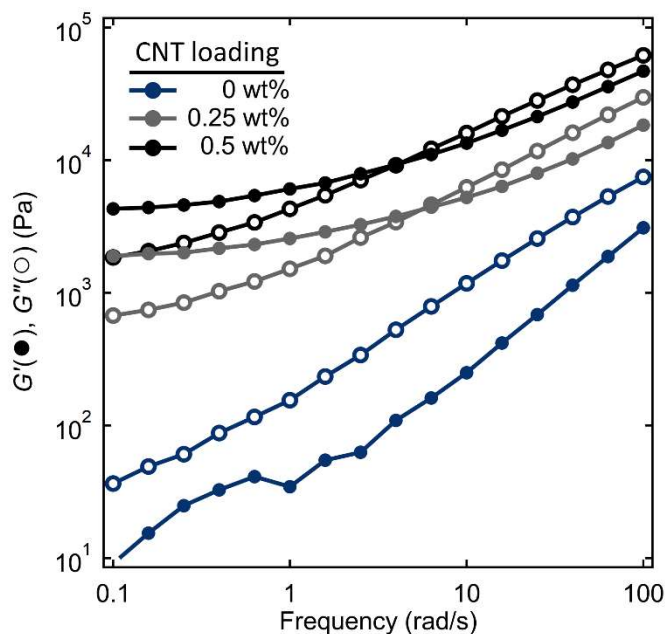


**Figure 50.** Frequency sweeps of the samples from **Figure 51** before curing. Samples with CNT-filler are elastic.

When cooled to room temperature, samples with 0, 0.25, and 0.5 wt% CNTs have shear moduli ( $G'$ ) of 31, 66, and 140 kPa, respectively. Another reported dynamic polyester CNT composite of similar filler loading (i.e., 0.25 wt% CNT) had a shear modulus of  $\approx 70$  MPa, nearly three orders of magnitude stiffer than the composites reported here.<sup>178</sup> Notably, a recently reported dynamic composite with a similar modulus (0.5 wt% CNT, 64 kPa) was achieved, but required 70 wt% solvent.<sup>180</sup> However, directly comparing modulus values of composites can be difficult as they are highly dependent on both the dispersion process and polymer matrix chemistry.<sup>176,181</sup>

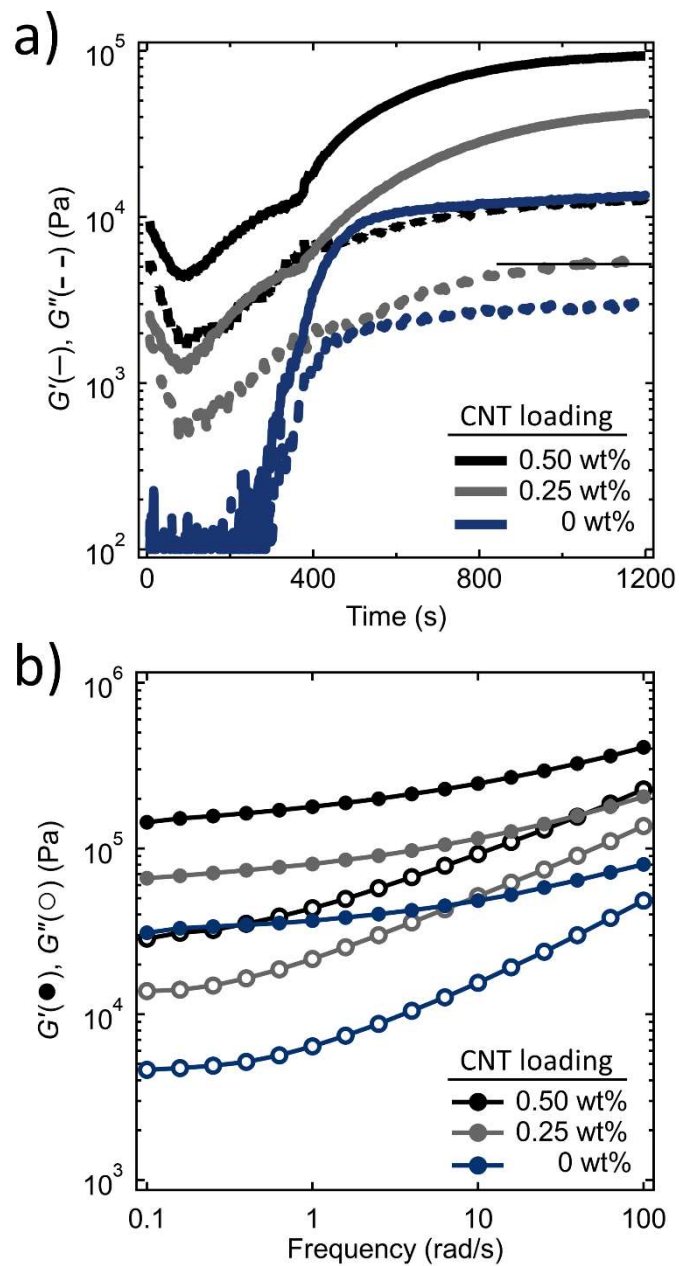


**Figure 51.** a) Composite bottlebrush polymer samples rapidly cure at 180 °C. b) Room temperature frequency sweeps after curing show a rubbery plateau.

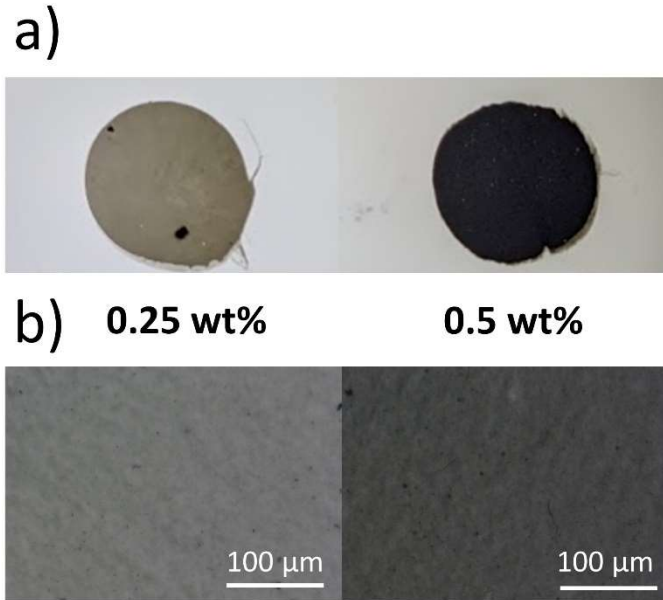


**Figure 52.** a) Optical images of two thin films with 0.25 wt% and 0.5 wt% CNTs. b) Optical microscopy (1000 $\times$  zoom) showing even CNT dispersion in the bottlebrush polymer matrix.

When heated beyond the 20 minutes which is required to cure the matrix network, the composite samples show a steady rise in modulus. This secondary curing process happens on a much longer timescale than the initial network formation and shows a nearly linear slope over time, in contrast to the characteristic S-shaped curing curves for samples without CNTs. We hypothesize that this secondary curing could stem from reactions between the bottlebrush polymer (specifically, terminal hydroxyl groups on the side chains) and functional group defects on the CNT surface (e.g., carboxylic acids and esters).<sup>182</sup> Interestingly, even in the absence of crosslinker and catalyst, this behavior persists (as shown in the experimental methods **Figure 59**), further indicating that deleterious side reactions between the bottlebrush polymer and the CNT surface could account for the rise in modulus.



*Electrical properties of bottlebrush/CNT composites*

The electrical properties of our bottlebrush–CNT composites were measured by AC impedance spectroscopy. Both the 0.25 and 0.5 wt% CNT composites exhibited stable conductivity across a wide frequency range (**Figure 53**). The samples had frequency-independent resistance and in-phase current and voltage (ideal resistor behavior) in this frequency range, with negligible capacitance (**Figure 54**). The DC conductivity,  $\sigma_{DC}$ , was calculated from the plateau value of the resistance in the low frequency limit (0.1 Hz). The 0.25 and 0.5 wt% samples had DC conductivities of 0.006 and 0.054 S/m, respectively. Conductivity increased with CNT loading as expected and the values were in the range of previously reported composites of similar CNT loadings.

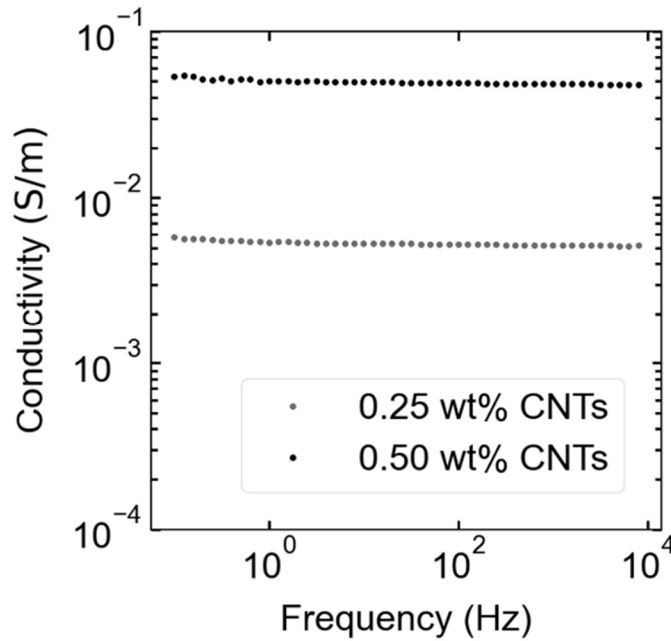


**Figure 53.** Conductivity of the 0.25 and 0.50 wt% CNT composite samples measured in the frequency range of 0.1 Hz to 10 kHz.

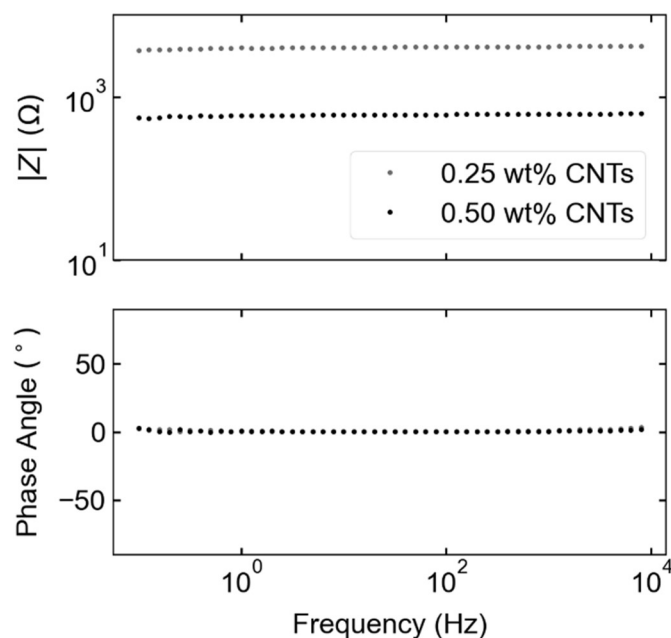


**Figure 54.** Bode plots of the 0.25 and 0.50 wt% CNT composite samples showing ideal resistor behavior in the range of 0.1 Hz to 10 kHz.

**Table 14.** Summary of P4MCL–CNT composite properties.

CNT Concentration (wt%)	Modulus (kPa)	Conductivity (S/m)
0	31	-
0.25	66	0.006
0.5	140	0.054

### *Self-healing*

Previously, polyester bottlebrush polymer networks have been shown to be dynamic and capable of efficient self-healing.<sup>40</sup> However, given the secondary curing that we observe during extended heating in the presence of CNTs, stress-relaxation experiments were not

performed at elevated temperatures on the composite networks. Instead, to gauge whether the dynamic bottlebrush matrix can be exploited in CNT composites, a simple self-healing experiment was attempted. Two rectangular samples were created; one was kept as a pristine control while the other was damaged, then re-healed by annealing in a mold at 180 °C for 1 hour. Macroscopically, the damaged pieces reformed a cohesive solid, but with a very apparent surface roughness. To more quantitatively evaluate healing efficiency, the moduli of the two samples were measured by DMA (**Figure 55a**). The pristine sample had a tensile modulus ( $E'$ ) of 200 kPa, which agrees with the value predicted from rheology under the assumption of volume-conserved deformation,  $E' = 3G' = 3(66) = 198$  kPa,<sup>162</sup> while the healed sample had a significantly lower  $E' = 82$  kPa. This result indicates that the material recovers approximately 40% of its original stiffness, lower than we would have expected from previous work on self-healing bottlebrush elastomers, perhaps due to the presence of the CNT filler particles.

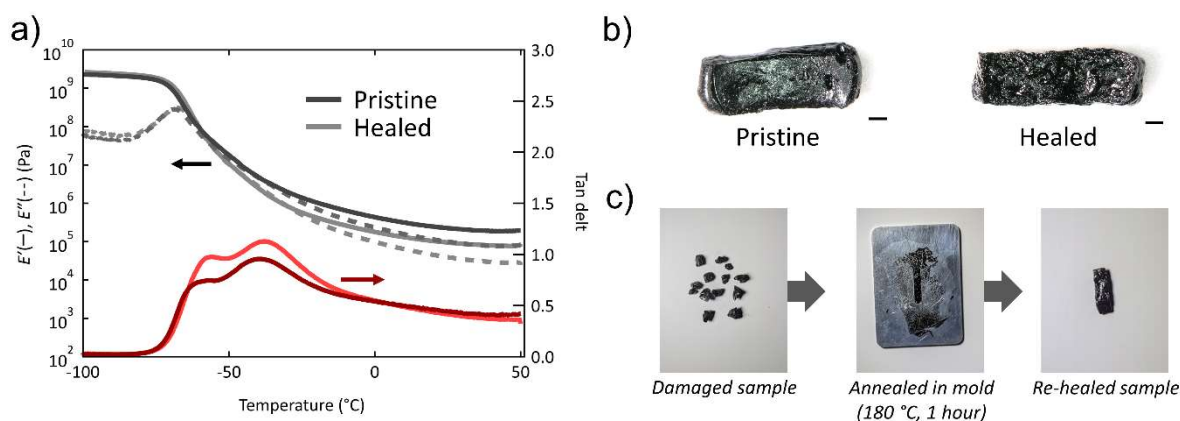


**Figure 55.** Self-healing study of a 0.25 wt% CNT composite sample with 0.5 wt% crosslinker. a) Dynamic mechanical thermal analysis showing partial recovery of the tensile modulus (measured on cooling ramp at 5 °C/min). b) Optical microscopy of pristine and healed samples; the scale bars are 1 mm. c) Pictures taken through the healing procedure.

## Conclusion

In this chapter, we explored a novel concept to access super-soft composites that exploits the bottlebrush polymer architecture. By using carbon nanotubes as the filler particles, the resulting composites achieve percolation at relatively low loadings. Specifically, two compositions were investigated with CNT loadings of 0.25 wt% and 0.5 wt%. Although stiffer than unfilled samples of similar composition ( $G' = 31$  kPa), the resulting composites had low modulus values ( $G' = 66$  kPa and 140 kPa) and comparable conductivities (0.006 and 0.054 S/m<sup>2</sup>) to linear analogues. We anticipate the findings reported here will be of significant interest to the community as a novel strategy for achieving composites with both high compliance and conductivity.

## Experimental methods

### *Reagents and solvents*

Reagents and solvents were used as received except where otherwise noted. Methylene chloride (“DCM”, ACS grade,  $\geq 99.5\%$ ), methanol (“MeOH”, 99%), and ethyl vinyl ether (“EVE”, 99%) were purchased from Fischer Scientific and used as received. Tin(II) ethyl hexanoate (Sn(Oct)<sub>2</sub>, Aldrich, 92.5–100%) was purified by fractional distillation (3 $\times$ ) under reduced pressure (0.05 Torr, 150 °C) and kept in a nitrogen-filled glovebox. 2,2'-(Ethylenedioxy)diethanethiol (95%), 2-cyclohexen-1-one ( $\geq 95\%$ ), and 3-chloroperbenzoic acid ( $>70\%$ ) were purchased from Millapore Sigma. 4-Methylcaprolactone (“4MCL”) was prepared according to previously reported methods<sup>113</sup> and further purified by three consecutive fractional distillations over calcium hydride (CaH<sub>2</sub>, Fisher Scientific, 93%). Macromonomer initiator (N-(hydroxyethyl)-cis-5-

norbornene-exo-2,3-dicarboximide, “NbOH”) was also prepared according to previously reported methods<sup>36</sup> and further purified by recrystallization from chloroform. Grubbs second-generation metathesis catalyst  $[(H_2IMes)(PCy_3)_2(Cl)_2Ru=CHPh]$ , “G2”] was generously provided by Materia. G2 was converted to Grubbs third-generation metathesis catalyst  $[(H_2IMes)(Pyr)_2(Cl)_2Ru=CHPh]$ , “G3”] following a previously reported method.<sup>163</sup>

#### *Size-exclusion chromatography instrumentation*

Size-exclusion chromatography with multi-angle light scattering detection (SEC-MALS) was performed using two Agilent columns (PLgel, 5 $\mu$ m Mini MIX-D, 250 $\times$ 4.6 mm) connected to a Waters Alliance HPLC System, 2690 separation module pump, Wyatt 18-angle DAWN HELEOS-II light scattering detector, and Wyatt REX differential refractive index detector using THF as the mobile phase. The absolute molar mass was determined by light scattering using online determination of  $dn/dc$  by assuming 100% mass elution under the peak of interest. Mass spectrometry data were collected on a Waters GCT Premier high-resolution time-of-flight mass spectrometer in the electron ionization mode. This instrument has a working mass range up to 800 m/z.

#### *Synthetic details*

Crosslinker was synthesized by a two-step method as shown in **Figure 48a**. In the first step, 2.6 g (14.2 mmol, 1 eq) of 2,2'-(ethylenedioxy)diethanethiol was diluted in 20 mL of dichloromethane. To the stirred solution, 0.14 g (1.4 mmol, 0.1 eq) of triethylamine was added and the reaction vessel was cooled to 0 °C. To the cooled solution, 3.0 g (31.2 mmol,

2.2 eq) of 2-cyclohexen-1-one is added dropwise. The reaction is stirred overnight and allowed to warm to room temperature, at which point the conversion was determined to be near quantitative. The product was isolated by removing the excess reagents *in vacuo*, giving 4.6 g (14.2 mmol, 98% yield), and used in the subsequent transformation without further purification. <sup>1</sup>H NMR (600 MHz, Chloroform-d)  $\delta$  = 3.60 (t,  $J$  = 6.8 Hz, 4H), 3.57 (s, 4H), 3.10 (tt,  $J$  = 10.3, 4.1 Hz, 2H), 2.71 (t,  $J$  = 6.69 Hz, 4H), 2.67 (m, 2H), 2.33 (ddd,  $J$  = 1.3, 10.56, 14.26 Hz, 4H), 2.27 (m, 2H), 2.1 (m, 4H), 1.67 (m, 4H).

For the following reaction, 2 g of the product from the previous reaction (5.3 mmol, 1 eq) is diluted in 50 mL dichloromethane and cooled to 0 °C. To the stirring and chilled solution, 11.1 g (48.1 mmol, 9 eq) of *meta*-chloroperoxybenzoic acid was added and allowed to react overnight. Conversion was monitored by NMR and upon complete conversion, the reaction was filtered (to remove precipitated *meta*-chlorobenzoic acid) and purified by column chromatography using a solvent gradient from pure dichloromethane to pure acetone. The final product was isolated as 1.46 g (58% yield) of a waxy solid. <sup>1</sup>H NMR (600 MHz, cdcl<sub>3</sub>)  $\delta$  = 4.34 (dd,  $J$  = 13.1, 5.5 Hz, 2H), 4.22 (dd,  $J$  = 13.2, 10.4 Hz, 2H), 3.93 – 3.83 (m, 4H), 3.60 (d,  $J$  = 4.2 Hz, 4H), 3.43 (td,  $J$  = 11.6, 2.8 Hz, 2H), 3.42 – 3.22 (m, 4H), 3.18 (dd,  $J$  = 13.8, 3.3 Hz, 2H), 2.93 (dd,  $J$  = 13.7, 11.6 Hz, 2H), 2.49 – 2.43 (m, 2H), 2.21 (dq,  $J$  = 14.8, 4.7 Hz, 2H), 2.01 – 1.91 (m, 2H), 1.90 – 1.81 (m, 2H). <sup>13</sup>C NMR (126 MHz, cdcl<sub>3</sub>)  $\delta$  171.52, 171.43, 70.40, 70.36, 70.30, 68.59, 68.57, 64.58, 64.46, 57.77, 57.69, 50.93, 50.86, 33.46, 33.40, 33.18, 32.64, 30.92, 27.27, 27.22, 27.14, 27.04, 26.83, 21.05.

Macromonomer and bottlebrush polymers were synthesized according to the synthetic procedures described in Chapter III. The SEC traces and characterization for the first macromonomer and bottlebrush system described are given below in

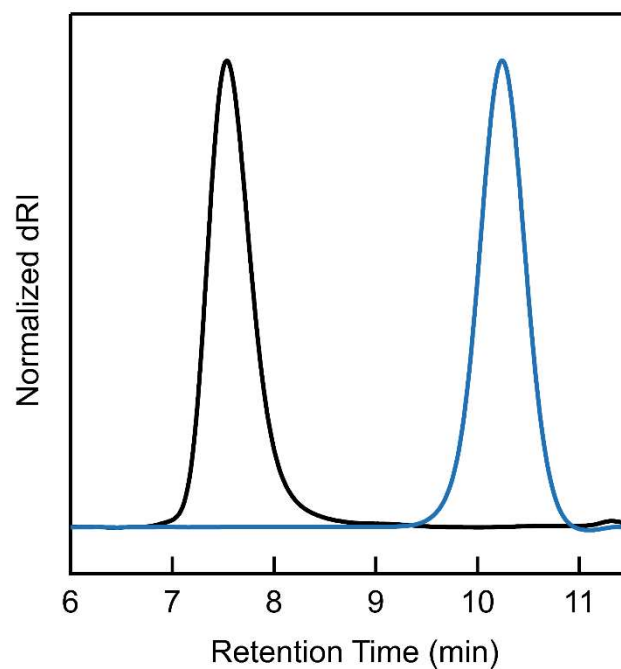


**Figure 56.** SEC trace of macromonomer ( $M_n = 2.1$  kDa,  $M_w = 2.3$  kDa,  $\mathcal{D} = 1.1$ ) and bottlebrush polymer ( $M_n = 170$  kDa,  $M_w = 190$  kDa,  $\mathcal{D} = 1.1$ ).

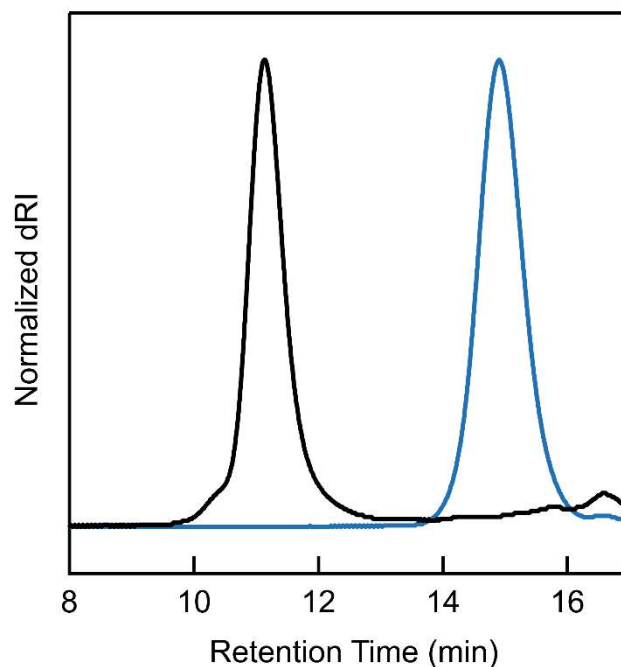


**Figure 57.** SEC trace of macromonomer ( $M_n = 1.7$  kDa,  $M_w = 1.9$  kDa,  $\bar{D} = 1.1$ ) and bottlebrush polymer ( $M_n = 150$  kDa,  $M_w = 170$  kDa,  $\bar{D} = 1.1$ ).

### *Carbon nanotube dispersion*

Single-walled carbon nanotubes (Single Walled Carbon Nanotubes 95, Cheap Tubes Inc.) were incorporated into P4MCL bottlebrush polymer using centrifugal mixing (FlackTek SpeedMixer) with ceramic cylinders to promote particle dispersion. Advantages of this dispersion method include solvent-free processing and safe, contained mixing suitable for powders such as CNTs; one requirement of this technique is a minimum batch size of approximately 1 g to achieve proper mixing. To help promote good mixing, the bottlebrush polymer was plasticized with approximately 14% by weight 4MCL monomer. The mixing



protocol began with a slow ramp in the mixing speed to 1500 RPM, at which point the sample was mixed for 45 minutes. The ceramic cylinders are not stable at speeds above 1750 RPM.

### *Mechanical analysis*

Frequency sweeps and *in situ* curing traces were obtained on a TA Instruments ARES-G2 with an 8 mm parallel-plate geometry and a nitrogen-purged forced convection oven. Strain sweeps were first collected to ensure the subsequent experiments would be within the linear viscoelastic regime (with a typical strain value being 1%). Frequency sweeps were collected from 100 rad/s to 0.1 rad/s and the reported plateau moduli correspond to the modulus as measured at the lowest frequency. Temperature-dependent modulus data were obtained on a TA Instruments DMA 850 with a film clamp geometry and a nitrogen-purged oven using a strain of 0.01% at a frequency of 1 Hz and a temperature ramp rate of 3 °C/min. Samples were approximately 3 mm by 8 mm by 1.5 mm.

### *Impedance spectroscopy*

The complex impedance was measured in the range of 0.1 Hz – 10 kHz using a Solartron 1260 Frequency Response Analyzer (100 mV AC amplitude, 4.5 V DC bias). Conductivity was extracted from the resistance using the electrode area and sample thickness.

### *Network formation procedure*

For samples without CNT filler, the crosslinker and catalyst were first weighed into a tared vial. 4MCL monomer was then added to help homogenize the crosslinker and catalyst

in solution. Lastly, P4MCL bottlebrush polymer was weighed into the vial and the contents were stirred until solution was well-mixed. The resulting viscous paste was held under vacuum overnight to facilitate the removal of any bubbles that formed during the mixing step. The reaction mixture was then loaded onto the parallel plates of the rheometer and cured *in situ* at 180 °C for 20 minutes. The full curing traces of the unfilled samples are given below in **Figure 58**.

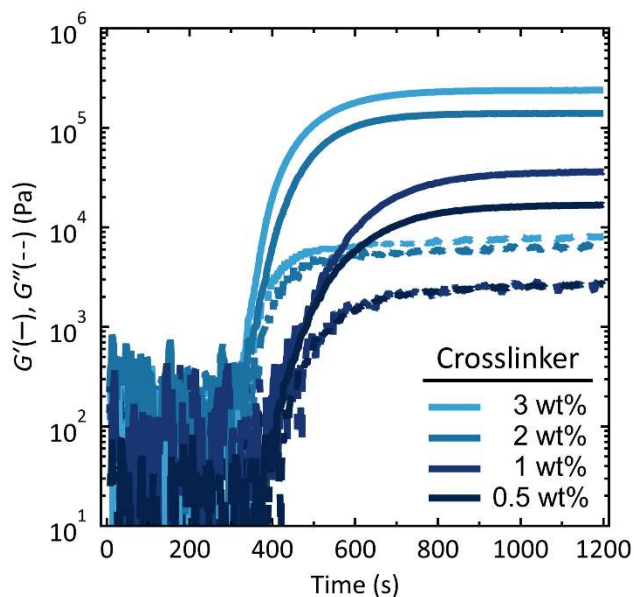


**Figure 58.** Non-truncated curing traces for unfilled samples.

For CNT-composite samples, a similar procedure was used. First, the crosslinker and catalyst were weighed into a tared vial. Then, a portion of the 4MCL monomer was added to help homogenize the crosslinker and catalyst in solution. Lastly, a mixture of P4MCL bottlebrush polymer with approximately 14% by weight 4MCL monomer and a variable amount of dispersed carbon nanotubes was added to the tared vial. This mixture was rigorously stirred until it was well-mixed. The resulting composite paste was held under vacuum overnight to facilitate the removal of any bubbles that formed during the mixing

step. The reaction mixture was loaded onto the parallel plates of the rheometer and cured *in situ* at 180 °C for 20 minutes, exactly analogous to the non-CNT samples.

Before curing, the non-filled samples flow like viscous polymers as expected, but the CNT-filled samples behave very differently. Once the CNT-filler is dispersed, the CNT/bottlebrush polymer mixture has a distinct elasticity. This is presumably due to mechanical percolation of the filler.

**Table 15.** Formulation details of the sample with 0.5 wt% crosslinker from **Figure 49**.

Compound	Molecular weight (g mol <sup>-1</sup> )	Mass (mg)	wt%	mmol × 10 <sup>3</sup>	Eq
P4MCL bottlebrush polymer	170,000	250.0	77.9%	1.47	1.0
4MCL monomer	470.13	64.2	20.0%	501	341
Crosslinker	405.12	1.7	0.5%	3.68	2.5
Sn(Oct) <sup>2</sup>	128.17	5.0	1.6%	12.4	8.4

**Table 16.** Formulation details of the sample with 1 wt% crosslinker from **Figure 49**.

Compound	Molecular weight (g mol <sup>-1</sup> )	Mass (mg)	wt%	mmol × 10 <sup>3</sup>	Eq
P4MCL bottlebrush polymer	170,000	250.0	77.4%	1.47	1.0
4MCL monomer	470.13	64.6	20.0%	504	343
Crosslinker	405.12	3.5	1.1%	7.35	5.0
Sn(Oct) <sup>2</sup>	128.17	5.0	1.5%	12.4	8.4

**Table 17.** Formulation details of the sample with 2 wt% crosslinker from **Figure 49**.

Compound	Molecular weight (g mol <sup>-1</sup> )	Mass (mg)	wt%	mmol × 10 <sup>3</sup>	Eq
P4MCL bottlebrush polymer	170,000	250.0	76.4%	1.47	1.0
4MCL monomer	470.13	65.5	20.0%	511	347
Crosslinker	405.12	6.9	2.1%	14.7	10.0
Sn(Oct) <sup>2</sup>	128.17	5.0	1.5%	12.4	8.4

**Table 18.** Formulation details of the sample with 3 wt% crosslinker from **Figure 49**.

Compound	Molecular weight (g mol <sup>-1</sup> )	Mass (mg)	wt%	mmol × 10 <sup>3</sup>	Eq
P4MCL bottlebrush polymer	170,000	250.0	75.4%	1.47	1.0
4MCL monomer	470.13	66.3	20.0%	518	352
Crosslinker	405.12	10.4	3.1%	22.1	15.0
Sn(Oct) <sup>2</sup>	128.17	5.0	1.5%	12.4	8.4

**Table 19.** Formulation details of the 0 wt% CNT composite sample from **Figure 51**.

Compound	Molecular weight (g mol <sup>-1</sup> )	Mass (mg)	wt%	mmol × 10 <sup>3</sup>	Eq
P4MCL bottlebrush polymer	170,000	350.0	77.9%	2.22	1.0
4MCL monomer	470.13	90.0	20.0%	702	317
Crosslinker	405.12	2.4	0.5%	5.10	2.3
Sn(Oct) <sup>2</sup>	128.17	6.7	1.5%	16.3	7.5
Carbon nanotubes	<i>n/a</i>	0.0	0.00%	<i>n/a</i>	<i>n/a</i>

**Table 20.** Formulation details of the 0.25 wt% CNT composite sample from **Figure 51**.

Compound	Molecular weight (g mol <sup>-1</sup> )	Mass (mg)	wt%	mmol × 10 <sup>3</sup>	Eq
P4MCL bottlebrush polymer	170,000	170.9	77.5%	1.08	1.0
4MCL monomer	470.13	44.6	20.2%	348	322
Crosslinker	405.12	1.2	0.5%	2.55	2.4
Sn(Oct) <sup>2</sup>	128.17	3.3	1.5%	8.15	7.5
Carbon nanotubes	<i>n/a</i>	0.5	0.25%	<i>n/a</i>	<i>n/a</i>

**Table 21.** Formulation details of the 0.5 wt% CNT composite sample from **Figure 51**.

Compound	Molecular weight (g mol <sup>-1</sup> )	Mass (mg)	wt%	mmol × 10 <sup>3</sup>	Eq
P4MCL bottlebrush polymer	170,000	171.6	77.5%	1.09	1.0
4MCL monomer	470.13	44.3	20.0%	345	318
Crosslinker	405.12	1.2	0.5%	2.55	2.4
Sn(Oct) <sup>2</sup>	128.17	3.3	1.5%	8.15	7.5
Carbon nanotubes	<i>n/a</i>	1.1	0.51%	<i>n/a</i>	<i>n/a</i>

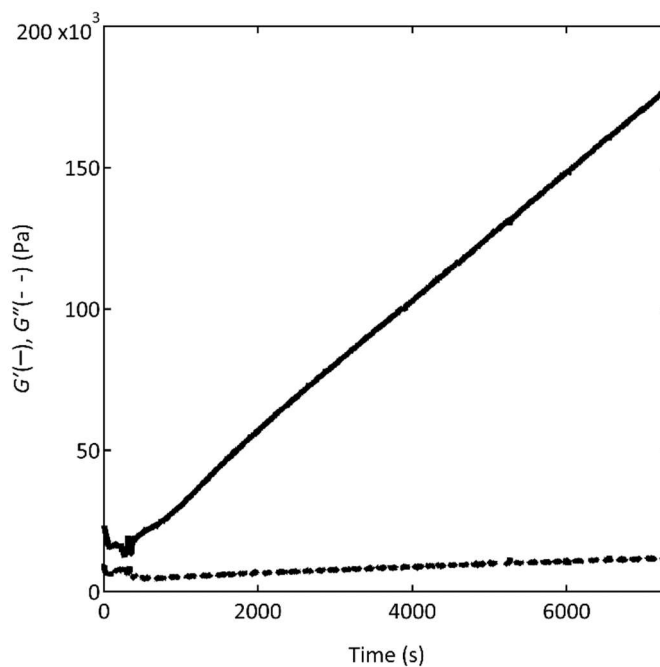


**Figure 59.** Curing of a 0.25 wt% CNT bottlebrush polymer mixture in the absence of catalyst or crosslinker shows secondary curing events over a long time-scale.

## Chapter V. References

- (1) Crespy, D.; Bozonnet, M.; Meier, M. 100 Years of Bakelite, the Material of a 1000 Uses. *Angew. Chemie Int. Ed.* **2008**, *47* (18), 3322–3328.  
<https://doi.org/10.1002/anie.200704281>.
- (2) Stern, M. D.; Tobolsky, A. V. Stress-Time-Temperature Relations in Polysulfide Rubbers. *J. Chem. Phys.* **1946**, *14* (2), 93–100. <https://doi.org/10.1063/1.1724110>.
- (3) Mochulsky, M.; Tobolsky, A. V. Chemorheology of Polysulfide Rubbers. *Ind. Eng. Chem.* **1948**, *40* (11), 2155–2163. <https://doi.org/10.1021/ie50467a030>.
- (4) Colodny, P. C.; Tobolsky, A. V. Chemorheological Study of Polyurethan Elastomers. *J. Am. Chem. Soc.* **1957**, *79* (16), 4320–4323.  
<https://doi.org/10.1021/ja01573a020>.
- (5) Johnson, D. H.; McLoughlin, J. R.; Tobolsky, A. V. Chemorheology of Some Specially Prepared Silicone Rubbers. *J. Phys. Chem.* **1954**, *58* (12), 1073–1075.  
<https://doi.org/10.1021/j150522a006>.
- (6) Osthoff, R. C.; Bueche, A. M.; Grubb, W. T. Chemical Stress-Relaxation of Polydimethylsiloxane Elastomers. *J. Am. Chem. Soc.* **1954**, *76* (18), 4659–4663.  
<https://doi.org/10.1021/ja01647a052>.
- (7) Bowman, C. Introduction to Chemistry for Covalent Adaptable Networks Polymer Chemistry Introduction to Chemistry for Covalent Adaptable Networks. *Polym. Chem* **2020**, *11*, 5295. <https://doi.org/10.1039/d0py90102d>.
- (8) Craven, J. CROSS-LINKED THERMALLY REVERSIBLE POLYMERS PRODUCED FROM CONDENSATION POLYMERS WITH PENDANT FURAN GROUPS CROSS-LINKED WITH MALEMDES. 3,435,003, June 1, 1969.

- (9) Diels, O.; Alder, K. Synthesen in Der Hydroaromatischen Reihe. *Justus Liebigs Ann. Chem.* **1928**, *460* (1), 98–122. <https://doi.org/10.1002/jlac.19284600106>.
- (10) Chen, X.; Dam, M. A.; Ono, K.; Mal, A.; Shen, H.; Nutt, S. R.; Sheran, K.; Wudl, F. A Thermally Re-Mendable Cross-Linked Polymeric Material. *Science* **2002**, *295* (5560), 1698–1702. <https://doi.org/10.1126/science.1065879>.
- (11) Montarnal, D.; Capelot, M.; Tournilhac, F.; Leibler, L. Silica-like Malleable Materials from Permanent Organic Networks. *Science* **2011**, *334* (6058), 965–968. <https://doi.org/10.1126/science.1212648>.
- (12) Scott, T. F.; Schneider, A. D.; Cook, W. D.; Bowman, C. N. Chemistry: Photoinduced Plasticity in Cross-Linked Polymers. *Science* **2005**, *308* (5728), 1615–1617. <https://doi.org/10.1126/science.1110505>.
- (13) Capelot, M.; Montarnal, D.; Tournilhac, F.; Leibler, L. Metal-Catalyzed Transesterification for Healing and Assembling of Thermosets. *J. Am. Chem. Soc.* **2012**, *134* (18), 7664–7667. <https://doi.org/10.1021/ja302894k>.
- (14) Porath, L. E.; Evans, C. M. Importance of Broad Temperature Windows and Multiple Rheological Approaches for Probing Viscoelasticity and Entropic Elasticity in Vitrimers. *Macromolecules* **2021**, *16*, acs.macromol.0c02800. <https://doi.org/10.1021/acs.macromol.0c02800>.
- (15) Li, Q.; Ma, S.; Wang, S.; Yuan, W.; Xu, X.; Wang, B.; Huang, K.; Zhu, J. Facile Catalyst-Free Synthesis, Exchanging, and Hydrolysis of an Acetal Motif for Dynamic Covalent Networks. *J. Mater. Chem. A* **2019**, *7* (30), 18039–18049. <https://doi.org/10.1039/c9ta04073k>.
- (16) Obadia, M. M.; Mudraboyina, B. P.; Serghei, A.; Montarnal, D.; Drockenmuller, E.

- Reprocessing and Recycling of Highly Cross-Linked Ion-Conducting Networks through Transalkylation Exchanges of C-N Bonds. *J. Am. Chem. Soc.* **2015**, *137* (18), 6078–6083. <https://doi.org/10.1021/jacs.5b02653>.
- (17) Hayashi, M.; Oba, Y.; Kimura, T.; Takasu, A. Simple Preparation, Properties, and Functions of Vitramer-like Polyacrylate Elastomers Using Trans-N-Alkylation Bond Exchange. *Polym. J.* **2021**, 1–6. <https://doi.org/10.1038/s41428-021-00472-4>.
- (18) Hendriks, B.; Waelkens, J.; Winne, J. M.; Du Prez, F. E. Poly(Thioether) Vitrimers via Transalkylation of Trialkylsulfonium Salts. *ACS Macro Lett.* **2017**, *6* (9), 930–934. <https://doi.org/10.1021/acsmacrolett.7b00494>.
- (19) Tang, Z.; Liu, Y.; Huang, Q.; Zhao, J.; Guo, B.; Zhang, L. A Real Recycling Loop of Sulfur-Cured Rubber through Transalkylation Exchange of C-S Bonds. *Green Chem.* **2018**, *20* (24), 5454–5458. <https://doi.org/10.1039/c8gc02932f>.
- (20) Park, H. Y.; Kloxin, C. J.; Abuelyaman, A. S.; Oxman, J. D.; Bowman, C. N. Stress Relaxation via Addition-Fragmentation Chain Transfer in High T<sub>g</sub>, High Conversion Methacrylate-Based Systems. *Macromolecules* **2012**, *45* (14), 5640–5646. <https://doi.org/10.1021/ma300228z>.
- (21) Sowan, N.; Song, H. B.; Cox, L. M.; Patton, J. R.; Fairbanks, B. D.; Ding, Y.; Bowman, C. N. Light-Activated Stress Relaxation, Toughness Improvement, and Photoinduced Reversal of Physical Aging in Glassy Polymer Networks. *Adv. Mater.* **2021**, *33* (5), 2007221. <https://doi.org/10.1002/adma.202007221>.
- (22) Cash, J. J.; Kubo, T.; Bapat, A. P.; Sumerlin, B. S. Room-Temperature Self-Healing Polymers Based on Dynamic-Covalent Boronic Esters. *Macromolecules* **2015**, *48* (7), 2098–2106. <https://doi.org/10.1021/acs.macromol.5b00210>.



- (23) Accardo, J. V.; Kalow, J. A. Reversibly Tuning Hydrogel Stiffness through Photocontrolled Dynamic Covalent Crosslinks. *Chem. Sci.* **2018**, *9* (27), 5987–5993. <https://doi.org/10.1039/c8sc02093k>.
- (24) Cromwell, O. R.; Chung, J.; Guan, Z. Malleable and Self-Healing Covalent Polymer Networks through Tunable Dynamic Boronic Ester Bonds. *J. Am. Chem. Soc.* **2015**, *137* (20), 6492–6495. <https://doi.org/10.1021/jacs.5b03551>.
- (25) Smithmyer, M. E.; Deng, C. C.; Cassel, S. E.; LeValley, P. J.; Sumerlin, B. S.; Kloxin, A. M. Self-Healing Boronic Acid-Based Hydrogels for 3D Co-Cultures. *ACS Macro Lett.* **2018**, *7* (9), 1105–1110. <https://doi.org/10.1021/acsmacrolett.8b00462>.
- (26) Brooks, W. L. A.; Sumerlin, B. S. Synthesis and Applications of Boronic Acid-Containing Polymers: From Materials to Medicine. *Chem. Rev.* **2016**, *116* (3), 1375–1397. <https://doi.org/10.1021/acs.chemrev.5b00300>.
- (27) Lascano, S.; Zhang, K. Da; Wehlauch, R.; Gademann, K.; Sakai, N.; Matile, S. The Third Orthogonal Dynamic Covalent Bond. *Chem. Sci.* **2016**, *7* (7), 4720–4724. <https://doi.org/10.1039/c6sc01133k>.
- (28) Ogden, W. A.; Guan, Z. Recyclable, Strong, and Highly Malleable Thermosets Based on Boroxine Networks. *J. Am. Chem. Soc.* **2018**, *140* (20), 6217–6220. <https://doi.org/10.1021/jacs.8b03257>.
- (29) Jiang, Z. C.; Xiao, Y. Y.; Yin, L.; Han, L.; Zhao, Y. “Self-Lockable” Liquid Crystalline Diels–Alder Dynamic Network Actuators with Room Temperature Programmability and Solution Reprocessability. *Angew. Chemie - Int. Ed.* **2020**, *59* (12), 4925–4931. <https://doi.org/10.1002/anie.202000181>.

- (30) Chou, C. I.; Liu, Y. L. High Performance Thermosets from a Curable Diels-Alder Polymer Possessing Benzoxazine Groups in the Main Chain. *J. Polym. Sci. Part A Polym. Chem.* **2008**, *46* (19), 6509–6517. <https://doi.org/10.1002/pola.22960>.
- (31) Chujo, Y.; Sada, K.; Saegusa, T. Reversible Gelation of Polyoxazoline by Means of Diels-Alder Reaction. *Macromolecules* **1990**, *23* (10), 2636–2641. <https://doi.org/10.1021/ma00212a007>.
- (32) Canary, S. A.; Stevens, M. P. Thermally Reversible Crosslinking of Polystyrene via the Furan–Maleimide Diels–Alder Reaction. *J. Polym. Sci. Part A Polym. Chem.* **1992**, *30* (8), 1755–1760. <https://doi.org/10.1002/pola.1992.080300829>.
- (33) Liu, Y.-L.; Chuo, T.-W. Self-Healing Polymers Based on Thermally Reversible Diels–Alder Chemistry. *Polym. Chem.* **2013**, *4* (7), 2194. <https://doi.org/10.1039/c2py20957h>.
- (34) Kuramoto, N.; Hayashi, K.; Nagai, K. Thermoreversible Reaction of Diels—Alder Polymer Composed of Difurfuryladipate with Bismaleimidodiphenylmethane. *J. Polym. Sci. Part A Polym. Chem.* **1994**, *32* (13), 2501–2504. <https://doi.org/10.1002/pola.1994.080321312>.
- (35) Michal, B. T.; Jaye, C. A.; Spencer, E. J.; Rowan, S. J. Inherently Photohealable and Thermal Shape-Memory Polydisulfide Networks. *ACS Macro Lett.* **2013**, *2* (8), 694–699. <https://doi.org/10.1021/mz400318m>.
- (36) Arrington, K. J.; Radzinski, S. C.; Drummey, K. J.; Long, T. E.; Matson, J. B. Reversibly Cross-Linkable Bottlebrush Polymers as Pressure-Sensitive Adhesives. *ACS Appl. Mater. Interfaces* **2018**, *10* (31), 26662–26668. <https://doi.org/10.1021/acsami.8b08480>.

- (37) Wang, Z.; He, Q.; Wang, Y.; Cai, S. Programmable Actuation of Liquid Crystal Elastomers: Via “Living” Exchange Reaction. *Soft Matter* **2019**, *15* (13), 2811–2816. <https://doi.org/10.1039/c9sm00322c>.
- (38) He, Q.; Wang, Z.; Wang, Y.; Song, Z.; Cai, S. Recyclable and Self-Repairable Fluid-Driven Liquid Crystal Elastomer Actuator. *ACS Appl. Mater. Interfaces* **2020**, *12* (31), 35464–35474. <https://doi.org/10.1021/acsami.0c10021>.
- (39) Chen, Q.; Wei, Y.; Ji, Y. Photo-Responsive Liquid Crystalline Vitriimer Containing Oligoanilines. *Chinese Chem. Lett.* **2017**, *28* (11), 2139–2142. <https://doi.org/10.1016/j.ccllet.2017.09.011>.
- (40) Self, J. L.; Sample, C. S.; Levi, A. E.; Li, K.; Xie, R.; de Alaniz, J. R.; Bates, C. M. Dynamic Bottlebrush Polymer Networks: Self-Healing in Super-Soft Materials. *J. Am. Chem. Soc.* **2020**, *142* (16), 7567–7573. <https://doi.org/10.1021/jacs.0c01467>.
- (41) Moazzen, K.; Rossegger, E.; Alabiso, W.; Shaukat, U.; Schlögl, S. Role of Organic Phosphates and Phosphonates in Catalyzing Dynamic Exchange Reactions in Thiol-Click Vitrimers. *Macromol. Chem. Phys.* **2021**, 2100072. <https://doi.org/10.1002/macp.202100072>.
- (42) Yang, Y.; Pei, Z.; Li, Z.; Wei, Y.; Ji, Y. Making and Remaking Dynamic 3D Structures by Shining Light on Flat Liquid Crystalline Vitriimer Films without a Mold. *J. Am. Chem. Soc.* **2016**, *138* (7), 2118–2121. <https://doi.org/10.1021/jacs.5b12531>.
- (43) Liu, W.; Schmidt, D. F.; Reynaud, E. Catalyst Selection, Creep, and Stress Relaxation in High-Performance Epoxy Vitrimers. *Ind. Eng. Chem. Res.* **2017**, *56* (10), 2667–2672. <https://doi.org/10.1021/acs.iecr.6b03829>.

- (44) Capelot, M.; Unterlass, M. M.; Tournilhac, F.; Leibler, L. Catalytic Control of the Vitrimer Glass Transition. *ACS Macro Lett.* **2012**, *1* (7), 789–792.  
<https://doi.org/10.1021/mz300239f>.
- (45) Self, J. L.; Dolinski, N. D.; Zayas, M. S.; Read De Alaniz, J.; Bates, C. M. Brønsted-Acid-Catalyzed Exchange in Polyester Dynamic Covalent Networks. *ACS Macro Lett.* **2018**, *7* (7), 817–821. <https://doi.org/10.1021/acsmacrolett.8b00370>.
- (46) Xu, X.; Ma, S.; Wang, S.; Wu, J.; Li, Q.; Lu, N.; Liu, Y.; Yang, J.; Feng, J.; Zhu, J. Dihydrazone-Based Dynamic Covalent Epoxy Networks with High Creep Resistance, Controlled Degradability, and Intrinsic Antibacterial Properties from Bioresources. *J. Mater. Chem. A* **2020**, *8* (22), 11261–11274.  
<https://doi.org/10.1039/d0ta01419b>.
- (47) Belowich, M. E.; Stoddart, J. F. Dynamic Imine Chemistry. *Chem. Soc. Rev.* **2012**, *41* (6), 2003–2024. <https://doi.org/10.1039/c2cs15305j>.
- (48) Taynton, P.; Ni, H.; Zhu, C.; Yu, K.; Loob, S.; Jin, Y.; Qi, H. J.; Zhang, W. Repairable Woven Carbon Fiber Composites with Full Recyclability Enabled by Malleable Polyimine Networks. *Adv. Mater.* **2016**, *28* (15), 2904–2909.  
<https://doi.org/10.1002/adma.201505245>.
- (49) Dhers, S.; Vantomme, G.; Avérous, L. A Fully Bio-Based Polyimine Vitrimer Derived from Fructose. *Green Chem.* **2019**, *21* (7), 1596–1601.  
<https://doi.org/10.1039/c9gc00540d>.
- (50) Song, F.; Li, Z.; Jia, P.; Zhang, M.; Bo, C.; Feng, G.; Hu, L.; Zhou, Y. Tunable “Soft and Stiff”, Self-Healing, Recyclable, Thermadappt Shape Memory Biomass Polymers Based on Multiple Hydrogen Bonds and Dynamic Imine Bonds. *J. Mater. Chem. A*

- 2019**, 7 (21), 13400–13410. <https://doi.org/10.1039/c9ta03872h>.
- (51) Chao, A.; Negulescu, I.; Zhang, D. Dynamic Covalent Polymer Networks Based on Degenerative Imine Bond Exchange: Tuning the Malleability and Self-Healing Properties by Solvent. *Macromolecules* **2016**, 49 (17), 6277–6284. <https://doi.org/10.1021/acs.macromol.6b01443>.
- (52) Zhao, S.; Abu-Omar, M. M. Recyclable and Malleable Epoxy Thermoset Bearing Aromatic Imine Bonds. *Macromolecules* **2018**, 51 (23), 9816–9824. <https://doi.org/10.1021/acs.macromol.8b01976>.
- (53) Lu, Y. X.; Tournilhac, F.; Leibler, L.; Guan, Z. Making Insoluble Polymer Networks Malleable via Olefin Metathesis. *J. Am. Chem. Soc.* **2012**, 134 (20), 8424–8427. <https://doi.org/10.1021/ja303356z>.
- (54) Lu, Y. X.; Guan, Z. Olefin Metathesis for Effective Polymer Healing via Dynamic Exchange of Strong Carbon-Carbon Double Bonds. *J. Am. Chem. Soc.* **2012**, 134 (34), 14226–14231. <https://doi.org/10.1021/ja306287s>.
- (55) He, C.; Shi, S.; Wang, D.; Helms, B. A.; Russell, T. P. Poly(Oxime-Ester) Vitrimers with Catalyst-Free Bond Exchange. *J. Am. Chem. Soc.* **2019**, 141 (35), 13753–13757. <https://doi.org/10.1021/jacs.9b06668>.
- (56) Saed, M. O.; Terentjev, E. M. Siloxane Crosslinks with Dynamic Bond Exchange Enable Shape Programming in Liquid-Crystalline Elastomers. *Sci. Rep.* **2020**, 10 (1), 1–10. <https://doi.org/10.1038/s41598-020-63508-4>.
- (57) Zheng, P.; McCarthy, T. J. A Surprise from 1954: Siloxane Equilibration Is a Simple, Robust, and Obvious Polymer Self-Healing Mechanism. *J. Am. Chem. Soc.* **2012**, 134 (4), 2024–2027. <https://doi.org/10.1021/ja2113257>.

- (58) Tretbar, C. A.; Neal, J. A.; Guan, Z. Direct Silyl Ether Metathesis for Vitrimers with Exceptional Thermal Stability. *J. Am. Chem. Soc.* **2019**, *141* (42), 16595–16599. <https://doi.org/10.1021/jacs.9b08876>.
- (59) Zych, A.; Pinalli, R.; Soliman, M.; Vachon, J.; Dalcanale, E. Polyethylene Vitrimers via Silyl Ether Exchange Reaction. *Polymer (Guildf)*. **2020**, *199*, 122567. <https://doi.org/10.1016/j.polymer.2020.122567>.
- (60) Nishimura, Y.; Chung, J.; Muradyan, H.; Guan, Z. Silyl Ether as a Robust and Thermally Stable Dynamic Covalent Motif for Malleable Polymer Design. *J. Am. Chem. Soc.* **2017**, *139* (42), 14881–14884. <https://doi.org/10.1021/jacs.7b08826>.
- (61) Podgórski, M.; Mavila, S.; Huang, S.; Spurgin, N.; Sinha, J.; Bowman, C. N. Thiol–Anhydride Dynamic Reversible Networks. *Angew. Chemie Int. Ed.* **2020**, *59* (24), 9345–9349. <https://doi.org/10.1002/anie.202001388>.
- (62) Podgórski, M.; Spurgin, N.; Mavila, S.; Bowman, C. N. Mixed Mechanisms of Bond Exchange in Covalent Adaptable Networks: Monitoring the Contribution of Reversible Exchange and Reversible Addition in Thiol-Succinic Anhydride Dynamic Networks. *Polym. Chem.* **2020**, *11* (33), 5365–5376. <https://doi.org/10.1039/d0py00091d>.
- (63) Podgórski, M.; Huang, S.; Bowman, C. N. Additive Manufacture of Dynamic Thiol–Ene Networks Incorporating Anhydride-Derived Reversible Thioester Links. *ACS Appl. Mater. Interfaces* **2021**, *13*, 12789–12796. <https://doi.org/10.1021/acsami.0c18979>.
- (64) Wen, Z.; Han, X.; Fairbanks, B. D.; Yang, K.; Bowman, C. N. Development of Thiourethanes as Robust, Reprocessable Networks. *Polymer (Guildf)*. **2020**, *202*,

122715. <https://doi.org/10.1016/j.polymer.2020.122715>.
- (65) Li, L.; Chen, X.; Torkelson, J. M. Reprocessable Polymer Networks via Thiourethane Dynamic Chemistry: Recovery of Cross-Link Density after Recycling and Proof-of-Principle Solvolysis Leading to Monomer Recovery. *Macromolecules* **2019**, *52* (21), 8207–8216. <https://doi.org/10.1021/acs.macromol.9b01359>.
- (66) Huang, S.; Podgórski, M.; Han, X.; Bowman, C. N. Chemical Recycling of Poly(Thiourethane) Thermosets Enabled by Dynamic Thiourethane Bonds. *Polym. Chem.* **2020**, *11* (43), 6879–6883. <https://doi.org/10.1039/d0py01050b>.
- (67) Chen, X.; Li, L.; Jin, K.; Torkelson, J. M. Reprocessable Polyhydroxyurethane Networks Exhibiting Full Property Recovery and Concurrent Associative and Dissociative Dynamic Chemistry: Via Transcarbamoylation and Reversible Cyclic Carbonate Aminolysis. *Polym. Chem.* **2017**, *8* (41), 6349–6355. <https://doi.org/10.1039/c7py01160a>.
- (68) Fortman, D. J.; Sheppard, D. T.; Dichtel, W. R. Reprocessing Cross-Linked Polyurethanes by Catalyzing Carbamate Exchange. *Macromolecules* **2019**, *52* (16), 6330–6335. <https://doi.org/10.1021/acs.macromol.9b01134>.
- (69) Shi, J.; Zheng, T.; Zhang, Y.; Guo, B.; Xu, J. Reprocessable Cross-Linked Polyurethane with Dynamic and Tunable Phenol-Carbamate Network. *ACS Sustain. Chem. Eng.* **2020**, *8* (2), 1207–1218. <https://doi.org/10.1021/acssuschemeng.9b06435>.
- (70) Chen, X.; Hu, S.; Li, L.; Torkelson, J. M. Dynamic Covalent Polyurethane Networks with Excellent Property and Cross-Link Density Recovery after Recycling and Potential for Monomer Recovery. *ACS Appl. Polym. Mater.* **2020**, *2* (5), 2093–2101.

- <https://doi.org/10.1021/acsapm.0c00378>.
- (71) Elizalde, F.; Aguirresarobe, R. H.; Gonzalez, A.; Sardon, H. Dynamic Polyurethane Thermosets: Tuning Associative/Dissociative Behavior by Catalyst Selection. *Polym. Chem.* **2020**, *11* (33), 5386–5396. <https://doi.org/10.1039/d0py00842g>.
- (72) Cox, L. M.; Sun, X.; Wang, C.; Sowan, N.; Killgore, J. P.; Long, R.; Wu, H. A.; Bowman, C. N.; Ding, Y. Light-Stimulated Permanent Shape Reconfiguration in Cross-Linked Polymer Microparticles. *ACS Appl. Mater. Interfaces* **2017**, *9* (16), 14422–14428. <https://doi.org/10.1021/acsami.7b02759>.
- (73) Denissen, W.; Droesbeke, M.; Nicola, R.; Leibler, L.; Winne, J. M.; Du Prez, F. E. Chemical Control of the Viscoelastic Properties of Vinylogous Urethane Vitrimers. *Nat. Commun.* **2017**, *8* (1), 1–7. <https://doi.org/10.1038/ncomms14857>.
- (74) Tellers, J.; Pinalli, R.; Soliman, M.; Vachon, J.; Dalcanale, E. Reprocessable Vinylogous Urethane Cross-Linked Polyethylene: Via Reactive Extrusion. *Polym. Chem.* **2019**, *10* (40), 5534–5542. <https://doi.org/10.1039/c9py01194c>.
- (75) Denissen, W.; Rivero, G.; Nicola, R.; Leibler, L.; Winne, J. M.; Du Prez, F. E. Vinylogous Urethane Vitrimers. *Adv. Funct. Mater.* **2015**, *25* (16), 2451–2457. <https://doi.org/10.1002/adfm.201404553>.
- (76) Bai, L.; Zheng, J. Robust, Reprocessable and Shape-Memory Vinylogous Urethane Vitriomer Composites Enhanced by Sacrificial and Self-Catalysis Zn(II)–Ligand Bonds. *Compos. Sci. Technol.* **2020**, *190*, 108062. <https://doi.org/10.1016/j.compscitech.2020.108062>.
- (77) Elling, B. R.; Dichtel, W. R. Reprocessable Cross-Linked Polymer Networks: Are Associative Exchange Mechanisms Desirable? *ACS Cent. Sci.* **2020**, *6* (9), 1488–



1496. <https://doi.org/10.1021/acscentsci.0c00567>.
- (78) Hsissou, R.; Seghiri, R.; Benzekri, Z.; Hilali, M.; Rafik, M.; Elharfi, A. Polymer Composite Materials: A Comprehensive Review. *Composite Structures*. Elsevier Ltd April 15, 2021, p 113640. <https://doi.org/10.1016/j.compstruct.2021.113640>.
- (79) Das, S. *THE COST OF AUTOMOTIVE POLYMER COMPOSITES: A REVIEW AND ASSESSMENT OF DOE'S LIGHTWEIGHT MATERIALS COMPOSITES RESEARCH*; Oak Ridge, Tennessee, 2001.
- (80) Zhou, Q.; Zhu, X.; Zhang, W.; Song, N.; Ni, L. Recyclable High Performance Epoxy Composites Based on Double Dynamic Carbon–Nitrogen and Disulfide Bonds. *ACS Appl. Polym. Mater.* **2020**, *2* (5), 1865–1873.  
<https://doi.org/10.1021/acsapm.0c00105>.
- (81) Kissounko, D. A.; Taynton, P.; Kaffer, C. New Material: Vitrimers Promise to Impact Composites. *Reinf. Plast.* **2018**, *62* (3), 162–166.  
<https://doi.org/10.1016/j.repl.2017.06.084>.
- (82) Yuan, Y.; Sun, Y.; Yan, S.; Zhao, J.; Liu, S.; Zhang, M.; Zheng, X.; Jia, L. Multiply Fully Recyclable Carbon Fibre Reinforced Heat-Resistant Covalent Thermosetting Advanced Composites. *Nat. Commun.* **2017**, *8* (1), 1–11.  
<https://doi.org/10.1038/ncomms14657>.
- (83) Suslu, H.; Fan, J.; Ibekwe, S.; Jerro, D.; Mensah, P.; Li, G. Shape Memory Alloy Reinforced Vitrimer Composite for Healing Wide-Opened Cracks. *Smart Mater. Struct.* **2020**, *29* (6), 065008. <https://doi.org/10.1088/1361-665X/ab85a7>.
- (84) Ji, F.; Liu, X.; Sheng, D.; Yang, Y. Epoxy-Vitrimer Composites Based on Exchangeable Aromatic Disulfide Bonds: Reprocessibility, Adhesive, Multi-Shape

- Memory Effect. *Polymer (Guildf)*. **2020**, *197*, 122514.  
<https://doi.org/10.1016/j.polymer.2020.122514>.
- (85) Jouyandeh, M.; Tikhani, F.; Hampp, N.; Akbarzadeh Yazdi, D.; Zarrintaj, P.; Reza Ganjali, M.; Reza Saeb, M. Highly Curable Self-Healing Vitriimer-like Cellulose-Modified Halloysite Nanotube/Epoxy Nanocomposite Coatings. *Chem. Eng. J.* **2020**, *396*, 125196. <https://doi.org/10.1016/j.cej.2020.125196>.
- (86) Legrand, A.; Soulié-Ziakovic, C. Silica-Epoxy Vitriimer Nanocomposites. *Macromolecules* **2016**, *49* (16), 5893–5902.  
<https://doi.org/10.1021/acs.macromol.6b00826>.
- (87) Memon, H.; Wei, Y. Welding and Reprocessing of Disulfide-Containing Thermoset Epoxy Resin Exhibiting Behavior Reminiscent of a Thermoplastic. *J. Appl. Polym. Sci.* **2020**, *137* (47), 49541. <https://doi.org/10.1002/app.49541>.
- (88) Qiu, M.; Wu, S.; Tang, Z.; Guo, B. Exchangeable Interfacial Crosslinks towards Mechanically Robust Elastomer/Carbon Nanotubes Vitrimers. *Compos. Sci. Technol.* **2018**, *165*, 24–30. <https://doi.org/10.1016/j.compscitech.2018.06.004>.
- (89) Ligon, S. C.; Liska, R.; Stampfl, J.; Gurr, M.; Mülhaupt, R. Polymers for 3D Printing and Customized Additive Manufacturing. *Chem. Rev.* **2017**, *117* (15), 10212–10290.  
<https://doi.org/10.1021/acs.chemrev.7b00074>.
- (90) Zhang, B.; Kowsari, K.; Serjouei, A.; Dunn, M. L.; Ge, Q. Reprocessable Thermosets for Sustainable Three-Dimensional Printing. *Nat. Commun.* **2018**, *9* (1), 1–7. <https://doi.org/10.1038/s41467-018-04292-8>.
- (91) Chen, Z.; Yang, M.; Ji, M.; Kuang, X.; Qi, H. J.; Wang, T. Recyclable Thermosetting Polymers for Digital Light Processing 3D Printing. *Mater. Des.* **2021**,

- 197, 109189. <https://doi.org/10.1016/j.matdes.2020.109189>.
- (92) Shi, Q.; Yu, K.; Kuang, X.; Mu, X.; Dunn, C. K.; Dunn, M. L.; Wang, T.; Jerry Qi, H. Recyclable 3D Printing of Vitrimer Epoxy. *Mater. Horizons* **2017**, *4* (4), 598–607. <https://doi.org/10.1039/c7mh00043j>.
- (93) Morgan, F. L. C.; Moroni, L.; Baker, M. B. Dynamic Bioinks to Advance Bioprinting. *Adv. Healthc. Mater.* **2020**, *9* (15), 1901798. <https://doi.org/10.1002/adhm.201901798>.
- (94) Huang, W.; Qi, C.; Gao, Y. Injectable Self-Healable Nanocomposite Hydrogels with Mussel-Inspired Adhesive Properties for 3D Printing Ink. *ACS Appl. Nano Mater.* **2019**, *2* (8), 5000–5008. <https://doi.org/10.1021/acsanm.9b00936>.
- (95) Nam, S.; Stowers, R.; Lou, J.; Xia, Y.; Chaudhuri, O. Varying PEG Density to Control Stress Relaxation in Alginate-PEG Hydrogels for 3D Cell Culture Studies. *Biomaterials* **2019**, *200*, 15–24. <https://doi.org/10.1016/j.biomaterials.2019.02.004>.
- (96) Lou, J.; Stowers, R.; Nam, S.; Xia, Y.; Chaudhuri, O. Stress Relaxing Hyaluronic Acid-Collagen Hydrogels Promote Cell Spreading, Fiber Remodeling, and Focal Adhesion Formation in 3D Cell Culture. *Biomaterials* **2018**, *154*, 213–222. <https://doi.org/10.1016/j.biomaterials.2017.11.004>.
- (97) Ula, S. W.; Traugott, N. A.; Volpe, R. H.; Patel, R. R.; Yu, K.; Yakacki, C. M. Liquid Crystal Elastomers: An Introduction and Review of Emerging Technologies. *Liq. Cryst. Rev.* **2018**, *6* (1), 78–107. <https://doi.org/10.1080/21680396.2018.1530155>.
- (98) Saed, M. O.; Gablier, A.; Terentjev, E. M. Exchangeable Liquid Crystalline Elastomers and Their Applications. *Chem. Rev.* **2021**.

- <https://doi.org/10.1021/acs.chemrev.0c01057>.
- (99) Davidson, E. C.; Kotikian, A.; Li, S.; Aizenberg, J.; Lewis, J. A. 3D Printable and Reconfigurable Liquid Crystal Elastomers with Light-Induced Shape Memory via Dynamic Bond Exchange. *Adv. Mater.* **2020**, *32* (1), 1905682.  
<https://doi.org/10.1002/adma.201905682>.
- (100) Wojtecki, R. J.; Meador, M. A.; Rowan, S. J. Using the Dynamic Bond to Access Macroscopically Responsive Structurally Dynamic Polymers. *Nat. Mater.* **2011**, *10* (1), 14–27. <https://doi.org/10.1038/nmat2891>.
- (101) Denissen, W.; Winne, J. M.; Du Prez, F. E. Vitrimers: Permanent Organic Networks with Glass-like Fluidity. *Chem. Sci.* **2016**, *7* (1), 30–38.  
<https://doi.org/10.1039/C5SC02223A>.
- (102) Kloxin, C. J.; Scott, T. F.; Adzima, B. J.; Bowman, C. N. Covalent Adaptable Networks (CANs): A Unique Paradigm in Cross-Linked Polymers. *Macromolecules* **2010**, *43* (6), 2643–2653. <https://doi.org/10.1021/ma902596s>.
- (103) Kloxin, C. J.; Bowman, C. N. Covalent Adaptable Networks: Smart, Reconfigurable and Responsive Network Systems. *Chem. Soc. Rev.* **2013**, *42* (17), 7161–7173.  
<https://doi.org/10.1039/C3CS60046G>.
- (104) Snyder, R. L.; Fortman, D. J.; De Hoe, G. X.; Hillmyer, M. A.; Dichtel, W. R. Reprocessable Acid-Degradable Polycarbonate Vitrimers. *Macromolecules* **2018**, *51* (2), 389–397. <https://doi.org/10.1021/acs.macromol.7b02299>.
- (105) Fortman, D. J.; Brutman, J. P.; Cramer, C. J.; Hillmyer, M. A.; Dichtel, W. R. Mechanically Activated, Catalyst-Free Polyhydroxyurethane Vitrimers. *J. Am. Chem. Soc.* **2015**, *137* (44), 14019–14022. <https://doi.org/10.1021/jacs.5b08084>.

- (106) Röttger, M.; Domenech, T.; Van Der Weegen, R.; Breuillac, A.; Nicolaÿ, R.; Leibler, L. High-Performance Vitrimers from Commodity Thermoplastics through Dioxaborolane Metathesis. *Science* **2017**, *356* (6333), 62–65.  
<https://doi.org/10.1126/science.aah5281>.
- (107) Ishibashi, J. S. A.; Kalow, J. A. Vitrimeric Silicone Elastomers Enabled by Dynamic Meldrum's Acid-Derived Cross-Links. *ACS Macro Lett.* **2018**, *7* (4), 482–486.  
<https://doi.org/10.1021/acsmacrolett.8b00166>.
- (108) Pang, K.; Kotek, R.; Tonelli, A. Review of Conventional and Novel Polymerization Processes for Polyesters. *Progress in Polymer Science (Oxford)*. Pergamon November 1, 2006, pp 1009–1037.  
<https://doi.org/10.1016/j.progpolymsci.2006.08.008>.
- (109) Kamber, N. E.; Jeong, W.; Waymouth, R. M.; Pratt, R. C.; Lohmeijer, B. G. G.; Hedrick, J. L. Organocatalytic Ring-Opening Polymerization. *Chemical Reviews*. American Chemical Society December 2007, pp 5813–5840.  
<https://doi.org/10.1021/cr068415b>.
- (110) Brutman, J. P.; Delgado, P. A.; Hillmyer, M. A. Polylactide Vitrimers. *ACS Macro Lett.* **2014**, *3* (7), 607–610. <https://doi.org/10.1021/mz500269w>.
- (111) Shi, W.; Zhao, J.; Yuan, X.; Wang, S.; Wang, X.; Huo, M. Effects of Brønsted and Lewis Acidities on Catalytic Activity of Heteropolyacids in Transesterification and Esterification Reactions. *Chem. Eng. Technol.* **2012**, *35* (2), 347–352.  
<https://doi.org/10.1002/ceat.201100206>.
- (112) Wiltshire, J. T.; Qiao, G. G. Degradable Core Cross-Linked Star Polymers via Ring-Opening Polymerization. *Macromolecules*. American Chemical Society June 27,

- 2006, pp 4282–4285. <https://doi.org/10.1021/ma060712v>.
- (113) Watts, A.; Kurokawa, N.; Hillmyer, M. A. Strong, Resilient, and Sustainable Aliphatic Polyester Thermoplastic Elastomers. *Biomacromolecules* **2017**, *18* (6), 1845–1854. <https://doi.org/10.1021/acs.biomac.7b00283>.
- (114) Zhao, Q.; Zou, W.; Luo, Y.; Xie, T. Shape Memory Polymer Network with Thermally Distinct Elasticity and Plasticity. *Sci. Adv.* **2016**, *2* (1), e1501297. <https://doi.org/10.1126/sciadv.1501297>.
- (115) Li, Q.; Barrett, D. G.; Messersmith, P. B.; Holten-Andersen, N. Controlling Hydrogel Mechanics via Bio-Inspired Polymer-Nanoparticle Bond Dynamics. *ACS Nano* **2016**, *10* (1), 1317–1324. <https://doi.org/10.1021/acsnano.5b06692>.
- (116) Edholm, O.; Blomberg, C. Stretched Exponentials and Barrier Distributions. *Chem. Phys.* **2000**, *252* (1–2), 221–225. [https://doi.org/10.1016/S0301-0104\(99\)00349-3](https://doi.org/10.1016/S0301-0104(99)00349-3).
- (117) Beckett, M. A.; Strickland, G. C.; Holland, J. R.; Sukumar Varma, K. A Convenient NMR Method for the Measurement of Lewis Acidity at Boron Centres: Correlation of Reaction Rates of Lewis Acid Initiated Epoxide Polymerizations with Lewis Acidity. *Polymer (Guildf)*. **1996**, *37* (20), 4629–4631. [https://doi.org/10.1016/0032-3861\(96\)00323-0](https://doi.org/10.1016/0032-3861(96)00323-0).
- (118) Imbernon, L.; Norvez, S.; Leibler, L. Stress Relaxation and Self-Adhesion of Rubbers with Exchangeable Links. *Macromolecules* **2016**, *49* (6), 2172–2178. <https://doi.org/10.1021/acs.macromol.5b02751>.
- (119) Arnett, E. M.; Mach, G. W. Solvent Effects in Organic Chemistry. VIII. Acidity Function Failure in Different Aqueous Acids. *J. Am. Chem. Soc.* **1966**, *88* (6), 1177–1183. <https://doi.org/10.1021/ja00958a019>.

- (120) Raamat, E.; Kaupmees, K.; Ovsjannikov, G.; Trummal, A.; Kütt, A.; Saame, J.; Koppel, I.; Kaljurand, I.; Lipping, L.; Rodima, T.; et al. Acidities of Strong Neutral Brønsted Acids in Different Media. *J. Phys. Org. Chem.* **2013**, *26* (2), 162–170. <https://doi.org/10.1002/poc.2946>.
- (121) Paenurk, E.; Kaupmees, K.; Himmel, D.; Kütt, A.; Kaljurand, I.; Koppel, I. A.; Krossing, I.; Leito, I. A Unified View to Brønsted Acidity Scales: Do We Need Solvated Protons? *Chem. Sci.* **2017**, *8* (10), 6964–6973. <https://doi.org/10.1039/c7sc01424d>.
- (122) Shamir, D.; Zilbermann, I.; Maimon, E.; Shames, A. I.; Cohen, H.; Meyerstein, D. Anions as Stabilizing Ligands for Ni(III)(Cyclam) in Aqueous Solutions. *Inorganica Chim. Acta* **2010**, *363* (12), 2819–2823. <https://doi.org/10.1016/j.ica.2010.03.057>.
- (123) Luong, B. X.; Petre, A. L.; Hoelderich, W. F.; Commarieu, A.; Laffitte, J. A.; Espeillac, M.; Souchet, J. C. Use of Methanesulfonic Acid as Catalyst for the Production of Linear Alkylbenzenes. *J. Catal.* **2004**, *226* (2), 301–307. <https://doi.org/10.1016/j.jcat.2004.05.025>.
- (124) Shroff, R.; Rulíšek, L.; Doubský, J.; Svatoš, A. Acid-Base-Driven Matrix-Assisted Mass Spectrometry for Targeted Metabolomics. *Proc. Natl. Acad. Sci. U. S. A.* **2009**, *106* (25), 10092–10096. <https://doi.org/10.1073/pnas.0900914106>.
- (125) Ugur, I.; Marion, A.; Parant, S.; Jensen, J. H.; Monard, G. Rationalization of the PKa Values of Alcohols and Thiols Using Atomic Charge Descriptors and Its Application to the Prediction of Amino Acid PKa's. *J. Chem. Inf. Model.* **2014**, *54* (8), 2200–2213. <https://doi.org/10.1021/ci500079w>.
- (126) Kim, S.; Thiessen, P. A.; Bolton, E. E.; Chen, J.; Fu, G.; Gindulyte, A.; Han, L.; He,

- J.; He, S.; Shoemaker, B. A.; et al. PubChem Substance and Compound Databases. *Nucleic Acids Res.* **2016**, *44* (D1), D1202–D1213.  
<https://doi.org/10.1093/nar/gkv951>.
- (127) Scheutz, G. M.; Lessard, J. J.; Sims, M. B.; Sumerlin, B. S. Adaptable Crosslinks in Polymeric Materials: Resolving the Intersection of Thermoplastics and Thermosets. *J. Am. Chem. Soc.* **2019**, *141* (41), 16181–16196.  
<https://doi.org/10.1021/jacs.9b07922>.
- (128) Zhao, S.; Abu-Omar, M. M. Catechol-Mediated Glycidylation toward Epoxy Vitrimers/Polymers with Tunable Properties. *Macromolecules* **2019**.  
<https://doi.org/10.1021/acs.macromol.9b00334>.
- (129) Lessard, J. J.; Garcia, L. F.; Easterling, C. P.; Sims, M. B.; Bentz, K. C.; Arencibia, S.; Savin, D. A.; Sumerlin, B. S. Catalyst-Free Vitrimers from Vinyl Polymers. *Macromolecules* **2019**, *52* (5), 2105–2111.  
<https://doi.org/10.1021/acs.macromol.8b02477>.
- (130) Chen, L.; Liu, R.; Hao, X.; Yan, Q. CO<sub>2</sub>-Cross-Linked Frustrated Lewis Networks as Gas-Regulated Dynamic Covalent Materials. *Angew. Chemie Int. Ed.* **2019**, *58* (1), 264–268. <https://doi.org/10.1002/anie.201812365>.
- (131) Ishibashi, J. S. A.; Fang, Y.; Kalow, J. A. Exploiting Block Copolymer Phase Segregation to Tune Vitriemer Properties. *ChemRxiv*. ChemRxiv December 13, 2019.  
<https://doi.org/10.26434/chemrxiv.10000232.v3>.
- (132) Lessard, J. J.; Scheutz, G. M.; Sung, S. H.; Lantz, K. A.; Epps, T. H.; Sumerlin, B. S. Block Copolymer Vitrimers. *J. Am. Chem. Soc.* **2020**, *142* (1), 283–289.  
<https://doi.org/10.1021/jacs.9b10360>.



- (133) Bates, F. S.; Hillmyer, M. A.; Lodge, T. P.; Bates, C. M.; Delaney, K. T.; Fredrickson, G. H. Multiblock Polymers: Panacea or Dandora's Box? *Science*. American Association for the Advancement of Science April 27, 2012, pp 434–440. <https://doi.org/10.1126/science.1215368>.
- (134) Ren, J. M.; McKenzie, T. G.; Fu, Q.; Wong, E. H. H.; Xu, J.; An, Z.; Shanmugam, S.; Davis, T. P.; Boyer, C.; Qiao, G. G. Star Polymers. *Chem. Rev.* **2016**, *116* (12), 6743–6836. <https://doi.org/10.1021/acs.chemrev.6b00008>.
- (135) Levi, A. E.; Lequeieu, J.; Horne, J. D.; Bates, M. W.; Ren, J. M.; Delaney, K. T.; Fredrickson, G. H.; Bates, C. M. Miktoarm Stars via Grafting-Through Copolymerization: Self-Assembly and the Star-to-Bottlebrush Transition. *Macromolecules* **2019**, *52* (4), 1794–1802. <https://doi.org/10.1021/acs.macromol.8b02321>.
- (136) Levi, A. E.; Fu, L.; Lequeieu, J.; Horne, J. D.; Blankenship, J.; Mukherjee, S.; Zhang, T.; Fredrickson, G. H.; Gutekunst, W. R.; Bates, C. M. Efficient Synthesis of Asymmetric Miktoarm Star Polymers. *Macromolecules* **2020**, *53* (2), 702–710. <https://doi.org/10.1021/acs.macromol.9b02380>.
- (137) Lin, T. P.; Chang, A. B.; Chen, H. Y.; Liberman-Martin, A. L.; Bates, C. M.; Voegtle, M. J.; Bauer, C. A.; Grubbs, R. H. Control of Grafting Density and Distribution in Graft Polymers by Living Ring-Opening Metathesis Copolymerization. *J. Am. Chem. Soc.* **2017**, *139* (10), 3896–3903. <https://doi.org/10.1021/jacs.7b00791>.
- (138) Laurent, B. A.; Grayson, S. M. Synthetic Approaches for the Preparation of Cyclic Polymers. *Chem. Soc. Rev.* **2009**, *38* (8), 2202–2213.

- <https://doi.org/10.1039/b809916m>.
- (139) Daniel, W. F. M.; Burdyńska, J.; Vatankhah-Varnoosfaderani, M.; Matyjaszewski, K.; Paturej, J.; Rubinstein, M.; Dobrynin, A. V.; Sheiko, S. S. Solvent-Free, Supersoft and Superelastic Bottlebrush Melts and Networks. *Nat. Mater.* **2016**, *15* (2), 183–189. <https://doi.org/10.1038/nmat4508>.
- (140) Pakula, T.; Zhang, Y.; Matyjaszewski, K.; Lee, H. il; Boerner, H.; Qin, S.; Berry, G. C. Molecular Brushes as Super-Soft Elastomers. *Polymer (Guildf)*. **2006**, *47* (20), 7198–7206. <https://doi.org/10.1016/j.polymer.2006.05.064>.
- (141) Zhang, M.; Müller, A. H. E. Cylindrical Polymer Brushes. *J. Polym. Sci. Part A Polym. Chem.* **2005**, *43* (16), 3461–3481. <https://doi.org/10.1002/pola.20900>.
- (142) Abbasi, M.; Faust, L.; Wilhelm, M. Comb and Bottlebrush Polymers with Superior Rheological and Mechanical Properties. *Adv. Mater.* **2019**, *31* (26), 1806484. <https://doi.org/10.1002/adma.201806484>.
- (143) Choinopoulos, I. Grubbs' and Schrock's Catalysts, Ring Opening Metathesis Polymerization and Molecular Brushes—Synthesis, Characterization, Properties and Applications. *Polymers (Basel)*. **2019**, *11* (2), 298. <https://doi.org/10.3390/polym11020298>.
- (144) Mukherjee, S.; Xie, R.; Reynolds, V. G.; Uchiyama, T.; Levi, A. E.; Valois, E.; Wang, H.; Chabinye, M. L.; Bates, C. M. Universal Approach to Photo-Crosslink Bottlebrush Polymers. *Macromolecules* **2020**, *53* (3), 1090–1097. <https://doi.org/10.1021/acs.macromol.9b02210>.
- (145) Vatankhah-Varnoosfaderani, M.; Daniel, W. F. M.; Everhart, M. H.; Pandya, A. A.; Liang, H.; Matyjaszewski, K.; Dobrynin, A. V.; Sheiko, S. S. Mimicking Biological

- Stress–Strain Behaviour with Synthetic Elastomers. *Nature* **2017**, *549* (7673), 497–501. <https://doi.org/10.1038/nature23673>.
- (146) Sarapas, J. M.; Chan, E. P.; Rettner, E. M.; Beers, K. L. Compressing and Swelling to Study the Structure of Extremely Soft Bottlebrush Networks Prepared by ROMP. *Macromolecules* **2018**, *51* (6), 2359–2366. <https://doi.org/10.1021/acs.macromol.8b00018>.
- (147) Bates, C. M.; Chang, A. B.; Momčilović, N.; Jones, S. C.; Grubbs, R. H. ABA Triblock Brush Polymers: Synthesis, Self-Assembly, Conductivity, and Rheological Properties. *Macromolecules* **2015**, *48* (14), 4967–4973. <https://doi.org/10.1021/acs.macromol.5b00880>.
- (148) Bates, C. M.; Chang, A. B.; Schulze, M. W.; Momčilovic, N.; Jones, S. C.; Grubbs, R. H. Brush Polymer Ion Gels. *J. Polym. Sci. Part B Polym. Phys.* **2016**, *54* (2), 292–300. <https://doi.org/10.1002/polb.23927>.
- (149) Liang, H.; Sheiko, S. S.; Dobrynin, A. V. Supersoft and Hyperelastic Polymer Networks with Brushlike Strands. *Macromolecules* **2018**, *51* (2), 638–645. <https://doi.org/10.1021/acs.macromol.7b02555>.
- (150) Roovers, J.; Toporowski, P. M. Characteristic Ratio and Plateau Modulus of 1,2-Polybutadiene. A Comparison with Other Rubbers. *Rubber Chem. Technol.* **1990**, *63* (5), 734–746. <https://doi.org/10.5254/1.3538286>.
- (151) Dossin, L. M.; Graessley, W. W. Rubber Elasticity of Well-Characterized Polybutadiene Networks. *Macromolecules* **1979**, *12* (1), 123–130. <https://doi.org/10.1021/ma60067a026>.
- (152) Reynolds, V. G.; Mukherjee, S.; Xie, R.; Levi, A. E.; Atassi, A.; Uchiyama, T.;

- Wang, H.; Chabinyo, M. L.; Bates, C. M. Super-Soft Solvent-Free Bottlebrush Elastomers for Touch Sensing. *Mater. Horizons* **2020**, *7* (1), 181–187.  
<https://doi.org/10.1039/c9mh00951e>.
- (153) Vatankhah-Varnoosfaderani, M.; Daniel, W. F. M.; Zhushma, A. P.; Li, Q.; Morgan, B. J.; Matyjaszewski, K.; Armstrong, D. P.; Spontak, R. J.; Dobrynin, A. V.; Sheiko, S. S. Bottlebrush Elastomers: A New Platform for Freestanding Electroactuation. *Adv. Mater.* **2017**, *29* (2), 1604209. <https://doi.org/10.1002/adma.201604209>.
- (154) Vatankhah-Varnosfaderani, M.; Keith, A. N.; Cong, Y.; Liang, H.; Rosenthal, M.; Sztucki, M.; Clair, C.; Magonov, S.; Ivanov, D. A.; Dobrynin, A. V.; et al. Chameleon-like Elastomers with Molecularly Encoded Strain-Adaptive Stiffening and Coloration. *Science* **2018**, *359* (6383), 1509–1513.  
<https://doi.org/10.1126/science.aar5308>.
- (155) Levental, I.; Georges, P. C.; Janmey, P. A. Soft Biological Materials and Their Impact on Cell Function. *Soft Matter* **2007**, *3* (3), 299–306.  
<https://doi.org/10.1039/B610522J>.
- (156) Vatankhah-Varnoosfaderani, M.; Sheiko, S. S.; Matyjaszewski, K.; Daniel, W. F. M.; Li, Q.; Morgan, B. J.; Spontak, R. J. Inherently Pre-Strained Elastomers with Self-Healing Property: New Generation of Freestanding Electroactuators. In *Electroactive Polymer Actuators and Devices (EAPAD) 2017*; Bar-Cohen, Y., Ed.; SPIE, 2017; Vol. 10163, p 29. <https://doi.org/10.1117/12.2261503>.
- (157) Hayashi, M.; Yano, R.; Takasu, A. Synthesis of Amorphous Low: T g Polyesters with Multiple COOH Side Groups and Their Utilization for Elastomeric Vitrimers Based on Post-Polymerization Cross-Linking. *Polym. Chem.* **2019**, *10* (16), 2047–

2056. <https://doi.org/10.1039/c9py00293f>.
- (158) Bowman, C. N.; Kloxin, C. J. Covalent Adaptable Networks: Reversible Bond Structures Incorporated in Polymer Networks. *Angew. Chemie Int. Ed.* **2012**, *51* (18), 4272–4274. <https://doi.org/10.1002/anie.201200708>.
- (159) Wu, J. B.; Li, S. J.; Liu, H.; Qian, H. J.; Lu, Z. Y. Dynamics and Reaction Kinetics of Coarse-Grained Bulk Vitrimers: A Molecular Dynamics Study. *Phys. Chem. Chem. Phys.* **2019**, *21* (24), 13267–13276. <https://doi.org/10.1039/c9cp01766f>.
- (160) Li, L.; Chen, X.; Jin, K.; Torkelson, J. M. Vitrimers Designed Both to Strongly Suppress Creep and to Recover Original Cross-Link Density after Reprocessing: Quantitative Theory and Experiments. *Macromolecules* **2018**, *51* (15), 5537–5546. <https://doi.org/10.1021/acs.macromol.8b00922>.
- (161) Creton, C. 50th Anniversary Perspective: Networks and Gels: Soft but Dynamic and Tough. *Macromolecules* **2017**, *50* (21), 8297–8316. <https://doi.org/10.1021/acs.macromol.7b01698>.
- (162) Rubenstein, M.; Colby, R. H. *Polymer Physics (Chemistry)*, 1st ed.; Oxford University Press, 2003.
- (163) Love, J. A.; Morgan, J. P.; Trnka, T. M.; Grubbs, R. H. A Practical and Highly Active Ruthenium-Based Catalyst That Effects the Cross Metathesis of Acrylonitrile. *Angew. Chemie Int. Ed.* **2002**, *41* (21), 4035–4037. [https://doi.org/10.1002/1521-3773\(20021104\)41:21<4035::aid-anie4035>3.0.co;2-i](https://doi.org/10.1002/1521-3773(20021104)41:21<4035::aid-anie4035>3.0.co;2-i).
- (164) Rogers, J. A.; Someya, T.; Huang, Y. Materials and Mechanics for Stretchable Electronics. *Science* **2010**, *327* (5973), 1603–1607. <https://doi.org/10.1126/science.1182383>.

- (165) Weigel, M.; Lu, T.; Bailly, G.; Oulasvirta, A.; Majidi, C.; Steimle, J. ISkin. In *Proceedings of the 33rd Annual ACM Conference on Human Factors in Computing Systems*; ACM: New York, NY, USA, New York, USA, 2015; Vol. 2015-April, pp 2991–3000. <https://doi.org/10.1145/2702123.2702391>.
- (166) Xu, S.; Zhang, Y.; Jia, L.; Mathewson, K. E.; Jang, K. I.; Kim, J.; Fu, H.; Huang, X.; Chava, P.; Wang, R.; et al. Soft Microfluidic Assemblies of Sensors, Circuits, and Radios for the Skin. *Science* **2014**, *344* (6179), 70–74. <https://doi.org/10.1126/science.1250169>.
- (167) Shih, B.; Shah, D.; Li, J.; Thuruthel, T. G.; Park, Y.-L.; Iida, F.; Bao, Z.; Kramer-Bottiglio, R.; Tolley, M. T. Electronic Skins and Machine Learning for Intelligent Soft Robots. *Sci. Robot.* **2020**, *5* (41), eaaz9239. <https://doi.org/10.1126/scirobotics.aaz9239>.
- (168) Amit, M.; Chukoskie, L.; Skalsky, A. J.; Garudadri, H.; Ng, T. N. Flexible Pressure Sensors for Objective Assessment of Motor Disorders. *Adv. Funct. Mater.* **2020**, *30* (20), 1905241. <https://doi.org/10.1002/adfm.201905241>.
- (169) Xu, J.; Wang, S.; Wang, G. J. N.; Zhu, C.; Luo, S.; Jin, L.; Gu, X.; Chen, S.; Feig, V. R.; To, J. W. F.; et al. Highly Stretchable Polymer Semiconductor Films through the Nanoconfinement Effect. *Science* **2017**, *355* (6320), 59–64. <https://doi.org/10.1126/science.aah4496>.
- (170) Shin, M.; Oh, J. Y.; Byun, K.-E.; Lee, Y.-J.; Kim, B.; Baik, H.-K.; Park, J.-J.; Jeong, U. Polythiophene Nanofibril Bundles Surface-Embedded in Elastomer: A Route to a Highly Stretchable Active Channel Layer. *Adv. Mater.* **2015**, *27* (7), 1255–1261. <https://doi.org/10.1002/adma.201404602>.

- (171) Song, E.; Kang, B.; Choi, H. H.; Sin, D. H.; Lee, H.; Lee, W. H.; Cho, K. Stretchable and Transparent Organic Semiconducting Thin Film with Conjugated Polymer Nanowires Embedded in an Elastomeric Matrix. *Adv. Electron. Mater.* **2016**, *2* (1), 1500250. <https://doi.org/10.1002/aelm.201500250>.
- (172) Moniruzzaman, M.; Winey, K. I. Polymer Nanocomposites Containing Carbon Nanotubes. *Macromolecules* **2006**, *39* (16), 5194–5205. <https://doi.org/10.1021/ma060733p>.
- (173) Kim, J. H.; Hwang, J. Y.; Hwang, H. R.; Kim, H. S.; Lee, J. H.; Seo, J. W.; Shin, U. S.; Lee, S. H. Simple and Cost-Effective Method of Highly Conductive and Elastic Carbon Nanotube/Polydimethylsiloxane Composite for Wearable Electronics. *Sci. Rep.* **2018**, *8* (1), 1375. <https://doi.org/10.1038/s41598-017-18209-w>.
- (174) Yu, Z.; Niu, X.; Liu, Z.; Pei, Q. Intrinsically Stretchable Polymer Light-Emitting Devices Using Carbon Nanotube-Polymer Composite Electrodes. *Adv. Mater.* **2011**, *23* (34), 3989–3994. <https://doi.org/10.1002/adma.201101986>.
- (175) Mutiso, R. M.; Winey, K. I. Electrical Properties of Polymer Nanocomposites Containing Rod-like Nanofillers. *Prog. Polym. Sci.* **2015**, *40* (1), 63–84. <https://doi.org/10.1016/j.progpolymsci.2014.06.002>.
- (176) Mensah, B.; Kim, H. G.; Lee, J.-H.; Arepalli, S.; Nah, C. Carbon Nanotube-Reinforced Elastomeric Nanocomposites: A Review. *Int. J. Smart Nano Mater.* **2015**, *6* (4), 211–238. <https://doi.org/10.1080/19475411.2015.1121632>.
- (177) Stopler, E. B.; Dodo, O. J.; Hull, A. C.; Weaver, K. A.; Chakma, P.; Edelman, R.; Ranly, L.; Zanjani, M. B.; Ye, Z.; Konkolewicz, D. Carbon Nanotube Enhanced Dynamic Polymeric Materials through Macromolecular Engineering. *Mater. Adv.*

- 2020**, *I* (5), 1071–1076. <https://doi.org/10.1039/d0ma00143k>.
- (178) Yuan, D.; Guo, H.; Ke, K.; Manas-Zloczower, I. Recyclable Conductive Epoxy Composites with Segregated Filler Network Structure for EMI Shielding and Strain Sensing. *Compos. Part A Appl. Sci. Manuf.* **2020**, *132*, 105837. <https://doi.org/10.1016/j.compositesa.2020.105837>.
- (179) Zhang, J.; Lei, Z.; Luo, S.; Jin, Y.; Qiu, L.; Zhang, W. Malleable and Recyclable Conductive MWCNT-Vitrimer Composite for Flexible Electronics. *ACS Appl. Nano Mater.* **2020**, *3* (5), 4845–4850. <https://doi.org/10.1021/acsanm.0c00902>.
- (180) Zhang, G.; Patel, T.; Nallepalli, P.; Bhagat, S.; Hase, H.; Jazani, A. M.; Salzmann, I.; Ye, Z.; Oh, J. K. Macromolecularly Engineered Thermoreversible Heterogeneous Self-Healable Networks Encapsulating Reactive Multidentate Block Copolymer-Stabilized Carbon Nanotubes. *Macromol. Rapid Commun.* **2021**, 2000514. <https://doi.org/10.1002/marc.202000514>.
- (181) Xie, X.; Mai, Y.; Zhou, X. Dispersion and Alignment of Carbon Nanotubes in Polymer Matrix: A Review. *Mater. Sci. Eng. R Reports* **2005**, *49* (4), 89–112. <https://doi.org/10.1016/j.mser.2005.04.002>.
- (182) Shaffer, M. S. P.; Fan, X.; Windle, A. H. Dispersion and Packing of Carbon Nanotubes. *Carbon N. Y.* **1998**, *36* (11), 1603–1612. [https://doi.org/10.1016/S0008-6223\(98\)00130-4](https://doi.org/10.1016/S0008-6223(98)00130-4).